RÉPUBLIQUE ALGÉRIENNE DÉMOCRATIQUE ET POPULAIRE

MINISTÈRE DE L'ENSEIGNEMENT SUPÉRIEUR ET DE LA RECHERCHE SCIENTIFIQUE

CENTRE UNIVERSITAIRE SALHI AHMED – NAAMA

INSTITUT DES TECHNOLOGIES

DÉPARTEMENT DE GÉNIE ÉLECTRIQUE

MÉMOIRE

En vue de l'obtention du diplôme de **Master** en :

Énergies Renouvelables

Option : **Énergies Renouvelables en Électrotechnique**

Intitulé:

OPTIMIZATION OF SILICON SOLAR CELLS USING PC1D SIMULATION

Présenté par :

- BOUAZZA Marwa
- BENKHEDDA Mohammed El Amine
- BERKOUK Rania Radja

Soutenu le : … 15/06/2023…. Devant le Jury :

Mr. BADAOUI Abdelhamid	***MCA***	***Centre Universitaire Naâma***	***Président***
Mlle. AMARA Zeyneb	***MCB***	***Centre Universitaire Naâma***	***Encadreur***
Mr. AMARA Hassen	***Master***	***Centre Universitaire Naâma***	***Co-Encadreur***
Mr. TAIBI Ibrahim	***MCA***	***Centre Universitaire Naâma***	***Examinateur***

Word of thanks

We thank **ALLAH** the Almighty for giving us the courage, the will and the patience to bring this work to an end.

Taking advantage of the opportunity offered to us, we have the great pleasure to express our heartfelt thanks to our supervisor .

Miss.AMARA ZEYNEB, who agreed to supervise us for the realization of this work, her knowledge, her judicious advice, her precious help, as well as our co-supervisor **Mr. AMARA HASSEN** for his immense effort.

Our thanks to the president of the jury **Mr.BADAOUI Abdelhamid** also to **Mr. TAIBI Ibrahim**, for having accepted to examine our work.

Finally, we would like to express our fervent thanks to all our teachers for their support and help during all the years of study.

Dedications

I dedicate this graduation thesis:

- To those whom I prefer over myself, for they sacrificed for me and make me happy, to the meaning of love, tenderness, devotion, to those whose supplication was the secret of my success, my dearest **parents.**
- To my **brothers** and **sisters** you are my happiness, may God grant you success to reach this moment .
- To a companion on the path, and a friend of all days, my dear **husband**, thank you for your motivation, continuous support, and your constant encouragement .
- To all my **precious family** and dear **colleagues .**

Berkouk Rania Radjaa

- To **Allah** first who give us the courage to finish this work .
- To my dear **parents** for all their sacrifices their love their tenderness their support and prayers throughout my studies .
- To my **sisters** .
- To all my **family** my **teachers** and **friends**

Bouazza Marwa

- To my beloved **parents,** without whom none of my success would be possible, whose love and support sustained me all along the path, I am forever grateful.
- To my dearest **brothers,** for being my lifelong companions and confidants.
- To my cherished **family** members, especially my dearest **aunties**, to whom I want to express my deepest gratitude.
- To my **favorite person** , lucky is to have you.
- To my dear **colleagues**, I am truly thankful for your commitment and devotion.

Benkhedda Mohammed El Amine

TABLE OF CONTENTS

Thanks
Dedications
LIST OF FIGURES
LIST OF TABLE
Abstract
General Introduction 1
CHARTER I: GENERALITIES ABOUT PHOTOVOLTAIC SOLAR CELLS ..... .
I. 1 Introduction 5
I. 2 History 5
I. 3 The photovoltaic effect 6
I. 4 Solar radiation 7
I. 4.1 Atmospheric Effects 9
I. 5 Semiconductor materials 10
I. 5.1. Intrinsic semiconductors 11
I. 6. Doping and silicon 12
I.6.1. N-type doping 12
I. 6.2. P-type doping 13
I. 7. The PN junction 13
I. 8.1. Ideal solar cell 14
I. 8.2. Real solar cell 15
I.10. PN junction solar cell under solar illumination 19
I.11. Illumination current in a homojunction PV cell 20
I.11.1. Neutral region type N 20
I.11.2. Neutral region type P 21
I.11.3. Region of the space load zone 22
I. 12. The different characteristics of a solar cell 22
I. 12.1. Short circuit current 23
I. 12.2. Open circuit voltage 23
I. 12.3.Maximum power 23
I. 12.4.Form factor FF 24

I.12.5. Conversion efficiency 24
I. 13. The different generations of PV solar cells 25
I.13.2. Second generation: CdTe, CIS/ CIGS, amorphous silicon microcrystalline 27
I. 13.3.Third generation Photo-electro-chemical technologies (Dye Sensitized Cell and Organic PV) 29
I. 14. Advantages and disadvantages of photovoltaic energy 30
I. 14.1. Advantages 30
I. 14.2. Disadvantages 31
I. 15. Conclusion 31
CHARTER II: PROPERTIES OF CRYSTALLINE AND AMORPHOUS SILICON……
II.1 Introduction 32
II.2 Features 32
..... 32
II.2.1 The diamond structure 33
II.3 The different states of silicon 34
II.3.1 Layers massive 34
II.3.2 Silicon-based thin films 36
II.4 Optoelectronic properties of crystalline silicon 37
II.4.1 monocrystalline silicon 37
II.4.2 polycrystalline silicon 39
II.5 Some properties of silicon 41
II.7 conclusion 45
CHARTER III: THE ANTI-REFLECTIVE LAYER 46
III.1. Introduction 47
III.2. Optical properties 47
III.2.1. Absorption 48
III.2.2. The transmission 48
III.2.3. The reflection 48
III.3. Optical Constants 49
III.3.1. Path difference 49
III.3.2. Phase shift 49
III.3.3. Refractive index 50
III.3.4. Absorption coefficient α 50

III.4. Thin film optics 51
III.4.1. Reflection in thin layers 52
III.4.1.1. Reflection coefficient 52
III.4.1.2. reflectivity 53
III.5. Special case of an anti-reflective layer 54
III.6. The anti-reflective layer for photovoltaic PV applications 55
III.6.1. Definition 55
III.6.2. The principle of the Anti-reflection coating 55
III.6.3. Characteristics Of Anti-Reflective Layer 55
III.7. Some materials used as Anti-reflection coating 55
III.7.1. Vanadium oxide (V_2O_5) 56
III.7.1.a. Electrical properties 56
III.7.1.b. Optical properties 56
III.7.2. Properties of ZnO 56
III.7.2.a. Crystal structure 56
III.7.2.b. Optical properties 57
III.7.2.c. Electrical properties 57
III.7.3. Applications of ZnO 59
III.8. Properties and applications of SnO_2 films 60
III.8.1. Properties 60
III.8.2. SnO_2 gap 61
III.8.3. Electronic structure of the bandgap of SnO_2 61
III.8.4. crystallographic Structure 62
III.8.5. Electrical structure 63
III.8.6. Optical properties 64
III.9. Photovoltaic applications 64
III.10. Conclusion 65
CHARTER IV: SIMULATION BY PC1D AND OPTIMIZATION 66
IV.1. Introduction 67
IV.2. Simulation Program PC1D 67
IV.3. Simulation results 70
IV.3.1.Influence of the area surface on the characteristic I-V/Power 70

IV.3.2. Influence of the thickness of the n-region on the I-V characteristic/Power and efficiency 73
IV.3.3.Influence of the texturing on the characteristic I-V/Power and the efficiency 75
IV.3.4.The influence of the angle of texuring on the characteristic I-V/Power and Efficiency 77
IV.3.5.Influence of the depth of texturation on the characteristic I-V/Power and Efficiency 79
IV.4.The Influence of the thickness of SnO_2 region on the characteristic I(V)/P(V) and Efficiency 82
IV.5.The Influence of the thickness of ZnO region on the characteristic I(V)/P(V) and Efficiency 86
GENERAL CONCLUSION 92
BIBLIOGRAPHY 93

LIST OF FIGURES

Chapter I: General information on photovoltaic solar cells.

Figure I.1: Functioning of the photovoltaic cell solar. [2] 6
Figure I.2: A fascinating photograph of the sun. [4] 7
Figure I.3: Solar irradiance and irradiation [2] 8
Figure I.4: Spectral distribution of radiation 9
Figure I.5: Types of solar radiation[11] 10
Figure I.6: forms four covalent bonds with a neighboring atom [14] 11
Figure I.7: semiconductor band diagram 11
Figure I.8: presented P-N doping 12
Figure I.9: The PN junction 13
Figure I.10: ideal solar cell model 15
Figure I.11: the equivalent diagram of a real solar cell 16
Figure I.12: Composition of a photovoltaic cell 17
Figure I.13: Principle of operation of the solar cell 19
Figure I.14: : Les courbes I = f (V) 22
Figure I.15: The different photovoltaic cell technologies. 25
Figure I.16: Manufacturing step cells [8] 26
Figure I.17: monocrystalline and polycrystalline cell [20] 26
Figure I.18: Cadmium Telluride glass-glass modules, efficiency of 9 to 11%. [17] 28
Figure I.19: flexible amorphous silicon α Si triple junction photovoltaic module for a 6.5% efficiency (Unisolar photo). [17] 28
Figure I.20: module combining microcrystalline and amorphous technology for efficiency [17] 29
Figure I.21: organic pv cell 30

Chapter II: Properties Of Crystalline And Amorphous Silicon

Figure II.1: Polycrystalline silicon 32
Figure II.2: Schematic band structure of a direct and indirect semiconductor 33
Figure II.3: Representation of SC conduction band minima 34
Figure II.4: Share of different technologies in the photovoltaic market in 2010 [7]. 35
Figure II.5: Crystallographic structure of silicon monocrystalline (diamond type) [13] 38
Figure II.6: Silicon band structure Monocrystalline .[13] 38
Figure II.7: Reflection coefficient R and absorption of monocrystalline silicon α um as a function of length of wav [12]. 39
Figure II.8: Density of states in logarithmic scale in the forbidden band of polycrystalline silicon in presence of defects (EV: valence band, EC: conduction band) [14]. 40
Figure II.9: photovoltaic Solar cell 43

Chapter III: The Anti-Reflective Layer

Figure III.1:Optical phenomena of the interaction of a light ray with a material medium. 48

Figure III.2: phenomenon of multiple reflections in a thin layer. [6] 52
Figure III.3: Schematic representation of the different crystal structures of ZnO 57
Figure III.4: Introduction to the Band Gap of Tin Oxide [32] 62
Figure III.5: Unit cell of SnO_2 (rutile structure) 62
Figure III.6: Energy diagram of SnO_2 63
Figure III.7: Schematic diagram of an Si-TCO electrode 65

Chapter IV: Simulation By Pc1d And Optimization

Figure IV.1: PC1D software window used in digital simulation [1] 68
Figure IV.2: The basic cell 69
Figure IV.3: characteristic of the basic cell. 69
Figure IV.4: Influence of the area on the I-V characteristic 70
Figure IV.5: Influence of the area on the Power characteristic 71
Figure IV.6: Influence of the thickness on the I-V characteristic 74
Figure IV.7: Influence of the thickness on the Power characteristic 74
Figure IV.8: Influence of the characteristic I-V With and without texturing 76
Figure IV.9: Influence of the characteristic Power with and without texturing 76
Figure IV.10: Influence of the texturing angle on the I-V characteristic 78
Figure IV.11: Influence of the texturing angle on the Power characteristic 78
Figure IV.12: Influence of the texturation angle on the I-V characteristic 80
Figure IV.13: Influence of the texturation angle on the Power characteristic 80
Figure IV.14: Cell SnO_2 81
Figure IV.15: Influence of the thickness of SnO_2 region on the I-V characteristic 83
Figure IV.16: Influence of the thickness of SnO_2 region on the Power characteristic 84
Figure IV.17: Cell ZnO 86
Figure IV.18: Influence of the thickness of ZnO region on the I-V characteristic. 88
Figure IV.19: Influence of the thickness of ZnO region on the Power characteristic 89

LIST OF TABLE

Chapter II: Properties of Crystalline and Amorphous Silicon

Table II.1: Efficiency of marketed solar modules. Performance measures are based on standard conditions. [9] 36
Table II.2: Some properties of silicon. 41

Chapter III: The Anti-Reflective Layer

Table III.1: refractive indices of some media 50
Table III.2: Resistivity, free carrier concentration, percent dopant of ZnO thin films with different types of impurities 58
Table III.3: Some physico-chemical properties of SnO_2 [30] 60

Chapter IV: Simulation By Pc1d And Optimization

Table IV.1: Comparison of different area values 72
Table IV.2: Comparison of different thickness values 75
Table IV.3: Cell comparison with texturing and without texturing 77
Table IV.4: Comparison of the different angle of texturing 79
Table IV.5: Comparison of the different depth texturations 81
Table IV.6: The parameters for the simulation SnO_2 82
Table IV.7: Comparison of the different thickness of ARL in SnO_2 region 84
Table IV.8: The parameters for the simulation ZnO 87
Table IV.9: Comparison of the different thickness of ARL in ZnO region 89

Abstract

Arabe

يركز عملنا على محاكاة ثلاث خلايا شمسية ، وهي **Si (N^+) / Si (P)** و **SnO_2 / Si (N^+) / Si (P)** و **ZnO / Si (N^+) / Si (P).** لقد درسنا معلمات مختلفة مثل) سطح المنطقة ، سمك المنطقة **N** ، التركيب ، زاوية التركيب ، عمق التركيب ، سمك منطقة **SnO_2** ، سمك منطقة **ZnO)** وقمنا بتحليل تأثيرها على الخاصية **I (V) / P** (ت) والكفاءة. استخدمنا **SnO_2** و **ZnO** كطبقات مضادة للانعكاس ، وأظهرت النتائج أن خلية غير متجانسة تؤدي أداءً أفضل بكثير من خلية متجانسة.

English

Our work focuses on the simulation of three solar cells, which are Si (N^+)/Si (P), SnO_2 /Si (N^+)/Si (P), ZnO /Si (N^+)/Si (P). We investigated different parameters such as (Area surface, Thickness of the N-region, Texturing, Angle of Texturing, Depth of Texturing, Thickness of SnO_2 region, Thickness of ZnO region) and analyzed their influence on the characteristic I (V)/P(V) and efficiency. We used SnO_2 and ZnO as anti-reflective layers, the results showed that a heterojunction cell performs far better than a homojunction cell.

French

Notre travail porte sur la simulation de trois cellules solaires, qui sont Si (N^+) /Si (P), SnO_2/Si (N^+) /Si (P), ZnO/Si (N^+) /Si (P). Nous avons étudié différents paramètres tels que (surface, épaisseur de la région N, texturation, angle de texturation, profondeur de texturation, épaisseur de la région SnO_2, épaisseur de la région ZnO) et analysé leur influence sur la caractéristique I (V) /P (V) et efficacité. Nous avons utilisé SnO_2 et ZnO comme couches antireflet, les résultats ont montré qu'une cellule à hétérojonction fonctionne bien mieux qu'une cellule à homojonction.

GENERAL INTRODUCTION

General Introduction

Photovoltaic cells are a very interesting solution for the production so-called green electricity. The rapid development of their technologies has made them currently fully capable of competing with conventional means based on fossil fuels. Their major handicap remains their relatively efficiency it rarely exceeds 20% [1].

Many teams around the world are currently working to improve their performance. The performance of a PV cell is highly dependent on the conditions weather, such as solar radiation, temperature and wind speed. The performance of the cell can be improved by optimizing the internal physical parameters to ensure both a short-circuit current, a form factor and a high open circuit voltage [2].

Bell Laboratories demonstrated the first practical solar cell in 1954 using a diffused silicon (Si) p–n junction having efficiency of 6% [3]. The Si based solar panels have become and are still most cost effective and practically feasible. Crystalline Si solar cells are approaching theoretical efficiency limit of 29.43% for a 110 μm thick solar cell [4] but the best-achieved conversion efficiency using commercial solar cells is not more than 22% [5].

Anti-reflective coating (ARC) layers on silicon (Si) solar cells usually play a vital role for light absorbed into the cell and a solution to reduce these losses and protect the device from environmental degradation [6]. Zinc oxide (ZnO) is an emerging material in the semiconductor industry due to its abundance and being environmentally friendly. The only major drawback of ZnO that hinders its use in the fabrication of a homojunction device is that it cannot be p-doped reliably and reproducibly. However, n-ZnO has been found to have applications in several optoelectronic devices, such as photovoltaic cells. Since the proposed use of n-ZnO as an emitter layer and antireflection (AR)

coating, several researchers have employed n-ZnO thin films to fabricate potentially high efficiency and low-cost solar cells [7].

Our attention brings us to the use of tin oxide SnO_2 as an antireflection coating; we are interested in the analysis of the influence of the parameters technological and geometric on the electrical and quantum response of a solar cell with PN homojunction using numerical simulation using PC1D software [8].

To describe this, this dissertation is presented in four chapters:

In the first chapter, we will focus on the solar cell theory photovoltaic.

In the second chapter, we recall polycrystalline silicon and report its properties optoelectronics through a bibliographic study.

In the third chapter, we first recall the theoretical principles concerning the optical properties and principle of antireflection coatings. Lastly, we present some materials used as an antireflection layer and will expose a study on tin dioxide SnO_2 and these essential properties in addition to some applications of this oxide in technology.

The fourth chapter is devoted to the presentation of the results obtained by the simulation of a SnO_2 (N)/Si (N+)/Si (P)/ZnO solar cell and their interpretations using the PC1D software.

General introduction references :

[1] MEMOIRE Pour l'obtention du diplôme de Master en PHYSIQUE Option : Physique des matériaux ELABORATION D'UN CODE DE CALCUL POUR L'ETUDE DES CELLULES SOLAIRES PHOTOVOLTAÏQUES A HAUT RENDEMENT APPLICATION A LA CELLULE A L'ARSENIURE DE GALLIUM (GAAS) Présenté par : Lamiss ABBAD ; Sara DJOUADI Soutenu le : 13 juillet 2021

[2] MEMOIRE Présenté pour l'obtention du diplôme de MAGISTER École doctorale

« Energies Renouvelables » Par: Amer HAMZAOUI Thème Soutenu le 2012 UNIVERSITE FERHAT ABBAS – SETIF

[3] K.A. Tsokos, Physics for the IB Diploma, 5th edition. Cambridge University Press, United Kingdom, 2012.

[4] A. Richter, M. Hermle, S.W. Glunz, Reassessment of the limiting efficiency for crystalline silicon solar cells, IEEE J. Photovolt. 3 (2013) 1184–1191.

[5] Babar Hussain, Abasifreke Ebong, Ian Ferguson Zinc oxide as an active n-layer and antireflection coating for silicon based heterojunction solar cell Solar Energy Materials & Solar Cells 2 April 2015

[6] Deb Kumar Shah, Devendra KC, Ahmad Umar, Hassan Algadi ,Mohammad Shaheer Akhtar and O-Bong Yang Article Influence of Efficient Thickness of Antireflection Coating Layer of HfO2 for Crystalline Silicon Solar Cell 12 October 2022.

[7] Babar Hussain, Aasma Aslam, Taj M Khan, Michael Creighton and Bahman Zohuri Article Electron Affinity and Bandgap Optimization of Zinc Oxide for Improved Performance of ZnO/Si Heterojunction Solar Cell Using PC1D Simulations 20 February 2019.

[8] MEMOIRE de ARBAOUI Kawter et MAZOUNI Mohamed Amin "Effet de la couche antireflet sur la réponse d'une cellule solaire" Université Djillali LIABES-Sidi Bel AbbesFaculté de Génie électrique Département d'électronique.

CHARTER I:

GENERALITIES ABOUT PHOTOVOLTAIC SOLAR CELLS

I. 1 Introduction

In this chapter, we draw on certain fundamental principles in the field of photovoltaic. We will start by discussing some ideas related to the photovoltaic energy source. Then, after giving a brief overview of the various current technical fields, we will describe semiconductors, P-N junctions, solar cells with their photovoltaic properties and briefly describe the different technologies sectors that exist. Finally, we discuss the advantages and disadvantages of photovoltaic energy. [1]

I. 2 History

It was in the first part of the 19th century when the photovoltaic effect was identified. The ability to convert light into electricity was discovered by young French physicist Alexandre Edmond Becquerel in 1839. Based on the photovoltaic effect, solar cells function. The most significant of these researchers are Charles Fritts, Edward Weston, Nikola Tesla, and Albert Einstein, who received the Nobel Prize in 1904 for his work on the "photoelectric effect." In the years that followed, a number of scientists worked to advance this effect and related technologies through their research. [2]

Nevertheless, because of high production rates, this technology has only started to advance more recently, in the late 1950 s of the 20th century, along with the growth of the semiconductor industry. The solar cells demonstrate themselves as a highly dependable and competitive technology during the 1960s when they are employed exclusively to power orbiting spacecraft in Earth orbit. Improvements in manufacturing occur in the 1970s, performance and efficiency of solar cells, while the impending oil crisis aids in lowering production costs and expanding the range of potential applications for solar cells. Electricity supply in areas far from the power grid has been acknowledged as being very well replaced by solar cells. [3]

Moreover, since the crisis of the 1970s, significant progress has been achieved in the creation of solar cells for usage in homes and businesses. [4]

One of the industries with the quickest growth over the past ten years is the production of solar modules and accompanying equipment, which is expanding at a rate of 40% annually as was already noted. The installed electricity capacity has grown to a staggering 17, 5 GW in the year 2010. [5]

I. 3 The photovoltaic effect

The photovoltaic effect, which is employed in solar cells, produces and transports positive and negative electrical charges in a semiconductor material under the influence of light. This directly turns the light energy of solar rays into electricity. [1]

Photons, or bundles of radiant energy, are the building blocks of sunlight. a PV cell can reflect or absorb photons, which allows them to pass right through the cell. Electricity is only produced by the absorbed photons. When photons are absorbed, their energy is transferred to the electrons in the solar cell's atoms. [2]

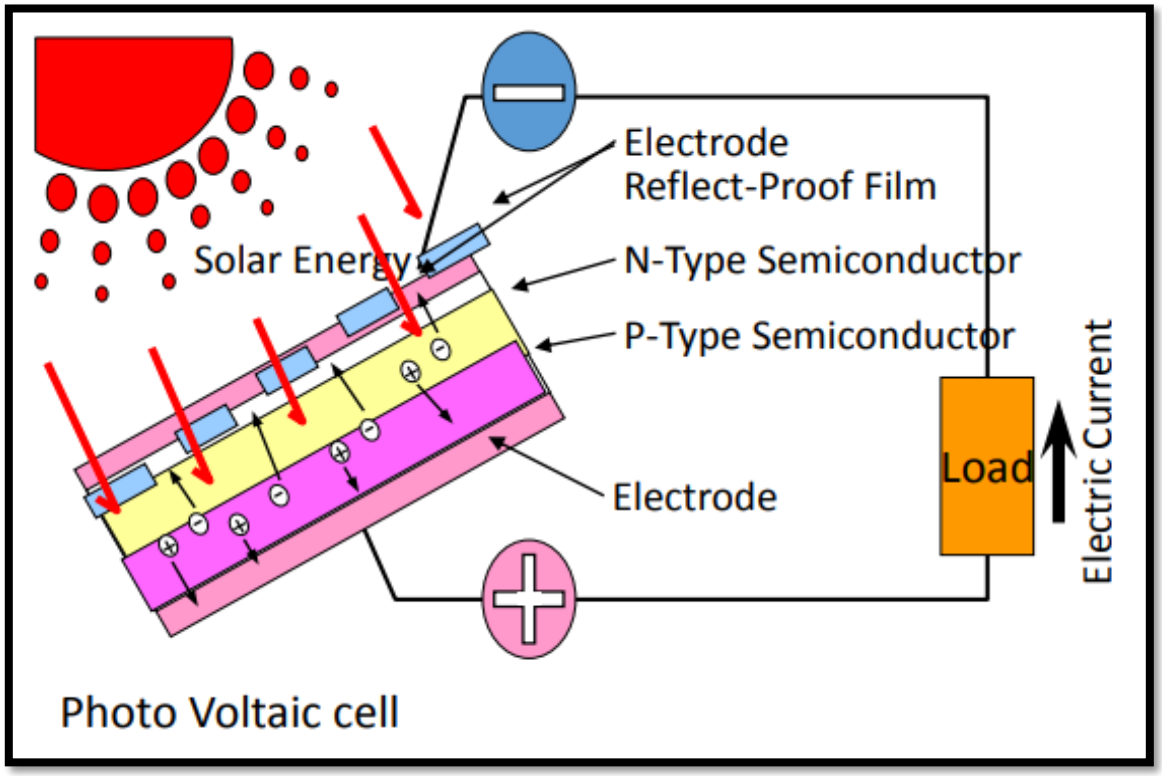

Figure I.1: Functioning of the photovoltaic cell solar. [2]

This is the photovoltaic effect's basic operating principle:

The process begins with "grains of light" (photons) striking the photovoltaic material's surface, which is arranged in cells or a thin layer. Next, they transfer their energy to the material's electrons, which become moved in a specific direction. Finally, very thin metal wires connected to one another and directed to the next cell collect the direct electric current produced. [1]

I. 4 Solar radiation

The sun continuously radiates a huge quantity of energy into the solar system, and only the planet intercepts a very small fraction of that energy. The solar constant, or 1367W/m^2, is the amount of energy that travels through each square meter of the Earth's atmosphere on average (for an average Earth-Sun distance of 150 million kilometers). [1]

Solar radiation is how the Sun's energy reaches the planet. The Sun's interior undergoes nuclear events that result in the fusion of hydrogen into helium. This process releases enormous quantities of energy, and the temperature there exceeds 15 million degrees Celsius. All activities, from photosynthesis to the generation of electricity in solar systems, are made possible by a portion of this energy, which arrives to Earth in the form of heat and light. [3]

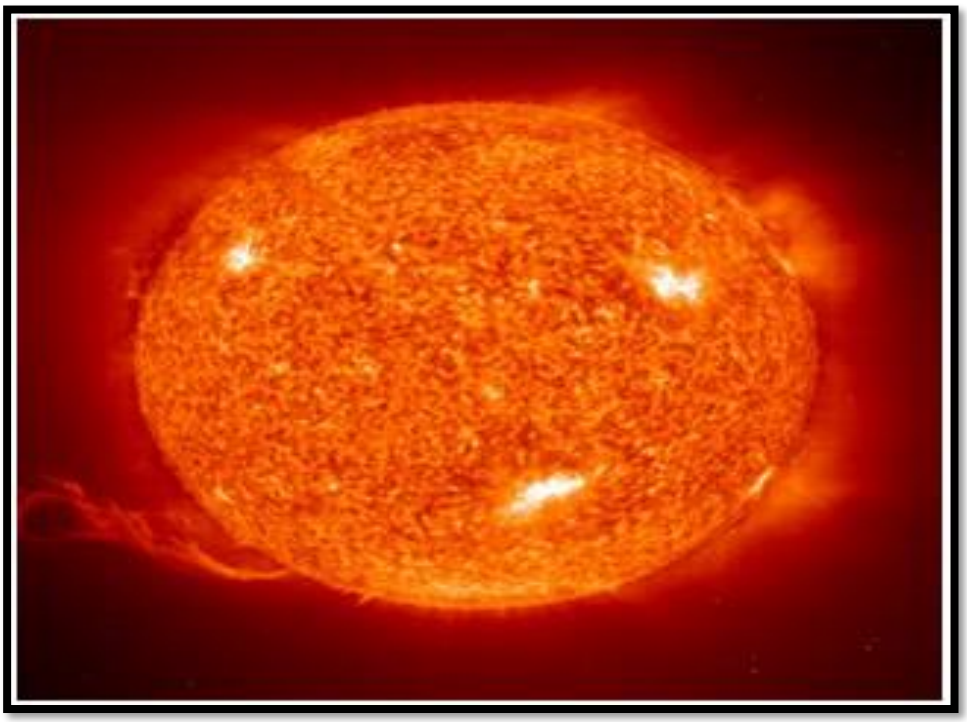

Figure I.2: A fascinating photograph of the sun. [4]

The amount of energy that the earth's surface receives in ideal circumstances 1.000 W/m^2 depends on the location, or latitude, as well as climatological location factors including the frequency of cloud cover and haze, air pressure, and other factors. [6]

Understanding the following ideas is important in order to properly consider the sun and the production of solar systems:

- Irradiation, average solar radiation power density (W/m^2), is equal to the solar radiation power divided by the surface of the plane perpendicular to the direction of this radiation. [7]
- Radiation is a unit of measurement for solar radiation (in Wh/m^2 or J/m^2) that is emitted on a particular surface at a given time. Depending on the period, it is sometimes stated as daily, monthly, or annual radiation in addition to hourly numbers. [3]

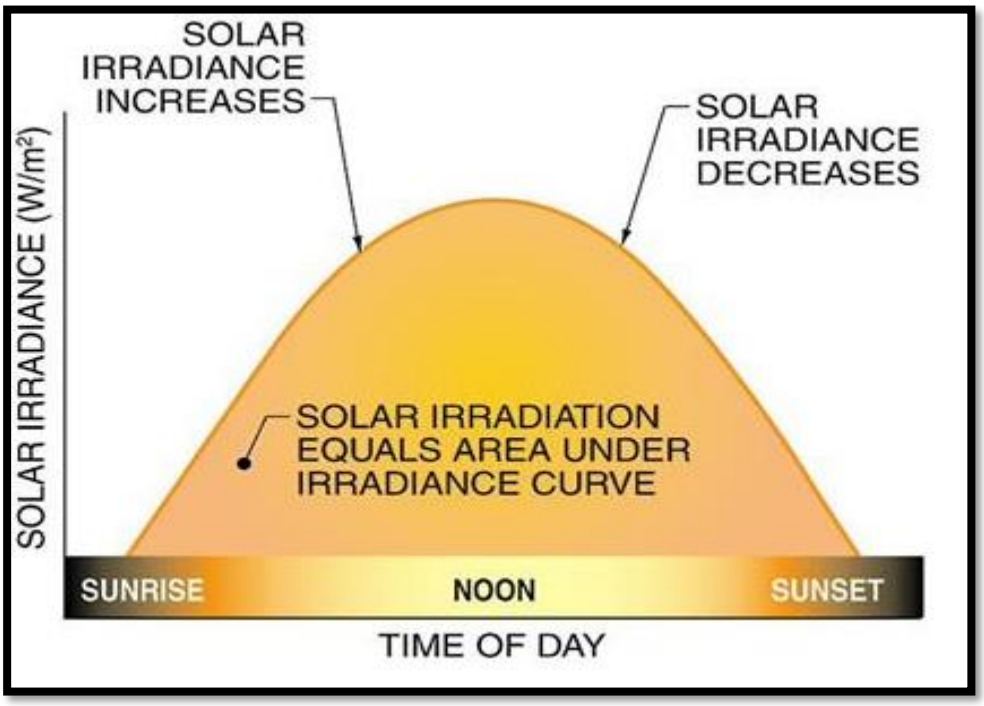

Figure I.3: Solar irradiance and irradiation [2]

- Most of the solar radiation that reaches Earth is made up of visible and infrared light. Only a small amount of ultraviolet radiation reaches the surface. [13]

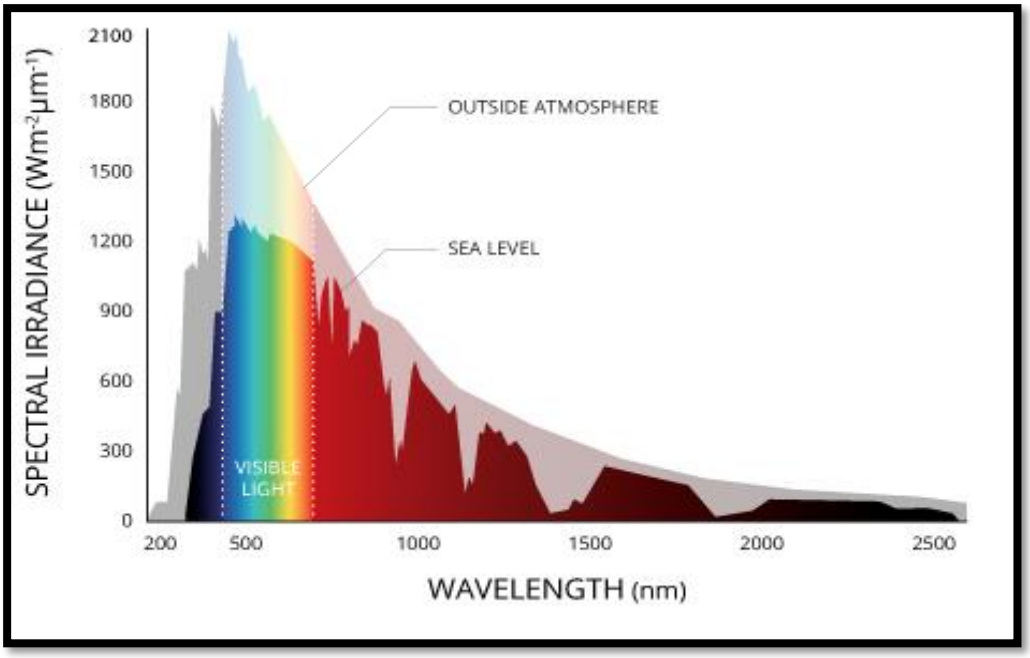

Figure I.4: Spectral distribution of radiation

- The proportion of energy that reaches earth's surface depends on how thick the atmosphere must be to pass through. The air mass number AM is used to describe this [8]

I. 4.1 Atmospheric Effects

The elements of the atmosphere absorb, scatter, and reflect solar light. This Earth is covered by the radioactive mountain, which extends from the interior to the upper atmosphere. [9]

A- Direct Normal Radiation (DIN): Radiation from the Earth that reaches the Earth without scattering

B- Diffuse Radiation (DIF): Radiation that is dispersed by the atmosphere and clouds and may reach from all directions.

C- Albedo: direct radiation, diffuse, radiation reflected from the Earth's surface (snow, lakes, etc.)

D- Global Horizontal Radiation (GHI): The total amount of short wave radiation received from the Earth's surface, this includes both direct normal radiation (DNI) and diffuse horizontal radiation (DHI).

E- Global in-plane radiation: the total amount of radiation (both DNI and DHI) received from a downward inclined surface. [10]

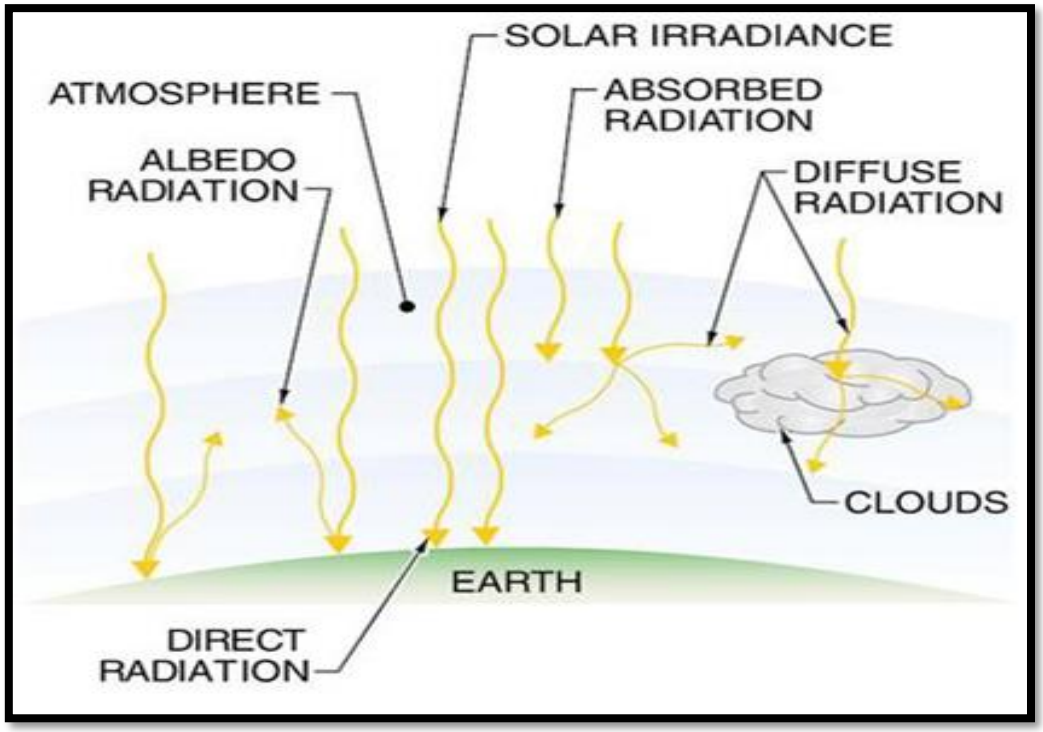

Figure I.5: Types of solar radiation [11]

I. 5 Semiconductor materials

Semiconductor materials are substances with a resistivity that is in the middle of that of insulators and conductors. The silicon atom's four valence electrons allow it to create four covalent connections with an atom nearby. In this situation, all of the electrons are used up and none is left over to produce electricity. [12]

The crystalline silicon (c-Si) solar cell, which now dominates the PV industry, has a straightforward structure and serves as a useful illustration of the construction of a conventional solar cell. [13]

Demonstrates the key characteristics of c-Si solar cells. A moderately doped p-type square wafer with a thickness of 300 nm and an area of 10 × 10 cm^2 or 12.5 × 12.5 cm^2 is generally used as an absorber material. A highly doped layer, which is n^+ type on the top side and p^{+-}type on the rear side of the c-Si wafer, respectively, is created on both sides of the wafer. These heavily doped layers aid in separating the c-Si wafer's bulk from the charge carriers produced by photography. The solar industry is moving toward wafers with a thickness of up to 250 nm and an area of 20 × 20 cm^2. [14]

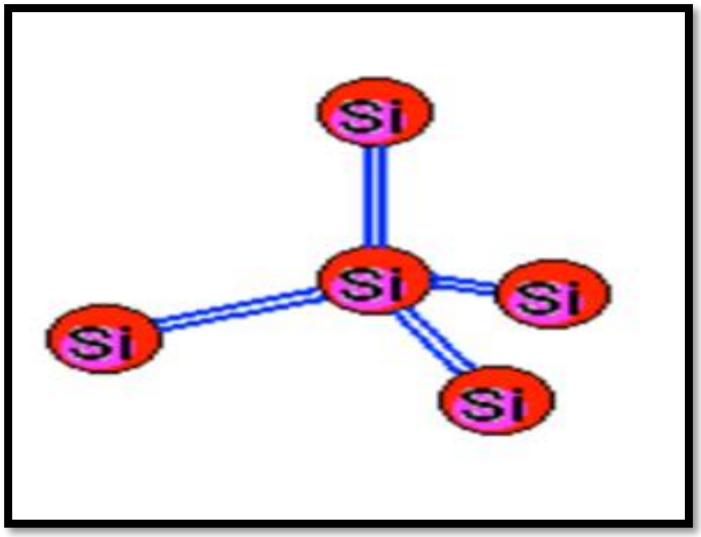

Figure I.6: forms four covalent bonds with a neighboring atom [14]

I. 5.1. Intrinsic semiconductors

The electrons located on the layer furthest from the nucleus, which take part in the covalent bonds can, under the effect of thermal agitation, become a carrier of charge.

The energy diagram consists of two bands (conduction and valence) separated by a band gap. To cross this band the electron must acquire energy (thermal, photon …) but the number of free electrons in an intrinsic semiconductor remains very weak. Here the number of hole and electron is equal. [15]

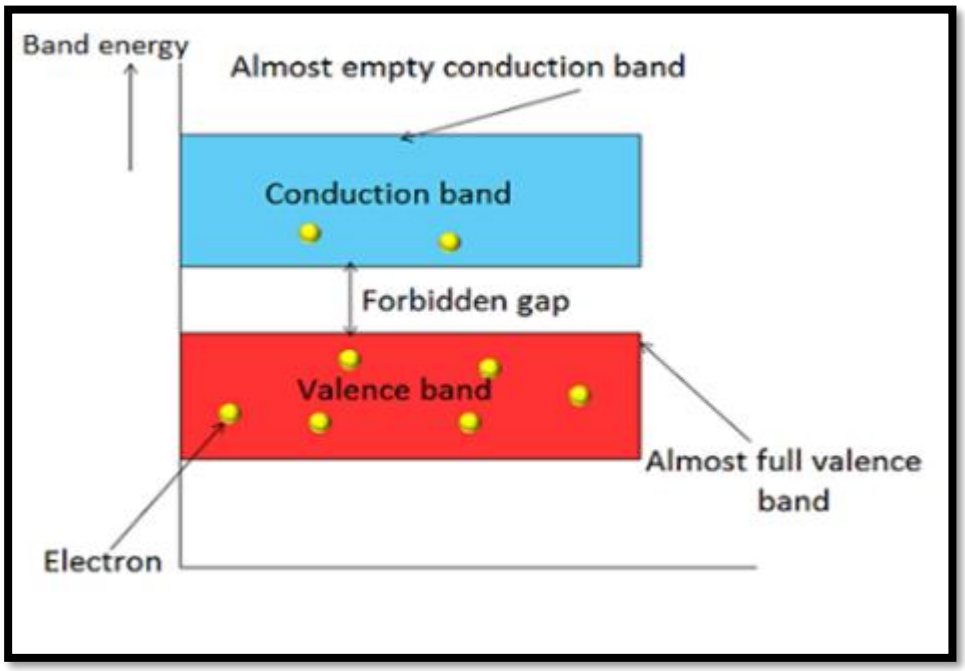

Figure I.7: semiconductor band diagram

I. 5.2. Extrinsic semiconductors

To increase the conductivity of semiconductors, impurities are introduced into them this process is called doping. [6]

I. 6. Doping and silicon

The conductivity is weak in a pure semiconductor due to the low number of carriers at ambient temperature. [7]

Why silicon?

Due to its electrical characteristics, silicon was selected to construct the photovoltaic solar cells. It is distinguished by having four electrons on the outer layer. Each atom in solid silicon is connected to four of its neighbors, and all of the peripheral layer's electrons are involved in the bonding [9].

If an atom with five peripheral electrons (such as phosphorus) is used in location of a silicon atom, the electron is no longer involved in the bonds and is free to wander throughout the network. When an electron conducts, the semiconductor is referred to as doped N. [16]

Contrarily, if an atom with three peripheral electrons (such as boron) replaces a silicon atom, an electron is needed to complete all of the bonds, and an electron can fill this hole. The semiconductor is then referred to as being p-type doped and there is stated to be conduction through a hole. [17]

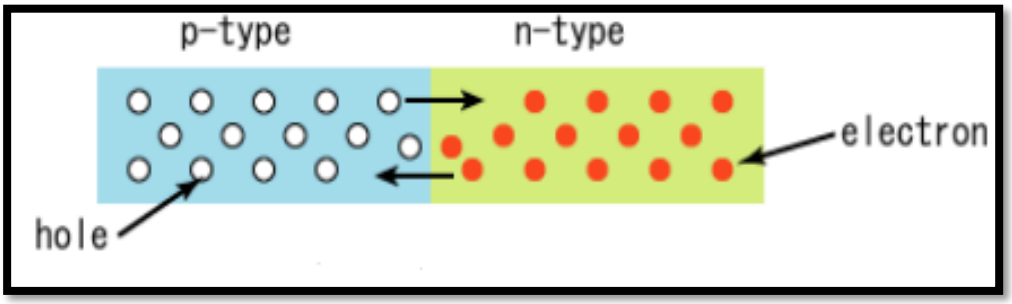

Figure I.8: presented P-N doping

I.6.1. N-type doping

A pentavalent atom takes the place of an atom of silicon. Four of these guarantee the bonds with the silicon atoms nearby, while the fifth one that is still free will be quickly stimulated toward the conduction band by thermal agitation. Because there are fewer holes than free electrons in this situation, the quantity of free electrons will rise significantly. Hence, an N-doped (negative) crystal is obtained. [18]

I. 6.2. P-type doping

Its three electrons will establish covalent connections with three adjacent atoms but leave a hole in the fourth, just as we did when we first introduced trivalent atoms. To produce a current, this hole in the crystal gradually travels. We acquire a P-doped crystal (positive) in this case because the number of holes is significantly larger than the intrinsic crystal's free electron count. Boron is frequently utilized as an impurity. [17]

I. 7. The PN junction

A P-doped area and an N-doped region come together to form a PN junction .The junction zone, also known as the transition zone, is where the free charge carriers attract and recombine during this assembly.

Just the ions are consequently left in this zone, which will produce an internal electrical field at the junction and prevent the remaining free charges in each zone from crossing the junction to recombine. [10]

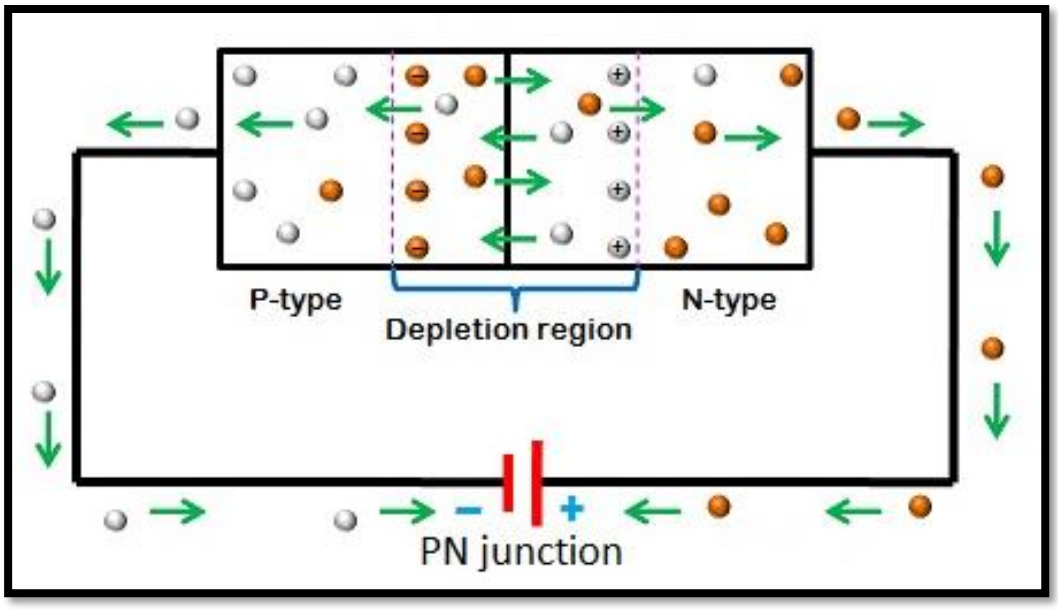

Figure I.9: The PN junction

I. 8. Operating principle of a PV solar cell

The solar cell is a large area PN junction photodiode that generates a electrical signal without the aid of an auxiliary power source. When the photons from the sun strike the cell, some are reflected and some are transmitted or absorbed in the solar cell, only the

absorbed photons participate in the effect photoelectric. Photovoltaic conversion involves three phenomena physical, intimately linked and simultaneous: [4]

- The absorption of light in the material
- Electric charge
- Load collection.

It follows that for photovoltaic conversion to be possible, the components of a solar cell must have precise optical and electrical characteristics. A field of electricity that allows the produced electron-hole pairs to be split apart is required in order to collect the pairs of electrons and holes. A PN junction is typically used for this. [15]

In the N-type, P, and space charge zones, the incoming photons produce electron-hole pairs. Depending on the area, the created electron-hole pairs act differently:

- Minority carriers disseminate in the N and P zone. The electric field propels what enters the space charge region toward the P zone (for the holes) and the N zone (for the electrons), where they will predominate. This movement of charge carriers produces the diffusion photocurrent. [10]
- In the space charge region, the photo generated electron hole pairs will be driven by the electric field towards the N region (electrons) and the P region (holes).This displacement of the photo carriers gives rise to a generation photocurrent. These two contributions together result in a total photocurrent Iph. It is a stream of minority carriers. It is proportional to the intensity luminous.[5]

I. 8.1. Ideal solar cell

If the junction is characteristic has the following form:$I = Is\left(e^{\frac{qv}{kT}} - 1\right)$. We can admit that in the presence of light there is appearance of a photocurrent additional, Iph whose direction is opposite to the direct current. By connecting a circuit outside on the clear cell, we collect this current. The current under light is worth. [5]

$$I = Iph - Is\left(e^{\frac{qv}{kT}} - 1\right). \quad (I.1)$$

Moreover, the voltage V is given by:

$$V = \frac{KT}{q}\ln\left(\frac{Iph + Is}{Is} - I\right). \quad (I.2)$$

With:

Iph: Photocurrent [A]

Is: Saturation current

q: Electron charge = 1.602. 10-^{19} Coulomb

K: Boltzmann constant = 1.38. 10^{-23} D/K

T: Actual cell temperature [Kelvin].

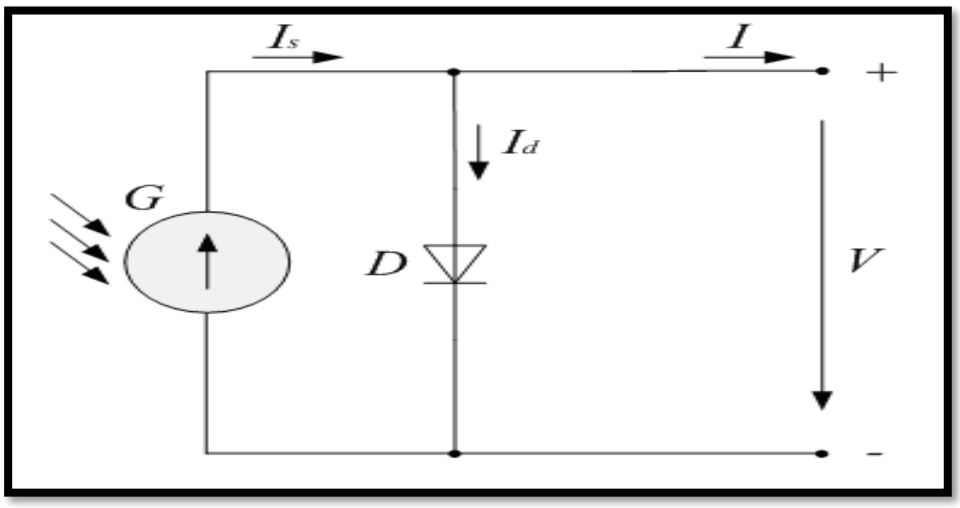

Figure I.10: ideal solar cell model

I. 8.2. Real solar cell

The figure. I .11 presents the equivalent diagram of a real solar cell, = where two parasitic resistances are introduced in this diagram, they will influence the characteristic I (V) of the cell. The first is the series resistance, this resistance is related to the impedance of the electrodes and the base, it follows that the voltage V at the terminals of the cell is different from the voltage at the terminals of the junction. [19]

The second is the shunt resistance Rsh, which corresponds to the losses in the surface and losses due to defects in the material, it results that this resistor will drive part of the current Iph and it cannot be delivered to the load. The equation of the I-V characteristic of the photovoltaic cell considering the resistances R sand Ish is therefore written [6].

$$I(V) = Iph - Id - Ish. \quad \text{(I. 3)}$$

$$I(V) = Iph - Is - \left(e^{\frac{q(V+RSI)}{KT}} - 1\right) - \frac{V + Rs}{Rsh}. \quad \text{(I. 4)}$$

With:

Rs: Series resistance [W]

Rsh: Shunt resistance [W]

Id: $diode\ current$

Ish: Shunt current

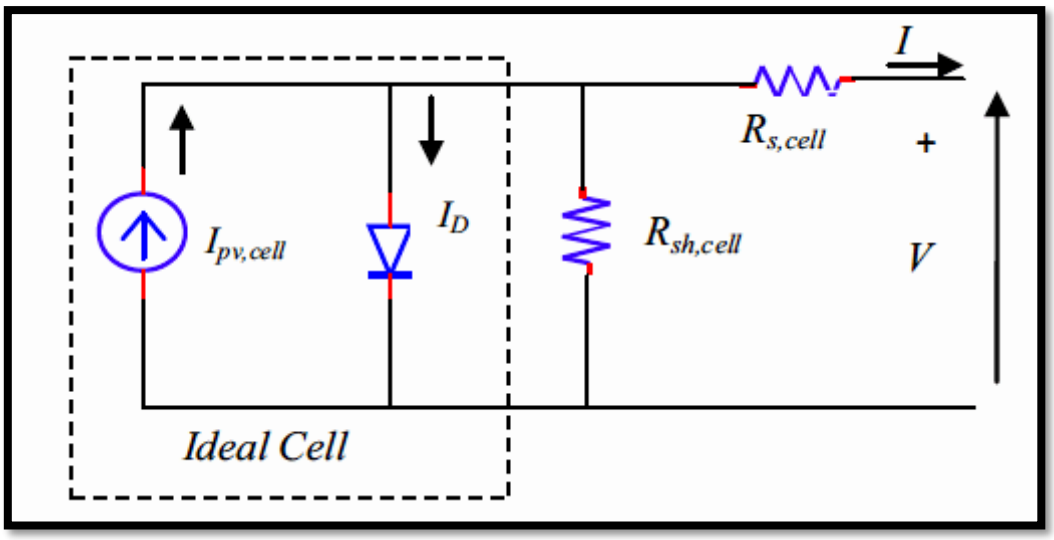

Figure I.11: the equivalent diagram of a real solar cell

I.9. The basic components of a photovoltaic cell (technology of a PV cell)

Although different structures are possible for the development of cells photovoltaics , similar parts are present in each component [23]. There structure of a photovoltaic cell with contacts on both sides is presented on the Figure I.12.

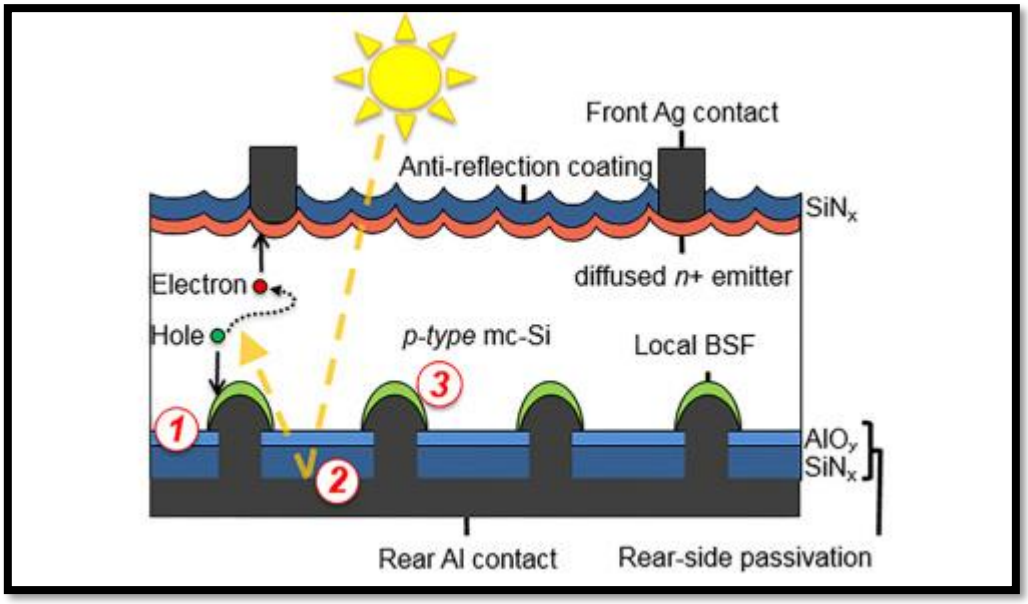

Figure I.12: Composition of a photovoltaic cell

- **Passivation of front and back sides**

The surface of semiconductors contains a high density of defects (bonds pendants, impurities, etc.) resulting in significant losses related to the surface recombination. Passivation consists of improving the electronic qualities of the surface and volume of the material by neutralizing the effects of its defects electrically assets. Various passivation layers are used in photovoltaic but the main ones are silicon oxide (SiO_2) and hydrogenated silicon nitride (SiNxH) [20].

- **Anti-reflective layer**

To minimize light reflection, an anti-reflective coating is used. The principle of action of the anti-reflection layers is based on the interference of the light beams in the thin dielectric layers [21].

For high efficiency photovoltaic cells, a double anti-reflection layer is used (with two different used (with two different dielectrics). Different materials are used in photovoltaics for the antireflection layer: TiO_2, SiO_2, ZnS, MgF_2, and SiNx.

- **Surface texturing**

Silicon texturing is used to decrease the reflectivity of the surface of the cell. This operation aims to develop a micrometric relief on the surface, generally pyramidal in shape.

The wavelength of the incident light being lower than the dimensions of the structures thus produced, the incident rays follow the laws of optics geometric.

Texturing leads to a reduction in reflection on the front face: a ray arriving at normal incidence (relative to the plane of the cell) on a pyramid will be reflected on the face of an adjacent pyramid. On the other hand, a ray of normal incidence will be transmitted in the cell with a refraction angle θ different from 0°. The path of this ray within the silicon will therefore be increased by a factor of 1/sin(θ) compared to the case of a flat surface and perpendicular to the illumination, which will have the effect of increasing the share of photons absorbed by the material. Also, texturing the surface results in more trapping significant amount of light entering the cell.

Different processes are used to texture the surface. For silicon, we find: chemical texturing (chemical attack of the surface with KOH or NaOH), mechanical texturing (cold rolling under a serrated comb) and laser texturing [20].

- **Front and rear contacts**

The metal contacts at the emitter and at the substrate serve to collect the current from photo-generated carriers. The contacts must be ohmic. The contact resistance is a very important parameter. High contact resistance increases series resistance of the cell and lowers the form factor and efficiency. Different processes are used to make contact. In the context of industrial photovoltaic cells in multicrystalline silicon, the contacts are generally made by screen-printing. For the high efficiency photovoltaic cells, sputtering or evaporation vacuum are used [20].

- **The BSF**

The back electric field (BSF: Back Surface Field) consists in creating a barrier of potential on the rear face of the cell to ensure passivation. The barrier of potential induced by the difference in doping level between the base and the BSF tends to confine the minority holders in the base. These are therefore kept away from the face back, which is characterized by a very high recombination rate. The BSF still does the subject of much research because the thickness of the plates is constantly reduced [21].

I.10. PN Junction Solar cell Under Solar illumination

- **Principle of operation**

The reverse current of a PN junction is a function on the one hand of the carrier densities minority in the neutral regions of the diode, and on the other hand the generation of pair's electron hole in the space charge region. In a photodiode, the radiation increases the reverse current by the creation of minority carriers in the regions neutrals and the generation of electron-hole pairs in the space charge region.

The principle of operation of a photovoltaic cell is illustrated in Fig. I.13. The incident photons create carriers in each region 1, 2 and 3 and the behavior of these free carriers differs according to the place of their creation.

In the electrically neutral regions P and N, the minority photo carriers diffuse, those that reach the space charge zone are propelled directly by the electric field towards the region where they become the majority.

These photo-carriers therefore contribute to the current by their diffusion, they create a scattering photocurrent. In the space charge region, the electron-hole pairs created by the photons are dissociated by the electric field, the electron is propelled towards the N-type region and the hole to the P-type region. These carriers give rise to a generation photocurrent. These different contributions add up to create a resultant photocurrent I_{PH} that contributes to the reverse current of the diode [22].

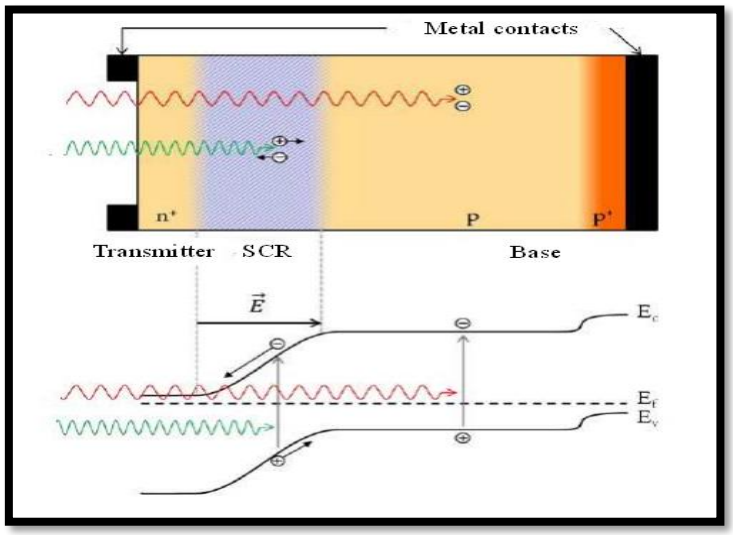

Figure I.13: Principle of operation of the solar cell

I.11. Illumination current in a homojunction PV cell

Consider a solar cell of thickness (L) illuminated with light containing photons with energy hv > Eg, the absorption of each photon by a valence electron will give rise to an electron-hole pair and all photo-generated pairs will contribute to the current. There are three regions: the neutral region of type N (front or emitter), the region P-type neutral (base) and the space charge zone (depletion zone) SCR [22, 23].

I.11.1. Neutral region type N

The current density of the minority carriers (holes) comes only from the diffusion current since the electric field is zero in this area [22, 24]:

$$J_P = -qD_P \frac{d\Delta P}{ds} \qquad (I.5)$$

The continuity equation is given by:

$$\frac{\partial pn}{\partial t} = Dp \frac{\partial^2 \Delta p}{\partial x^2} - \frac{\Delta p}{\tau p} + G_{opt} \qquad (I.6)$$

Where is the lifetime of the holes and G_{opt} the optical generation term.

The optical generation term G_{opt} due to an external mechanism (light) is expressed by:

$$G_{opt} = \alpha\phi\ (1 - R)\ exp\ (-\alpha x) \qquad (I.7)$$

Where α is the absorption coefficient of the semiconductor, the incident photon flux, R the reflection coefficient of the semiconductor, x the flux absorption depth light from the surface of the semiconductor [21].

In steady state $\frac{\partial pn}{\partial t} = 0$, then equation (I.10) becomes:

$$Dp \frac{\partial^2 \Delta p}{\partial x^2} + \alpha\emptyset(1 - R)\exp(-\alpha x) - \frac{\Delta p}{\tau p} = 0 \qquad (I.8)$$

The general solution is in the form:

$$\Delta p = A'ch\left(\frac{x}{Lp}\right) + B'sh\left(\frac{x}{Lp}\right) + \frac{\alpha\phi(1-R)}{1-\alpha^2 L^2 p}\tau_p exp(-\alpha x) \qquad (I.9)$$

The constants A' and B' are deduced from the two boundary conditions, which arise in the following form [24]:

$$Dp\frac{\partial \Delta p}{\partial x}\Big| 0_{x=0} = Sp\Delta p \qquad (I.10)$$

At the surface, the superficial recombination originating from the defects materializes by a Sp recombination rate.

$$\Delta p|c_{x=dn} = 0 \qquad (I.11)$$

At the boundary of the space charge region, all excess minority carriers are recombined.

The photocurrent density generated in the front area of the junction, for x = dn is then:

$$Jp(\lambda) = \frac{q(\alpha Lp)^2\phi(1-R)}{1-\alpha^2 Lp^2}\left[\exp(-\alpha dn) - \frac{1}{\alpha Lp}\frac{\left[1+\frac{\alpha Dp}{Sp}\right] - \exp(-\alpha dn)\left[ch\left(\frac{dn}{Lp}\right) + \frac{Dp}{LpSp}sh\left(\frac{dn}{Lp}\right)\right]}{sh\left(\frac{dn}{Lp}\right) + \frac{Dp}{LpSp}ch\left(\frac{dn}{Lp}\right)}\right] \qquad (I.12)$$

I.11.2. Neutral region type P

In the same way as in the previous case, we calculate the photocurrent density generated in the region P [21].

The boundary conditions are expressed as follows:

- For x = dn+W, at the boundary of the space charge region, the excess carrier density is zero: Δn=0.
- For x = L, the backside of the solar cell must be a zone of ohmic contact, thus of total recombination.

If the back contact is ohmic, the recombination rate can be considered as infinitely large, then Δn = 0, and the photocurrent density generated in this area, with x=dn+W is written:

$$Jn(\lambda) = \frac{q(\alpha Ln)^2\phi(1-R)}{\alpha^2 Ln^2 - 1}\left[\exp\left(-\alpha(dn+W)\right) + \frac{1}{\alpha Ln}\frac{\exp(-\alpha L) - \exp\left(-\alpha(dn+W)\right)ch\left(\frac{dn}{Lp}\right)}{sh\left(\frac{dp}{Ln}\right)}\right] \qquad (I.13)$$

If the recombination rate takes a value Sn for x = L, the formulation general current density of this zone is expressed by:

$$Jn(\lambda) = \frac{q(\alpha Ln)^2 \phi(1-R)}{\alpha^2 Ln^2 - 1}\left[\exp(-\alpha(dn+W)) + \frac{1}{\alpha Ln}\frac{\exp(-\alpha L)\left[1+\frac{\alpha Dn}{Sn}\right] - \exp(-\alpha(dn+W))\left[ch\left(\frac{dp}{Ln}+\frac{Dn}{LnSn}sh\left(\frac{dp}{Ln}\right)\right)\right]}{sh\left(\frac{dp}{Lp}\right)+\frac{Dn}{LnSn}ch\left(\frac{dp}{Ln}\right)}\right] \quad (I.14)$$

I.11.3. Region of the space load zone

It is assumed that the excess carriers generated are carried out of this region by the electric field region by the electric field that reigns there, before they can recombine. The density of photocurrent in this region is given by [25]:

$$J_{dr}(\lambda) = q\phi(1-R)exp\,(-\alpha d_n)[1-exp\,(-\alpha W)] \quad (I.15)$$

The total illumination current density (photocurrent) in short circuit for each incident radiation wavelength is given by:

$$J_E = J_{PK} = Jp\,(\lambda) + J_n(\lambda) + J_{dr}(\lambda) \quad (I.16)$$

I. 12. The different characteristics of a solar cell

Each photovoltaic cell is distinguished by an I-V curve that represents all of the possible electrical configurations for the cell under a certain light. This curve's three physical parameters are as follows:

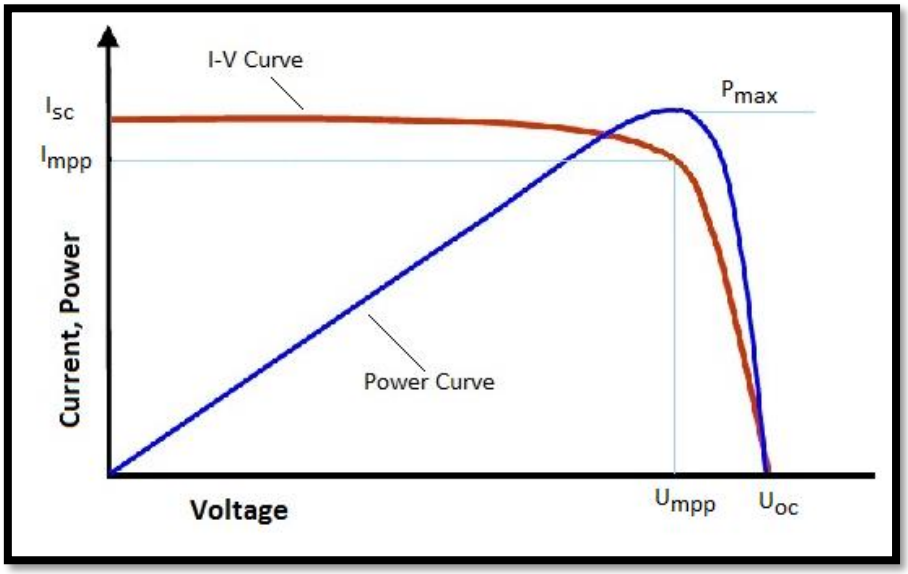

Figure I.14: : Les courbes I = f (V)

To allow a comparison of the efficiency of different cells, these characteristics are defined under very specific test conditions (STC = Standard Test Conditions). These conditions are light emission of 1000 W/m², temperature of 25°C, spectral conditions Air Mass 1.5 (composition of the spectrum identical to the solar spectrum when it crosses a thickness and a half of atmosphere, which corresponds to an angle of incidence of 41.8° with respect to the horizontal). [19]

I. 12.1. Short circuit current

The short-circuit current is the current started by the cell under illumination in short circuit the output. That is Isc= (V = 0) for an ideal solar cell the short circuit current is equal to the photovoltaic current Iph. [6]

I. 12.2. Open circuit voltage

As its name suggests, it is the voltage across the cell when it is not connected to a load or when connected to an infinite resistance load. She essentially depends on the type of solar cell (PN junction, Schottky junction), materials of the active layer and the nature of the contacts of the active layer electrode. She depends more on the illumination of the cell [7].

For an ideal solar cell the open circuit voltage is given:

$$Vco = \frac{KT}{q}\ln\left(\frac{Iph}{Is}+1\right) \approx Vco = \frac{KT}{q}\ln\left(\frac{Iph}{Is}\right). \quad \text{(I. 17)}$$

With:

q: Electron charge = 1.602. 10^{-19} Coulomb

K: Boltzmann constant = 1.38. 10^{-23} D/K

T: Actual cell temperature [Kelvin].

I. 12.3.Maximum power

The power delivered by a solar cell is maximum when the product V.I is maximum. If Vm and Im are the voltage and the current for which we have this maximum, the maximum power is the area of the largest rectangle with sides Vm and Im which can be written under the curve I (V). [8]

$P_M = I_M V_M$. (I.18)

P_M: Maximum power

I_M: Maximum current

V_M: Maximum voltage

I. 12.4.Form factor FF

The usual operating point of a solar cell is a point on the I (V) curve, which corresponds to a maximum power dissipated by the load. In FF (Fill Factor) form, the quantity: [7]

$$FF = \frac{P_M}{Isc\ Vco}. \quad (I.19)$$

Isc: Short-circuit current

Vco: Open circuit voltage

I.12.5. Conversion efficiency

Finally, the efficiency of a photovoltaic cell is given by the report enter here power output at the point of maximum power and the light output available

$$\eta \equiv \frac{Pm}{Pi}. \quad (I.20)$$

Where: Pi is the incident power of solar radiation at the ground. [11]

I. 13. The different generations of PV solar cells

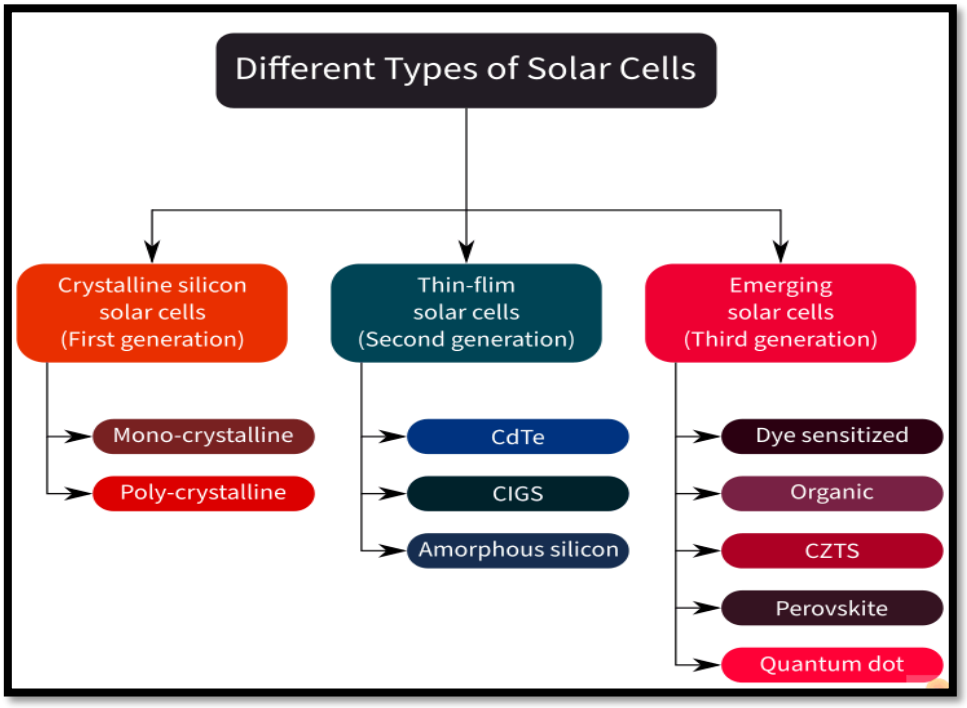

Figure I.15: The different photovoltaic cell technologies.

There are a large number of technologies implementing the photovoltaic effect. Many are still in the research and development phase [8]. The main technologies industrialized in quantity to date are: silicon mono or polycrystalline (more than 80% of world production) and silicon in thin film based on amorphous silicon or CIS (Copper Indium Selenium). [9]

I. 13.1. First generation: Crystalline silicon (mono and poly)

Wafers (thin slices) of crystalline silicon serve as the foundation for this type of cell. The silicon ingots made from these wafers are sawn. These ingots are the end product of a purifying procedure that produced a substance that contains 99.99999% silicon. [20]

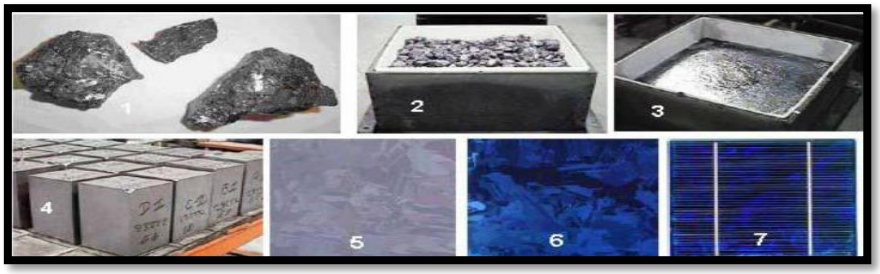

Figure I.16: Manufacturing step cells [8]

1) silicon ore
2) refining (to increase purity)
3) Molten silicon yielding ingot
4) After solidification
5) wafer obtained by sawing the ingot
6) surface treatment by physic-chemical processes
7) Finished cell with electrodes.

Crystalline cells are subdivided into 2 categories: mono- and polycrystalline depending on the type of structure. These two types of cells come from a process of different purification and solidification processes (Czochralski (Cz) process and Siemens). The Cz and Siemens purification processes have structures different supply chains and are generally carried out by industries different Figure I.17. [20]

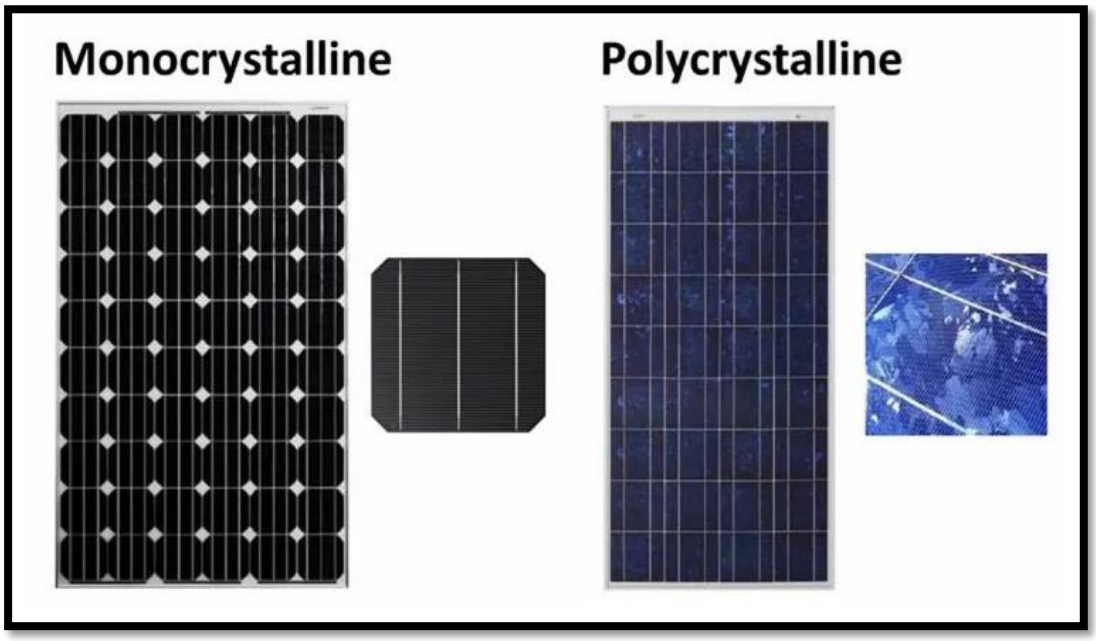

Figure I.17: monocrystalline and polycrystalline cell [20]

Monocrystalline cells may be identified by their uniform appearance and broken edges. The orientation of the various crystal lattices with regard to the cutting plane gives the polycrystalline cells a more iridescent look. [20]

I.13.2. Second generation: CdTe, CIS/ CIGS, amorphous silicon microcrystalline

This generation of cell relies on the thin-layer deposition of semiconductor materials (thin film). These materials are placed on a substrate using procedures like PECVD (Plasma Enhanced Chemical Vapor Deposition). The layer might be anything from a few nanometers to tens of micrometers thick. Because to their reduced weight per peak watt and initial cost, these technologies were only used in applications space and concentration technologies. The cost price of these technologies has decreased to be competitive with first-generation crystalline technologies, as manufacturing volumes have increased. [19]

Among the thin film technologies that are industrially exploited (mass production), we distinguish: CdTe: Cadmium Telluride (Telluride from cadmium), CIS / CIGS: Copper Indium Gallium Selenide, Silicon layer thin: amorphous silicon α-Si and microcrystalline. Note that the telluride of cadmium is a heavy metal alloy, very toxic, and can – like lead or mercury- concentrating in the food chain. The EU has banned its use for electrical devices... except for PV cells... [17]

Figure I.18: Cadmium Telluride glass-glass modules, efficiency of 9 to 11%. [17]

Figure I.19: flexible amorphous silicon α Si triple junction photovoltaic module for a 6.5% efficiency (Unisolar photo). [17]

Figure I.20: module combining microcrystalline and amorphous technology for efficiency [17]

I. 13.3.Third generation Photo-electro-chemical technologies (Dye Sensitized Cell and Organic PV)

Organic photovoltaic cells are solar cells that contain at least some organic molecules in the active layer. Generally, there are 2 types:

- Molecular organic photovoltaic cells.
- Organic polymer photovoltaic cells

These technologies, which first emerged in the 1990s, are meant to lower the price of producing power. The cheap cost of organic semiconductors and future manufacturing process simplifications are advantageous for organic photovoltaic cells. They provide the possibility of continuous production (roll-to-roll), which might significantly lower the cost of the solar panel. [14]

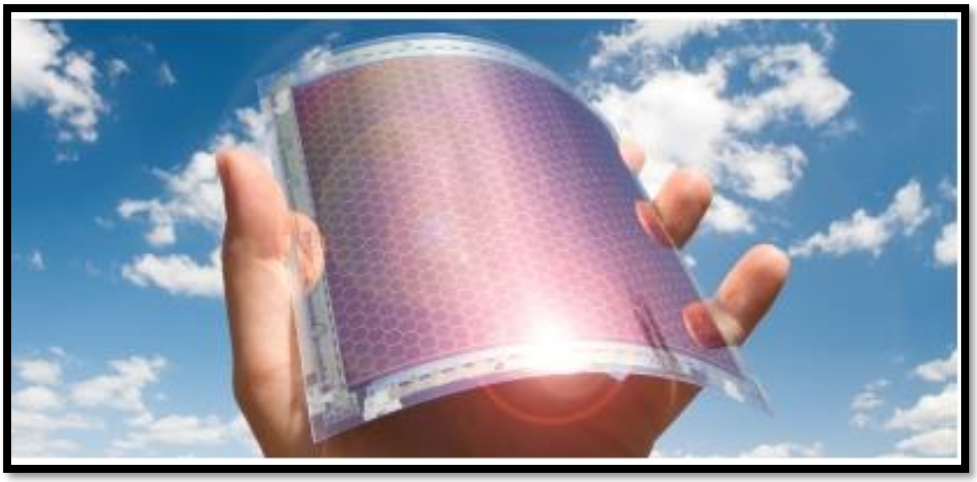

Figure I.21: organic pv cell

Practically, these technologies are only used commercially today in the consumer electronics sector (mobile phone charger/ portable MP3) where the lifetime of the cell and the associated product are approximately equal (2 years). By improving service life or reducing production costs, other applications should emerge in the years to come. [4]

I. 14. Advantages and disadvantages of photovoltaic energy

I. 14.1. Advantages

High reliability; modules are guaranteed for 25 years by most builders.

- As it has no moving components, it is especially suited for distant locations. It is used on gear gears for this purpose.
- The modular design of solar panels enables easy and flexible mounting to meet diverse energy demands. Systems may be made in sizes ranging from milliwatts to megawatts for power applications.
- With the decreased maintenance, their operational costs are extremely minimal, and they don't need gasoline, transportation, or highly skilled workers.
- From an ecological standpoint, photovoltaic technology provides advantages since the finished product is non-polluting, quiet, and waste-free. [10]

I. 14.2. Disadvantages

- The production of solar modules involves advanced technology and expensive capital.
- Use of space for substantial installations
- A module's actual conversion efficiency is low (a crystalline silicon cell's theoretical maximum efficiency is 28%).
- Only in distant places with low energy consumption can photovoltaic generators compete with diesel generators.
- Last but not least, the price of the solar generator increases when chemical energy storage (battery) is required. Yet, as long as the battery and the related regulatory components are wisely chosen, the dependability and system performance stay the same. [19]

I. 15. Conclusion

In this chapter, we have provided background material about photovoltaic cells that will help us comprehend the next chapters. We began by describing the photovoltaic effect, which is the key to harnessing photovoltaic energy. The properties of a p-n junction, which forms the core of solar cells, were then covered.

We next turned our attention to silicon, which accounts for more than 90% of the materials utilized in the construction of solar cells. We introduced crystalline silicon and amorphous silicon, which are the primary components of solar cells.

CHARTER II:

PROPERTIES OF CRYSTALLINE AND AMORPHOUS SILICON

II.1 Introduction

In this chapter, we will review the different states of silicon and recall the performance required for an efficient photovoltaic conversion according to of the different states. Silicon is the most used semiconductor material for the manufacture of microelectronic devices as well as photovoltaic cells.

II.2 Features

Figure II.1: Polycrystalline silicon

Silicon crystals are gray to black, needle-shaped or hexahedral (shape cubic). The amorphous phase is a dark brown powder. Silicon is a semiconductor, its electrical conductivity is much lower than that of metals [1].

It is insoluble in water (except at high temperature). Hydrofluoric acid (HF) or a mixture of hydrofluoric acid/nitric acid (HNO3) depending on the phase attacks it. Silicon has bluish metallic reflections, but is not at all as ductile as metals [2].

There are three natural isotopes of silicon: ^{28}Si (92.18%), ^{29}Si (4.71%) and ^{30}Si (3.12%). He are also unstable artificial isotopes: ^{25}Si, ^{26}Si and ^{27}Si which are β^+ emitters, as well as ^{31}Si to ^{34}Si which are β^- emitters [1].

Silicon, like germanium and the diamond form of carbon, has a structure like «diamond», shape derived from the face-centered cubic (fcc) structure, with a parameter of mesh of 0.5430710 nm [3].

II.2.1 The diamond structure

In the diamond structure, each atom is surrounded by 4 nearest neighbors, which allows forming covalent bonds. It can be described as being formed of 2 structures fcc. Displaced relative to each other along the main diagonal [4].

The band structure is the relationship between the energy of the particle and its vector k: E (k). We represent the evolution of the energy's by the curve E (k) by forcing the wave vector k to remain in a remarkable direction of space k, which has to say crystallographic direction of the reciprocal lattice [3].

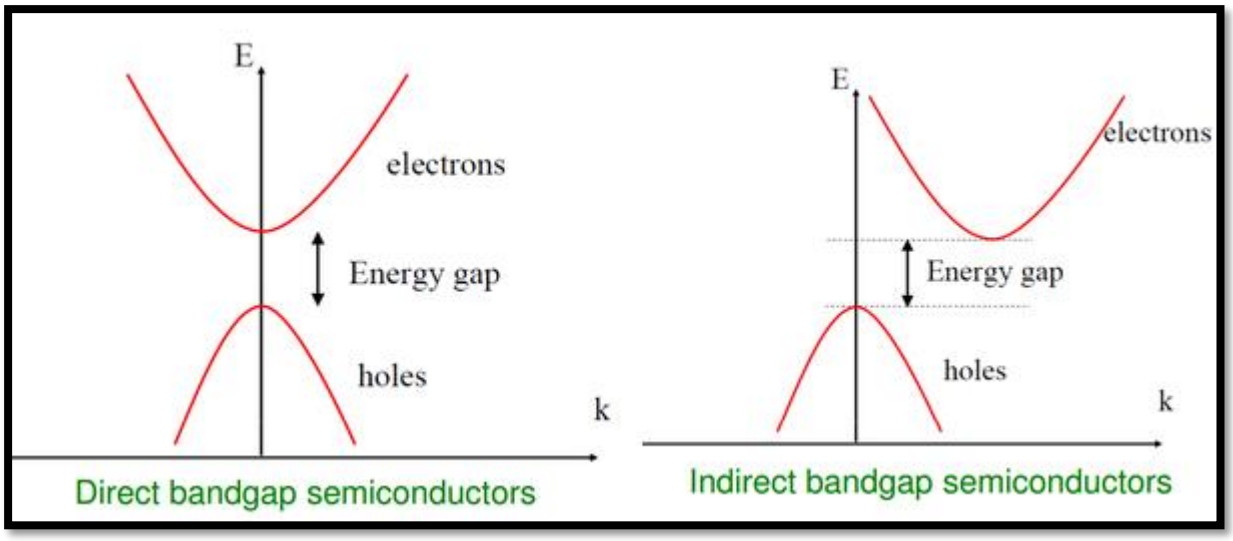

Figure II.2: Schematic band structure of a direct and indirect semiconductor

The band structure of silicon has been the subject of several studies which have enabled the know with great precision. The conduction band minimum of silicon is in the direction [010] and therefore, by symmetry, also in the directions [0 10], [001], [00 1], [100], [100] i.e. a total of six minima [5].

On the contrary, for germanium, the minimum of the conduction band takes place in the directions corresponding to the diagonals of the cube, so we are in the presence of 8 minimum [2]

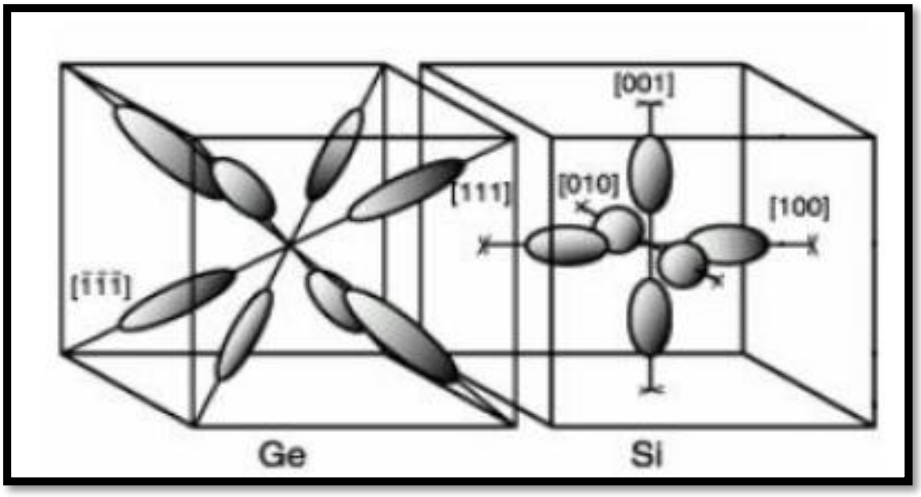

Figure II.3: Representation of SC conduction band minima

II.3 The different states of silicon

Silicon exists in different forms:

- In multicrystalline and monocrystalline form for massive layers
- In amorphous and polycrystalline form for thin layers.

These different forms are distinguished by the thickness of the layer but also by the size of the grains. We will briefly describe their mode of production and indicate their effectiveness in the photovoltaic conversion in particular [6].

II.3.1 Layers massive

Monocrystalline silicon is the material with the best electronic properties thanks to its great purity and its structure composed of a single grain. It is produced using the process Czochralski or by zone fusion purification. These processes are carried out at very high temperature, in the liquid phase. At the end of the process, the product is in the form of ingots of monocrystalline pure silicon. These ingots are then cut into wafers of 300 µm thick. This thickness is necessary to ensure mechanical stability. The step of cutting results in a significant loss of material, up to 50%. In addition to the method process, these losses make the material very expensive [7].

Multicrystalline silicon is made from the residue from silicon manufacturing monocrystalline. The crystallization process consists of the recasting of these residues

followed by a unidirectional resolidification in the form of a coarse-grained multicrystalline columnar structure, whose size is between 1 mm and 10 cm. It also comes in the form of an ingot, which requires a step of cutting into thin plates. Despite its lower purity compared to monocrystalline silicon, this material is the most used in the photovoltaic industry thanks to its advantageous cost and its efficiency which is not the least (up to 15,16% efficiency for a multicrystalline silicon based module versus 19.20% for a monocrystalline silicon module). Figure II.4 shows the market share of different technologies in the industry photovoltaic. We can notice that multicrystalline silicon alone occupies 43.4% of the shares. It is closely followed by monocrystalline silicon with 42.4% of the shares [7].

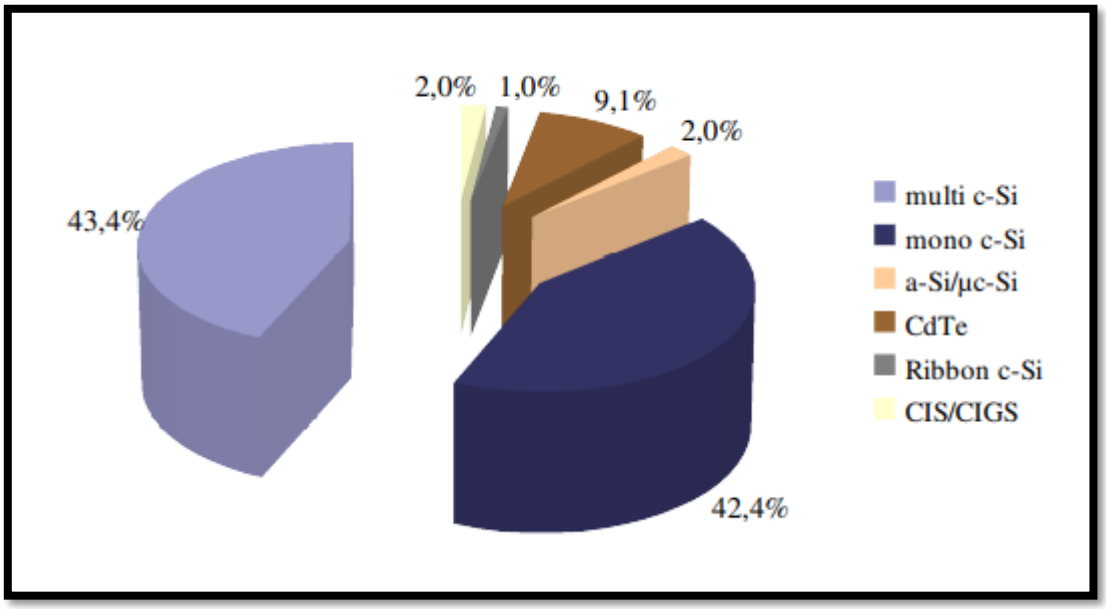

Figure II.4: Share of different technologies in the photovoltaic market in 2010 [7].

The silicon ribbon technique is another technology that involves the production of fine multicrystalline silicon wafers (<200 µm) from a flexible carbon ribbon passing through a bath of molten silicon. The silicon crystallizes along the carbon ribbon by adhesion. The carbon located between the crystallized silicon wafers is eliminated by burning under oxygen [8]. This technique makes it possible to dispense with the manufacture of ingots and of the cutting step that leads to a great loss of material. However, it only represents 1% production due to low purity, lower crystal quality, and low production speed. Nevertheless, the optimum conversion efficiency is between 1516% [5].

For the sake of reducing silicon production costs, various solutions have been proposed and studied such as the reduction in the thickness of the silicon layers. Indeed, in the

massive film solar cell technology (monocrystalline, multicrystalline and ribbon in silicon), half of the production cost is due to the manufacture of the ingots and the cutting into platelets. However, a minimum thickness of 200 µm is necessary to avoid a embrittlement that can lead to cracks [8].

Table II.1: Efficiency of marketed solar modules. Performance measures are based on standard conditions. [9]

Technology	Thin films					Crystalline Silicon		Concentration PV[1]
	a-Si	CdTe	CI(G)S	a-Si/µcSi	Dye solar cells	Mono	Multi	Multi-Junction
Cell efficiency	4-8 %	10-11 %	7-12 %	7-9%	2-4%	16-22 %	14--18 %	30-38 %
Module Efficiency						13-19 %	11--15 %	~25 %
Area needed per KW (for modules)	~15 m^2	~10 m^2	~10 m^2	~12 m^2		~7 m^2	~8 m^2	

Furthermore, the reduction in the thickness of the silicon is not without consequence on the photovoltaic conversion since the absorption coefficient of the silicon is extremely low as we will see later. Great thicknesses are therefore necessary for a total absorption of the light spectrum, including in the infrared. A reduction in the thickness of monocrystalline or multicrystalline silicon is limited, hence the alternative thin layers of amorphous and polycrystalline silicon on substrate [8].

II.3.2 Silicon-based thin films

The idea of thin layers involves manufacturing very thin silicon films (a few tens of nanometers to a few microns thick) on an appropriate substrate using chemical or physical methods. This technology offers a number of important benefits, including the ability to reduce the amount of raw materials required by up to 100 times, the use of inexpensive large-area substrates (glass, metal, and plastic), and authorization from the procedures for generating the materials. In fact, the ability to deposit on surfaces as large as 1 m^2 makes this

technology particularly intriguing for use in photovoltaics and the production of flat screens. For the latter specifically, a decrease in thickness is intended to restrict the volume recombination's of the charge carriers at thickness values comparable to the minority carriers' diffusion length. The Both polycrystalline and amorphous thin silicon films can be deposited [10].

Indeed, the hydrogenated amorphous silicon absorbs visible light 50 times more than monocristalline silicone that favors the reduction of its thickness to a few microns for solar applications [9]. Its production is restricted to less than 5% of the global module market share solar despite its significantly lower cost than crystalline technologies. Its low performance conversion rate, from 4 to 8%, is in fact its main limitation. This limitation is due to a very low electron mobility (<1 $cm^2 .V^{-1}.s^{-1}$) and the difficulty of achieving effective doping of the because of its disordered structure [11].

II.4 Optoelectronic properties of crystalline silicon

In this part, we present the generalities on the optoelectronic properties of the monocrystalline silicon then those of polycrystalline silicon; the aim is to recall the consequences of the presence of crystallographic defects (grain boundaries, twins, dislocations) and chemicals (hydrogen, oxygen) on the electrical properties of crystalline silicon[12].

II.4.1 Monocrystalline silicon

The crystallographic structure of monocrystalline silicon (Fig II.5) is a cubic structure diamond in which two face-centered cubic lattices interpenetrate. Each atom of a of the networks is surrounded by 4 close neighbors equidistant from the other network forming a tetrahedron [12]. The bonds between the atoms are of the covalent type with an interatomic distance of 2.35 Å and a mesh parameter a=5.43 Å [13]. The forbidden band (gap), separating the band valence of the conduction band is equal to Eg=1.12 eV at room temperature. It corresponds to an indirect gap since the minimum of the conduction band is located at a point other than the maximum of the valence band in the Brillouin zone. Figure II.6 represents the distribution energy levels of monocrystalline silicon and illustrates the indirect gap.

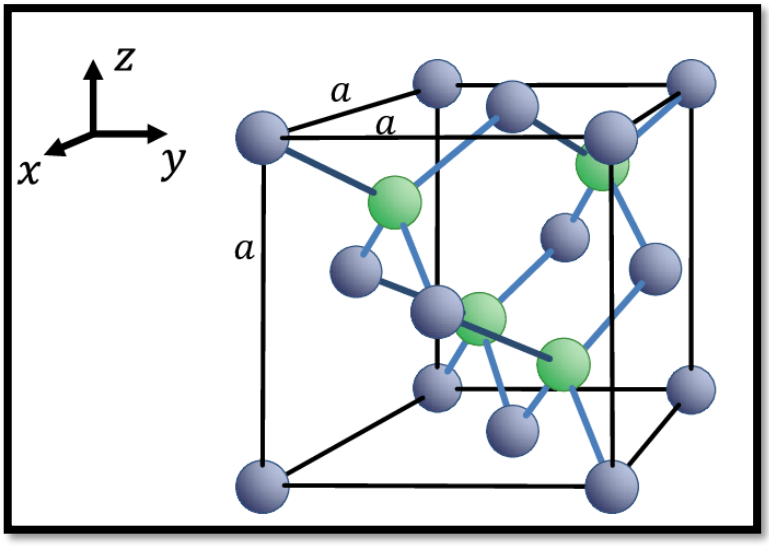

Figure II.5: Crystallographic structure of silicon monocrystalline (diamond type) [13]

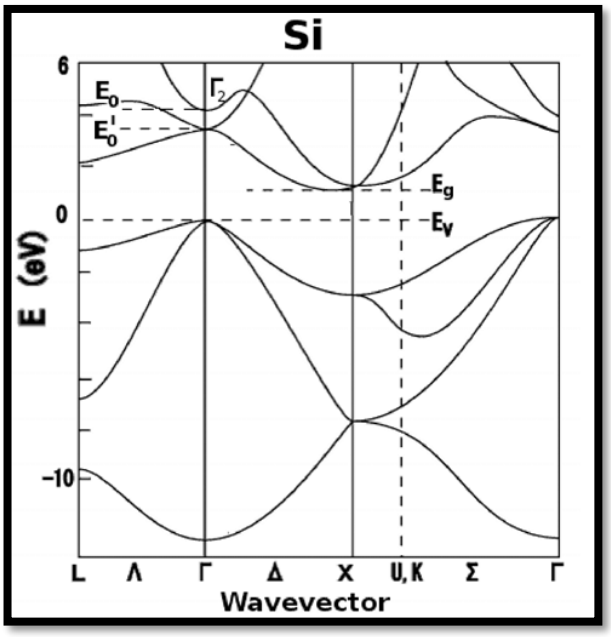

Figure II.6: Silicon band structure Monocrystalline. [13]

Figure II.7 shows the variation of the optical properties of monocrystalline silicon, namely the reflection coefficient R and the absorption coefficient in α as a function of the wavelength, measured at room temperature [14]. The spectrum of the reflection coefficient reveals 2 peaks located around λ =275 nm and λ =365 nm, characteristic of monocrystalline silicon. These peaks are associated respectively with the long-range and short-range order in the structure crystalline. The absorption coefficient is low in the infrared because of the low energies of excitement. The absorption length for which 63% of the light beam is absorbed in the material is 100 μm for photons of wavelength λ =2 μm. However, it takes very low values

at low wavelengths, down to 10 nm in the ultraviolet. In particular, we can be noted that at the wavelength 808 nm, the reflection coefficient of monocrystalline Si is 0.35 and the absorption coefficient is approximately equal to $7x10^3$ cm^{-1} **[12].**

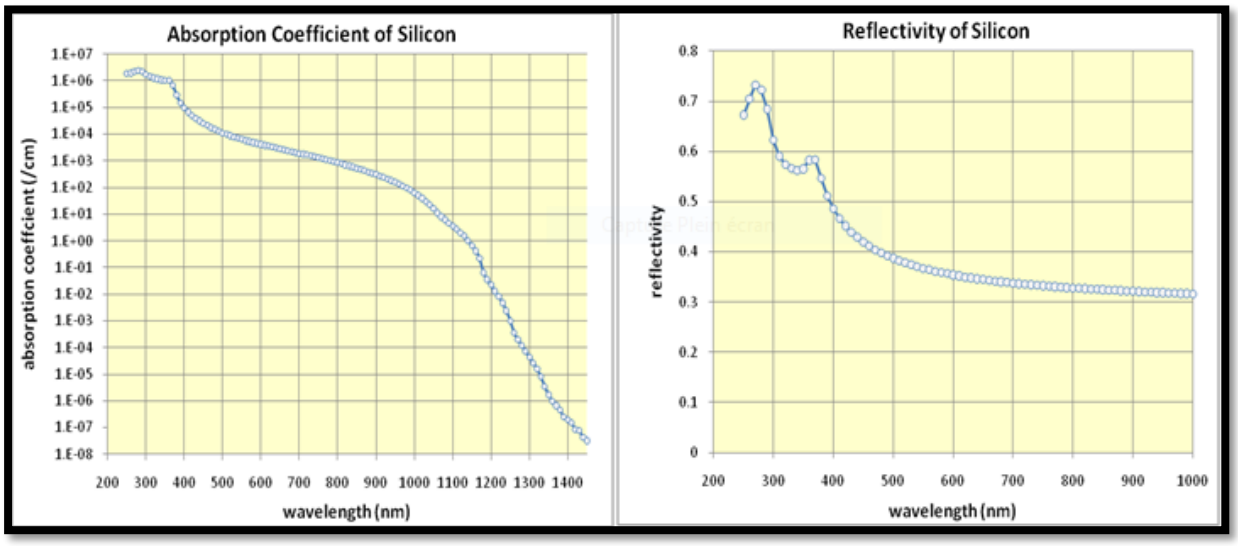

Figure II.7: Reflection coefficient R and absorption of monocrystalline silicon α um as a function of length of wav [12].

II.4.2 Polycrystalline silicon

Polycrystalline silicon has a structure that falls between between amorphous and monocrystalline silicon. Depending on the conditions of manufacturing, it is made up of grains with sizes ranging from a few hundred nanometers to a few millimeters that are divided from one another by grain boundaries. Disordered zones, frequently compared to amorphous silicon, are created by the grain boundaries separating grains with different orientations. Similar to that of amorphous silicon, Figure II.8 depicts the density of states in the forbidden band of polycrystalline silicon **[14]**.

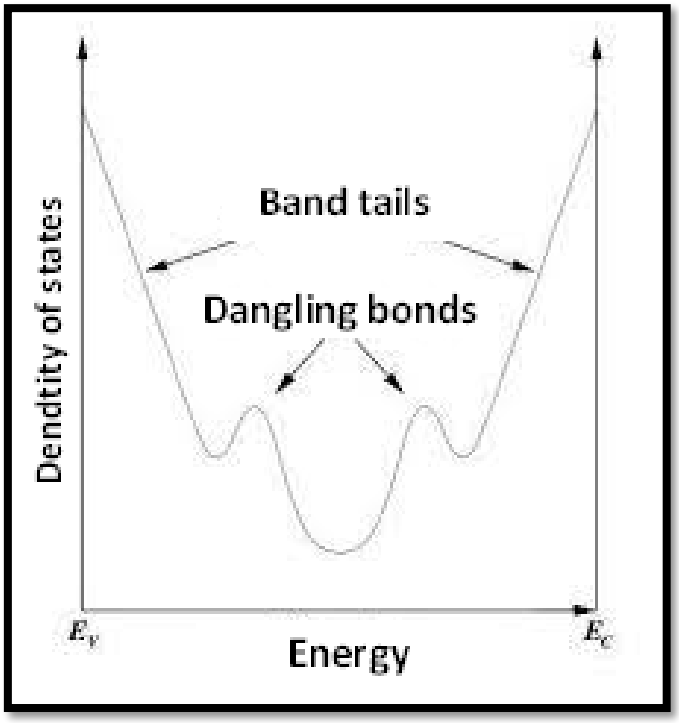

Figure II.8: Density of states in logarithmic scale in the forbidden band of polycrystalline silicon in presence of defects (EV: valence band, EC: conduction band) [14].

A dispersion of electronic states results from disorder brought on by grain boundaries and bond deformation between silicon atoms. This causes localized states to manifest as strip tails at the level of the conduction and valence bands in the forbidden band. In the center of the gap, dangling bonds (unsatisfied bonds) introduce two states electronics [15].

Several sizes of grains are possible. The density of the intragranular flaws, such as dislocations, subjoints, and twin joints, determines the crystalline quality of the material. The silicon band structure can be altered when these flaws are present. Contrarily, compared to monocrystalline silicon, polycrystalline silicon layers are less pure. The diffusion length of minority carriers in applications like photovoltaics is constrained by contaminants like oxygen, carbon, and metal transitions that can be inserted into the layer during the production of silicon polycrystalline. The layer may purposefully contain additional contaminants for doping or defect passivation [13].

The density of states can vary depending on the number of faults in the layer, but it will always resemble that shown in figure II.8 because grain boundaries are inevitable in polysilicon[16].

II.5 .Some properties of silicon

Due to its multiple applications, silicon is one of the materials with the most better known. Even the behavior of most impurities in silicon has been the subject of numerous publications. Current research efforts focus more on impurity-impurity, impurity-defect interaction in silicon and passivation of these imperfections [17].

Table II.2: Some properties of silicon.

Mass Volumetric at 300K	Mass Volumetric at 1687K	Gain in density liquid-solid	Conductivity thermal at 300K	Temperature fusion	gap at 300k
2.32 g/cm^3	2.51 g/cm^3	+9.1%	1.5w.cm^{-1} k $^{-1}$	1687k	1.12ev

II.6 Fabrication Techniques for Silicon Modules

There are various phases in the typical manufacturing process for solar systems. The crystalline silicon industry is covered by the following justifications. In 2011, crystalline silicon technology still accounted for 88% of the solar industry. The document "Photovoltaic systems: manufacturing and environmental effect" goes into further depth on each of these phases [18].

STEP 1: Refining the Silicon

In 2019, 160,000 tonnes of polycrystalline silicon were produced, with the solar sector receiving 83% of that amount (source US Geological Survey). (Warning: the term polycrystalline is commonly abused to talk about multicrystalline modules, however polycrystalline silicon only comes into play at the beginning and subsequently is changed into monocrystalline or multicrystalline silicon). The solar sector generated 10 GWp of photovoltaic panels made of crystalline silicon based on a demand of 18 t/MWp. The process of refining that results in the acquisition of this substance may be divided into two primary stages [19]:

- The transformation of quartz into metallurgical grade silicon or MG-Si.

It is done in an arc furnace, a common piece of equipment in the metallurgical sector. Around 98 to 99% of MG-Si is pure.

- converting silicon metal to solar grade silicon, also known as SoG-Si, which has a purity of 99.9999%.

It is produced by the Siemens process, inherited from electronics and uses chemical reactors to synthesize polycrystalline silicon or poly-Si. Of the entire photovoltaic module production chain, this stage consumes the most energy. Due to the cost of this step and the fact that a lower purity can be tolerated, techniques for producing solar silicon from new chemical but also metallurgical processes, the Elkem process in particular, are being explored [20].

STEP 2: Crystallization of the Silicon and Shaping Of the Plates

At this stage and until the manufacture of the module, know-how specific to the photovoltaic industry is brought into play.

The silicon will be purified again, uniformly doped and cut into slabs once cooled. The crystallization technique consists of gradually solidifying the molten polysilicon in a controlled manner. It is in the molten silicon charge that the doping element will be added, generally boron that gives p-type doping. The material ultimately presents a crystal lattice, which is an ordered arrangement of silicon atoms. The removal of impurities is done by segregation. More soluble in the liquid phase than in the solid phase, the impurities will migrate towards the zones which solidify last. In the case of bottom cooling, they will concentrate on the top of the ingot [21].

For crystallization, three main routes are possible, depending on the technological choice made by the manufacturer.

- The Czochralski pull, to produce cylindrical ingots of single-crystal silicon (sc-Si).

Monocrystalline silicon is obtained by growing or stretching a cylindrical ingot from a "stem" single crystal using the Czochralski or CZ process. The final cells of monocrystalline silicon have one of the best yields (15%), but for a greater energy expenditure at this stage [22].

- Directional solidification gives bricks of multicrystalline silicon (mc-Si).

Multicrystalline silicon is obtained by casting in an ingot mold in which slow cooling takes place, of the order of a few tens of hours. Its development is less energy consuming, and the final yield of the cells is around 12%.

The sawing of the plates (mc-Si and sc-Si): The monocrystalline ingots and the multicrystalline bricks are after the first stage cut into slices by a wire saw, to a thickness of approximately 250 µm. The operation is carried out in the presence of slurry, an organic solution containing abrasives in suspension. It should be noted that there is a significant loss of material during sawing (30 to 40% non-recycled). On the diagrams, we notice that the corners of the monocrystalline silicon are rounded because the plate is cut from a cylindrical ingot [23].

- Ribbon pulling to give multicrystalline silicon in ribbon.

This last technological option combines the steps of crystallization and shaping of the silicon, and has the advantage of minimizing material loss. It is obtained by driving a silicon ribbon on a flat or tubular support from a molten silicon bath. It is a process almost abandoned in the industry in 2019.

STEP 3: Manufacturing the Cells

Once the plates have been cut, the cells are manufactured, which will make it possible to exploit the semiconductor properties of silicon and transform the light energy captured into electrical energy.

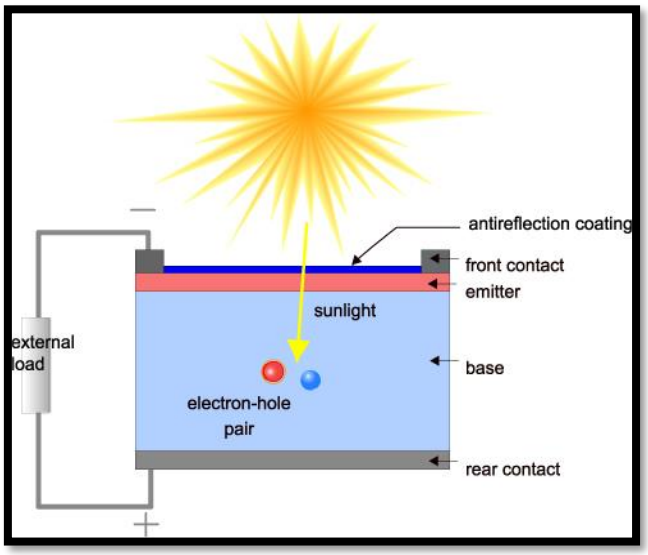

Figure II.9: photovoltaic Solar cell

The plate must be of the order of a hundred microns to absorb the incident photons. The rear face is p+ doped by aluminum diffusion and acts as an ohmic conductor with the rear electrode. The front zone is n+ doped. An anti-reflective layer is deposited on it [24].

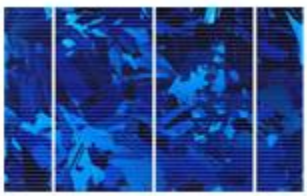

STEP 4: Assembling the Modules

The function of the modules is to protect the cells from the external environment and to facilitate their implementation, while limiting as much as possible optical losses and reductions in efficiency due to the heating of the cells in operation.

1. The cells are first connected in several chains to form a final matrix.
2. The matrix is encapsulated by hot rolling: the laminates are brought up to temperature and pressed under vacuum. The EVA film placed between the glass (front side) or the tedlar (back side) and the cells ensures the cohesion of the whole [25].
3. Depending on the case, the module is framed. It is then equipped with a junction box allowing its electrical connection.
4. The modules are finally subjected to a test under calibrated artificial light in order to measure their actual electrical characteristics.

II.7 conclusion

Silicon solar cells are without a doubt the future of the solar panel industry with so many benefits. Because there are so many of these cells, they will not become outdated in the upcoming years. They are nevertheless more expensive than electrical systems while being more affordable than other cells. The main obstacle facing the solar sector is this additional expense. The makers are always seeking for a fix for this issue. If silicon solar cells can be manufactured more reasonably priced than they are currently, they will probably dominate the market.

Crystalline silicon (c-Si) cells are made from thin slices of silicon (wafers) that are 160-240 m thick and are cut from a single crystal or a block. The manufacturing procedure used to create silicon wafers determines the sort of crystalline cell that is created.

In the next chapter, we will study the role of the anti-reflective layer and explain how anti-reflective layers' optical features are used to reduce reflectivity at the surface of photovoltaic solar cells.

CHARTER III:

THE ANTI-REFLECTIVE LAYER

III.1. Introduction

The conversion of incident solar energy into electrical energy is optimal when the reflection of incident light at the surface of the cell is minimal, which causes losses in the efficiency of the cell, in order to reduce the losses by reflection, the surface of the cell must be covered by an antireflection layer. In this chapter, we will detail how the optical properties of anti-reflective layers are exploited to minimize the reflectivity at the surface of the solar cells photovoltaic.

III.2. Optical properties

Light is made up of photons when it passes from one medium to another, three phenomena are observed. [1]

- Part of the light is absorbed by the medium.
- Another part emerges from the middle, it is transmitted.
- A third part does not cross the interface and is reflected.

If I_0 is the initial light intensity: $I_0 = I_A + I_T + I_R$. This intensity is the energy received during time t by a unit area perpendicular to the direction of spread. It is expressed in W/m².

With:

I_A: absorbed light intensity.

I_T: transmitted light intensity.

I_R: reflected light intensity.

These three phenomena are also expressed in terms:

Absorptivity:

$$\mathbf{A} = \frac{IA}{I0} \qquad \textbf{(III.1)}$$

Transmissivity:

$$\mathbf{T} = \frac{IT}{I0} \qquad \textbf{(III.2)}$$

Of reflectivity:

$$\mathbf{R} = \frac{IR}{I0} \qquad \textbf{(III.3)}$$

These quantities are connected by A + T + R = 1.

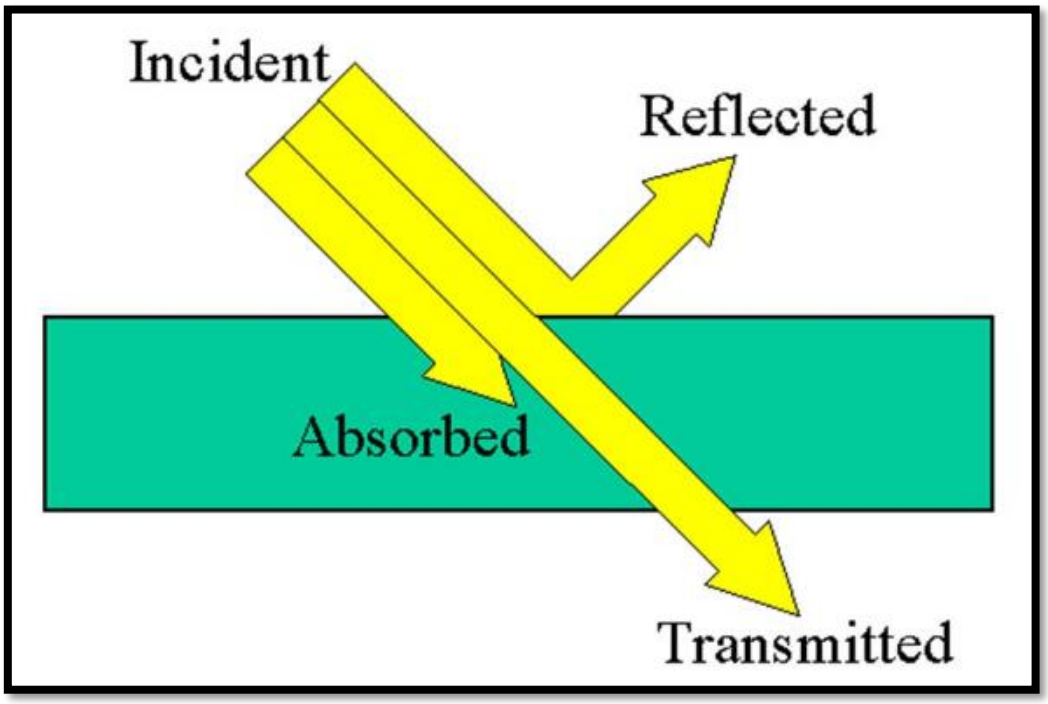

Figure III.1:Optical phenomena of the interaction of a light ray with a material medium.

III.2.1. Absorption

Absorption of light is an optical phenomenon in which the energy light or electromagnetic is absorbed by any substance [2].

III.2.2. The transmission

It is the ability to move energy from one point to another. We study it either through transmitted energy, or transmitted power. The notions of dissemination and diffraction are specific cases of transmission.

III.2.3. The reflection

When light reaches a new medium, part of it is refracted while the other part is returned to the first medium, this light is said to undergo a reflection [3].

III.3. Optical Constants

III.3.1. Path difference

In the presence of two different optical paths taken by two consecutive reflected rays, there is a path difference δ, which introduces a phase shift between these light rays [4].

The path difference δ is given by:

$\delta = n(IJ+JK) - IH$ **(III.4)**

The parameters IJ, JK, IH are determined below:

$$IJ = JK = \frac{d}{\cos\beta} \quad \textbf{(III.5)}$$

$$IH = IK \sin\theta \text{ et } IK = 2.d.\tan\beta \quad \textbf{(III.6)}$$

$$\Rightarrow IH = 2.d.\tan\beta.\sin\theta \quad \textbf{(III.7)}$$

$$\delta = \frac{2nd}{\cos\beta}\left[1 - \frac{\sin\beta.\sin\theta}{n}\right] \quad \textbf{(III.8)}$$

The law of Snell-Descartes $n_1 \sin\theta = n_2 \sin\beta$, authorizes us to write:

$$\sin\theta = n\sin\beta \Rightarrow \sin\beta = \frac{\sin\theta}{n} \quad \textbf{(III.9)}$$

This allows us to write:

$$\delta = \frac{2nd}{\cos\beta}[1 - \sin^2\beta] = \frac{2nd}{\cos\beta}\cos^2\beta \quad \textbf{(III.10)}$$

SO:

$$\delta = 2nd\cos\beta \quad \textbf{(III.11)}$$

III.3.2. Phase shift

Any path difference has the effect of generating a phase shift ϕ, which is expressed in the general case by [5]:

$$\varphi = \omega t \qquad \text{With} \qquad \omega = \frac{2\pi}{T} \quad \textbf{(III.12)}$$

Where T represents the period of the signal.

To cover a distance identified by the difference in rate δ, the wave moving at speed v must have a time equal to:

$$t = \frac{\delta}{v} \quad \textbf{(III.13)}$$

In the case of an electromagnetic wave, the speed v is identified with the speed of light c, so it follows:

$$\varphi = \omega t = \frac{2\pi}{T}.\frac{\delta}{c} \quad \text{or} \quad \lambda = cT \Rightarrow \varphi = \frac{2\pi\pi}{\lambda}.\delta \quad \textbf{(III.14)}$$

III.3.3. Refractive index

Any medium can be described by the complex optical index ñ, in the general case: [2]

$$\tilde{n} = n + ik \quad \textbf{(III.15)}$$

The real part n is the refractive index.

$$n(\lambda) = \left(\frac{1+R(\lambda)}{1-R(\lambda)}\right) - \sqrt{\frac{4R(\lambda)}{(1-R(\lambda))^2 - K^2}} \quad \textbf{(III.16)}$$

And the imaginary part K is the extinction coefficient given by:

$$K = \frac{\alpha\lambda}{4\pi} \quad \textbf{(III.17)}$$

Or:

λ: Wavelength.

A: Reflectivity

The following table summarizes the refractive indices of a few media:

Table III.1: refractive indices of some media

Media	Refraction index
The void	1.0000
The air	1.0008
The water	1.3300
The diamond	2.4600

III.3.4. Absorption coefficient α

- **Lambert-Bouguer Law:**

The intensity I of the radiation decreases when the light beam passes through a material medium. The intensity follows the Lambert-Bouguer law, whose expression is: [2]

$$I = I_0 . e^{-\alpha r} \quad \textbf{(III.18)}$$

α: is the absorption coefficient of the medium.

On the other hand, we also know that the luminous intensity is proportional to the square of the module of the electric field E, that is:

$$I \propto E^2{}_0 . e^{-2\omega \frac{k}{c}\vec{r}} \quad \textbf{(III.19)}$$

By comparing the expressions of the intensities, we obtain:

$$\alpha = 2\omega . \frac{k}{r} = 2 . \frac{2\pi}{T} . \frac{k}{c} \Rightarrow \alpha = \frac{4\pi k}{\lambda} \quad \textbf{(III.20)}$$

The medium is all the more transparent as the absorption coefficient α is small.

In a homogeneous and isotropic conductive medium (necessarily absorbent), and taking into account Ohm's law (J=σE), Maxwell's equations are written in this case:

$$\overrightarrow{rot}.\vec{E} = -\frac{\partial \vec{B}}{\partial t} \quad \textbf{(III.21)}$$

$$\overrightarrow{\mathrm{rot}\vec{B}} = \mu_0.\sigma.\vec{E} + \varepsilon.\mu_0.\frac{\partial \vec{E}}{\partial t} \quad \textbf{(III.22)}$$

$\mathrm{div}(\vec{E}) = 0$ (generally neutral environment). **(III.23)**

$$\mathrm{div}(\vec{B}) = 0 \quad \textbf{(III.24)}$$

Given the equality: $\overrightarrow{\mathrm{rot}}(\overrightarrow{\mathrm{rot}}.\vec{E}) = \overrightarrow{\mathrm{grad}}(\mathrm{div}\vec{E}) - \Delta\vec{E}$,one will have:

$$\overrightarrow{\mathrm{rot}}(\overrightarrow{\mathrm{rot}}\vec{E}) = \overrightarrow{\mathrm{rot}}\left(-\frac{\partial \vec{B}}{\partial t}\right) = -\frac{\partial \overrightarrow{E^2}}{\partial \overrightarrow{r^2}} \quad \textbf{(III.25)}$$

$$\Rightarrow -\frac{\partial \overrightarrow{\mathrm{rot}}\vec{B}}{\partial \vec{t}} = -\frac{\partial^2 \vec{E}}{\partial \overrightarrow{r^2}} \Rightarrow -\varepsilon\mu_0.\frac{\partial^2 \vec{E}}{\partial \overrightarrow{t^2}} - \mu_0\delta\frac{\partial \vec{E}}{\partial \vec{t}} = \frac{\partial^2 \mathrm{E}}{\partial \overrightarrow{r^2}} \quad \textbf{(III.26)}$$

That is $$:\frac{\partial^2 \vec{E}}{\partial \vec{t}^2} + \frac{\delta}{\varepsilon}.\frac{\partial \vec{E}}{\partial \vec{t}} = \frac{1}{\mu_0.\varepsilon}.\frac{\partial^2 \vec{E}}{\partial \overrightarrow{r^2}} \quad \textbf{(III.27)}$$

By replacing $\overrightarrow{E} = \overrightarrow{E_0}.e^{-i\omega(t-\frac{\vec{r}}{v})}$ in the previous equation, it follows:

$$-\omega^2.\vec{E} + \frac{\delta}{\varepsilon}(-i\omega).\vec{E} = -\frac{1}{\mu_0\varepsilon}.\frac{\omega^2}{v^2}\vec{E} \quad \textbf{(III.28)}$$

$$\omega + i\frac{\delta}{\varepsilon} = \frac{\omega}{\varepsilon_r}.\frac{\widetilde{n^2}}{\mu_0.\varepsilon_0.c^2} = \frac{\omega}{\varepsilon_r}(n + i\mathcal{k})^2 = \frac{\omega}{\varepsilon_r}[(n^2 - \mathcal{k}^2) + 2in\mathcal{k}] \quad \textbf{(III.29)}$$

It therefore follows:

$$\varepsilon_1 = \varepsilon_r = (n^2 - \mathcal{k}^2) \quad \textbf{(III.30)}$$

$$\varepsilon_2 = 2n\mathcal{k} = \frac{\sigma}{\varepsilon_0.\omega} \quad \textbf{(III.31)}$$

Solving this system in n and k leads to the following results:

$$n = \sqrt{\left(\frac{\sqrt{\varepsilon_1^2+\varepsilon_2^2}+\varepsilon_1}{2}\right)} \quad \textbf{(III.32)}$$

$$\mathcal{k} = \sqrt{\left(\frac{\sqrt{\varepsilon_1^2+\varepsilon_2^2}-\varepsilon_1}{2}\right)} \quad \textbf{(III.33)}$$

III.4. Thin film optics

T= a thin layer is generally obtained on a physical support called a substrate. The inevitable existence of this support and the presence of a thin layer seriously complicates the optical study of such a system. We then witness the appearance of a phenomenon of multiple reflections of the incident rays, which often give rise to an interference phenomenon. It should be noted that such results are never observed during studies of massive materials.

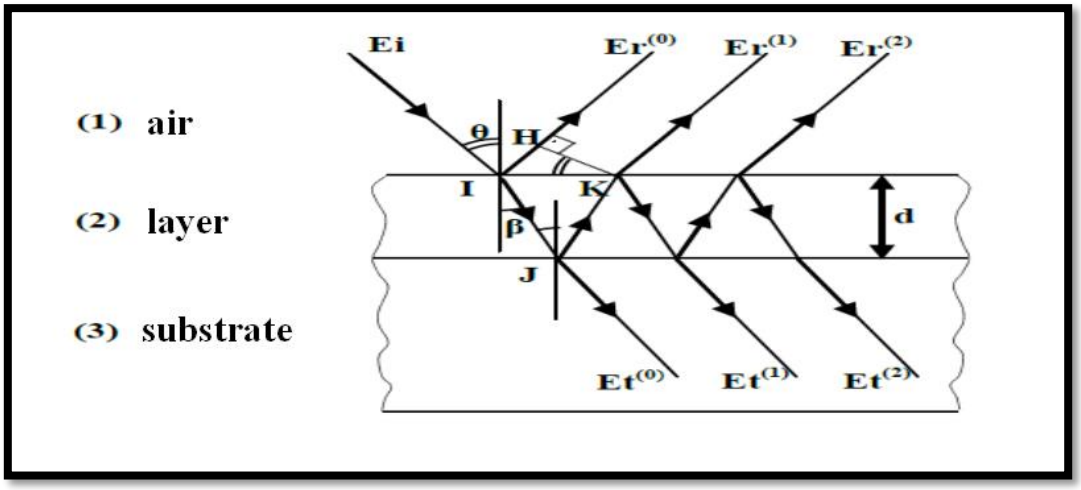

Figure III.2: phenomenon of multiple reflections in a thin layer. [6]

The calculation of the transmission and reflection coefficient of the system will be done in two steps:

Considering the optical path taken by each of the rays, we note the existence of a constant path difference between two consecutive rays.

- The first step will consist in determining this path difference due to the presence of the thin layer.
- The second step, the calculation of the reflection coefficient will be undertaken taking into account the contribution of all the reflected rays.

III.4.1. Reflection in thin layers

III.4.1.1. Reflection coefficient

The study of figure III.2 allows us to arrive at the following equations: [7]

$$E_r^{(0)} = r_{12}.E_i \quad \textbf{(III.34)}$$

$$E_r^{(1)} = t_{12}.t_{21}.r_{23}..e^{-2j\varphi}.E_i \quad \textbf{(III.35)}$$

$$E_r^{(2)} = t_{12}.t_{21}.r_{21}.r_{23}^2.e^{-4j\varphi}.E_i \quad \textbf{(III.36)}$$

The reflection coefficient r, result of the contribution of all the reflected fields is therefore evaluated at:

$$r = \frac{E_r^{(0)}+E_r^{(1)}+E_r^{(3)}+\cdots.}{E_i} \quad \textbf{(III.37)}$$

$$r = r_{12} + t_{12}.t_{21}.r_{23}.e^{-2j\varphi} + t_{12}.t_{21}.r_{21}.r_{23}^2.e^{4j\varphi} + \cdots \quad \textbf{(III.38)}$$

$$r = r_{12} + t_{12}.t_{21}.r_{23}e^{-2j\varphi}\left[1 + r_{12}r_{23}.e^{-2j\varphi} + r_{21}^2.r_{23}^2.e^{-4j\varphi} \ldots\right] \quad \textbf{(III.39)}$$

$$r = r_{12} + \frac{t_{12}.t_{21}.r_{23}.e^{-2j\varphi}}{1-r_{21}.r_{23}.e^{-2j\varphi}}\ldots\ldots \quad \textbf{(III.40)}$$

Taking into account the following equalities:

$$r_{12} = \frac{\tilde{n}_1 - \tilde{n}_2}{\tilde{n}_1 + \tilde{n}_2} \quad \textbf{(III.41)}$$

$$t_{12} = \frac{2\tilde{n}_1}{\tilde{n}_1 + \tilde{n}_2} \quad \textbf{(III.42)}$$

It is easy to establish the relations:

$$r_{12} = -r_{21} \quad \textbf{(III.43)}$$

$$r_{12}^2 + t_{12}.t_{21} = 1 \quad \textbf{(III.44)}$$

The reflection coefficient becomes:

$$\boxed{r = \frac{r_{12} + r_{23}.e^{-2j\varphi}}{1 + r_{12}.r_{23}.e^{-2j\varphi}}} \quad \textbf{(III.45)}$$

III.4.1.2. Reflectivity

The reflectivity is identified with the square of the modulus of the reflection coefficient that has to say [8]:

$$R = r.r^* = |r|^2 \quad \textbf{(III.46)}$$

On the other hand, if we also consider the absorption of light, which takes place in the layer of thickness d, the reflection coefficient determined previously and given by the relation (III.45) becomes:

$$r = \frac{r_{12} + r_{23}.e^{-2j\varphi}.e^{2(-\frac{\alpha}{2}.d)}}{1 + r_{12}.r_{23}.e^{-2j\varphi}.e^{2(-\frac{\alpha}{2}d)}} = \frac{r_{12} + r_{23}.e^{-2j\varphi}.e^{-\alpha.d}}{1 + r_{12}.r_{23}.e^{-2j\varphi}.e^{-\alpha d}} \quad \textbf{(III.47)}$$

Writing the reflectivity coefficients r_{12} and r_{23} respectively as:

$$r_{12} = \rho_{12}.e^{-j\theta_{12}} \quad \textbf{(III.48)}$$

$$r_{23} = \rho_{23}.e^{-j\theta_{23}} \quad \textbf{(III.49)}$$

The reflectivity coefficient r becomes:

$$r = \frac{\rho_{12}.e^{j\theta_{12}} + \rho_{23}.e^{j(\theta_{23} - 2\varphi)}.e^{-\alpha d}}{1 + \rho_{12}.\rho_{23}.e^{j(\theta_{12} - \theta_{23} - 2\varphi)}.e^{-\alpha d}} \quad \textbf{(III.50)}$$

The reflectivity is obtained by calculating $R=|r|^2$, and then we get:

$$R = |r|^2 = \frac{\rho_{12}^2 + \rho_{23}^2.e^{-2\alpha d} + 2.\rho_{12}.\rho_{23}.e^{-\alpha d}.\cos(\theta_{12} + \theta_{23} - 2\varphi)}{1 + \rho_{12}^2.\rho_{23}^2.e^{-2\alpha d} + 2\rho_{12}.\rho_{23}.e^{-\alpha d}.\cos(\theta_{12} + \theta_{23} - 2\varphi)} \quad \textbf{(III.51)}$$

- **Determination of parameters ρ_{ij} and θ_{ij} :**

Knowing the expression of the complex refractive index $\tilde{n} = n + i\mathcal{k}$ and that of the reflection coefficient $r = \rho_{ij}.e^{j\theta_{ij}}$, one can easily determine the parameters mentioned above. In general, in a plane interface, we know that the reflection coefficient is given by:

$$r_{ij} = \frac{\tilde{n}_i - \tilde{n}_j}{\tilde{n}_i + \tilde{n}_j} = \frac{(n_i - n_j) + i(\mathcal{k}_i - \mathcal{k}_j)}{(n_i + n_i) + i(\mathcal{k}_i + \mathcal{k}_j)} \quad \textbf{(III.52)}$$

It therefore follows that:

$$\rho_{ij} = \sqrt{\frac{(n_i - n_j)^2 + (k_i - k_j)^2}{(n_i + n_j)^2 + (k_i - k_j)^2}} \quad \textbf{(III.53)}$$

$$\theta_{ij} = arc\tan\frac{(n_i + n_j).(k_i - k_j) - (n_i - n_j).(k_i + k_j)}{(n_i + n_i).(n_i - n_j) + (k_i + k_j)(k_i - k_j)} \quad \textbf{(III.54)}$$

III.5. Special case of an anti-reflective layer

Now considering the case where an antireflection layer of refractive index (n_2) is inserted between the air medium of index (n_1) and the substrate of index n_3 under an incidence normal, the reflected amplitude is given by equation (III.45) [9]

With a path difference after two crossings of the layer until the reflection of the incident wave.

$\delta = 2\,\phi$ **(III.55)**

With:

$\phi = \omega.t = 2\pi.\ f.t = 2\pi.(c/\lambda).t = 2\pi.t.(v/\lambda).n2 = 2\pi(d/\lambda).n2$ **(III.56)**

$$r_{12} = \frac{n_1 - n_2}{n_1 + n_2} \quad \textbf{(III.57)}$$

And:

$$r_{23} = \frac{n_2 - n_3}{n_2 + n_3} \quad \textbf{(III.58)}$$

As r_{12}, r_{23} are the individual reflection amplitudes at the air-layer interface antireflection and antireflection layer –substrate (semiconductor) respectively, (d) is the geometric thickness of the layer and λ the wavelength expressed in the same units as (d).

For a path difference $\delta = \pi$ making it possible to cancel the reflection.

$\delta = 2.2\pi\ (d/\lambda).\ n2 = \pi$ **(III.59)**

We thus find that the thickness "d" of this antireflection layer:

$$d = (\lambda/4).n2 \quad \textbf{(III.60)}$$

This value is called the quarter wave thickness.

The antireflection layer can therefore be seen as a quarter-wave plate, which goes to eliminate the reflection for a given wavelength. For apps photovoltaic, the refractive index and the thickness of the antireflection layer are chosen to minimize reflection at a chosen wavelength.

III.6. The anti-reflective layer for photovoltaic PV applications

III.6.1. Definition

It is an ideally transparent and thin layer deposited on the surface of the solar cell to reduce the intensity of the reflected light.

III.6.2. The principle of the Anti-reflection coating

In a solar cell, we seek to capture most of the useful photons of the solar spectrum, to increase the efficiency of the photovoltaic conversion. So he need to optimize the absorption of the solar flux while reducing the optical losses by reflection, the deposition of an anti-reflective layer on the surface of the wafer makes it possible to reduce the reflectivity of the sun's rays.

Anti-reflective layers are generally deposited by vacuum evaporation, sputtering, chemical vapor deposition screen-printing or by other chemical techniques such as pyrolysis spray**.**

III.6.3. Characteristics of Anti-Reflective Layer

By taking the case of an ARL on silicon. Knowing that the refractive indices of different elements (air, anti-reflective layer, silicon) are respectively n_0, n_1, n_2. We can show that the anti-reflective coating is obtained if the following two conditions are fulfilled:

1. n0<n1<n2 **(III.61)**
2. The thickness of the antireflection layer is given by:

$$n_0 d = \frac{\lambda_0}{4} + \frac{k\lambda_0}{2} \quad \textbf{(III.62)}$$

Based on these two conditions we can have a minimum reflectivity R, which is given by the following relationship:

$$R_{min} = \frac{(n^2{}_1 - n^2{}_2)}{(n^2{}_1 + n^2{}_2)} \quad \textbf{(III.63)}$$

III.7. Some materials used as Anti-reflection coating

There are many materials in the oxide form that can be used as an anti-reflective layer such as vanadium oxide V_2O_5, zinc oxide ZnO, tin oxide, tantalum oxide Ta_2O_5, etc. In this part, we will cite some properties of some oxides. In this, our choice is focused on SnO_2 as a layer antireflection, the properties of this material will be given in more detail in the chapter following.

III.7.1. Vanadium oxide (V_2O_5)

Vanadium has a complex chemistry. In minerals, its oxidation state can be +2, +3, +4 or +5. For solutions in water, V^{3+} and V^{4+} are rapidly oxidized to the +5 degree, constituting the most stable form of vanadium **[10].**

III.7.1.a. Electrical properties

It is a degenerate n-type semiconductor. The electrical conductivity of vanadium oxide vanadium oxide results from the vacant oxygen or existing bonds of the vanadium atoms and is of the order of vanadium atoms, it is of the order of $6.10^{-4}\Omega^{-1}$ cm^{-1}**.**

III.7.1.b. Optical properties

Vanadium oxide has indirect and direct optical gaps of the order of 2eV and 3.3 eV. Its refractive index and its absorption coefficient vary according to the conditions of elaboration.

III.7.2. Properties of ZnO

Zinc oxide is a wide gap semiconductor, it is transparent in the visible and near infrared **[8, 9]**. It has a set of properties that can be mentioned: its high thermal conductivity, high heat capacity, medium dielectric constant, and high resistivity, researchers around the world have been attracted, in the past and in the present, by all these interesting properties of ZnO.

III.7.2.a. Crystal structure

Zinc oxide is known in three crystallographic forms: the cubic form (Rocksalt), the blende form, and the hexagonal form (Würtzite) **[10, 11]**. The most thermodynamically stable is the compact hexagonal structure, called zincite, with a Würtzite-like structure, shown in Figure (III.3), with the following lattice parameters: a = 3.25 Å c = 5.12 Å. The zinc and oxygen atoms are located in the special Wyckoff positions 2b of the space group P63mc.

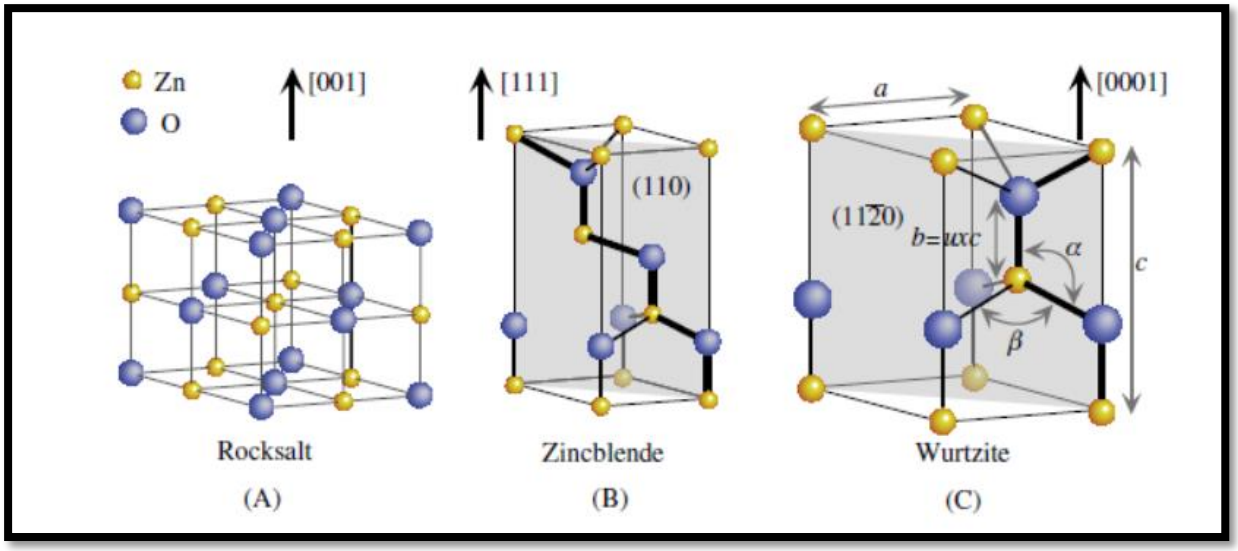

Figure III.3: Schematic representation of the different crystal structures of ZnO

III.7.2.b. Optical properties

Zinc oxide is a transparent material whose refractive index is close to 2 when the material is in the solid form [12]. When it is in the form of thin layers, its refractive index and absorption coefficient vary depending on the processing conditions (ex: by the 'IRASCVD: InfraRed Assisted Spray Chemical Vapor Deposition' method and by the 'USCVD: Ultrasonic Spray Chemical Vapor Deposition' method the absorption coefficient is equal to 10^{+4} cm^{-1}[13]). The refractive index has a value that varies between 1.70 and 2.20 depending on the author [14, 15]. Doped zinc oxide belongs to the class of transparent conductive oxides (TCO). With very little doping, it can be used in luminescence.

III.7.2.c. Electrical properties

Zinc oxide is an n-type semiconductor of group II-VI which has a band gap of about 3.3 eV [16, 17], which makes it possible to classify it among the wide bandgap semiconductors. This band gap value can vary according to the mode of preparation and the doping rate, between 3.2 eV and 3.39 eV [18, 19, 20, and 12]. It is possible to widely modify the properties of zinc oxide by doping:

- Either by deviating from the ZnO stoichiometry, mainly by introducing excess zinc atoms in interstitial position, or by creating oxygen vacancies (the created centers then behave as electron donors) [21, 12].
- Or by substituting zinc or oxygen atoms in the lattice with foreign atoms of different valence (group III element: F, Cl). It is interesting to note here that doping ZnO with aluminum decreases the concentration of Zn in the interstitial position, thereby

reducing the rate of oxidation of Zn [14]. This phenomenon may be of great importance since it would significantly reduce oxygen adsorption, which has been one of the main causes of limitation in the use of ZnO as a transparent conductor.

In practice, n-type conductivity is easily obtained by doping. The doping rates obtained can be very high (of the order of 10^{20} atoms/cm^3), allowing to reach very low resistivities (of the order of 10^{-4} Ω.cm [13]) (see. Table (III.2)).

High n-type conductivity (> 5.103 $Ω^{-1}.cm^{-1}$) is possible in ZnO, due to intrinsic defects, group III and VII dopants (Al, In, Ga, B, F) or in combination.

Table III.2: Resistivity, free carrier concentration, percent dopant of ZnO thin films with different types of impurities .

Dopant	Dopant percentage (%)	Resistivity(10^{-4}Ω.cm)	Concetration of free carriers($10^{20}cm^{-3}$)
Al	1.6-3.2	1.3	15.0
Ga	1.7-6.1	1.2	14.5
B	4.6	2.0	5.4
Y	2.2	7.9	5.8
In	1.2	8.1	3.9
Sc	2.5	3.1	6.7
Si	8.0	4.8	8.8
Ge	1.6	7.4	8.8
Ti	2.0	5.6	6.2
Zr	5.4	5.2	5.5
Hf	4.1	5.5	3.5
F	0.5	4.0	5.0

Regarding its electrical properties, many studies have been carried out on the ZnO crystal and its fabrication methods. In general, the various thin film vapor deposition processes result in polycrystalline layers that is layers composed of grains that can be oriented along various crystallographic directions [9, 12, 22, and 23]. This aspect is very important in particular for understanding the behavior of the mobility (μ) of charge carriers, which are electrons in the case of ZnO. The mobility (μ) is a determining factor for the electrical conduction of *TCO*. Indeed, the higher the mobility (μ), the higher the conductivity (σ) of

TCO. The mobility (μ) is influenced by the phenomenon of diffusion of free charge carriers in the material. The greater this phenomenon, the lower the mobility (μ) will be. Charge carrier diffusion is mainly due to three factors [22]:

1. The presence of ionized or neutral impurities: the more impurities the ZnO layer has (such as boron atoms or interstitial zinc atoms), the more they cause the diffusion of charge carriers. The study of the importance of this diffusion according to the different types of impurities is very complex and subject to many discussions and theories.
2. The presence of grain boundaries in the material: this type of diffusion only occurs in polycrystalline materials. Grain boundaries represent potential barriers that the electrons must cross. The more grain boundaries there are, the more the electrons are slowed down, and thus the more their mobility is reduced.
3. The presence of optical or acoustic phonons: the various vibrations of the ZnO atomic lattice can cause the scattering of electrons and thus decrease their mobility.

The p-type conductivity can be obtained with difficulty. This is achieved by doping ZnO with group I (Li, Na, K, Cu, Ag) and group V (N, P...) elements [13].

Numerous studies have shown that adequate heat treatment after the growth of ZnO crystals (high temperature annealing) can significantly change the electrical properties of the crystals. For example it has been noticed that for ZnO crystals with high resistivity and high concentration of charge carriers [23, 24, 25, 26], can change under air or oxygen treatment and gives crystals with low resistivity [27, 28].

III.7.3. Applications of ZnO

Zinc oxide and through these properties, it has been used in a large number of applications such as varistors used in large voltage interruptions (polycrystalline ceramic electronic devices with non-linear current-voltage characteristics). It can also find applications in optoelectronics, electroluminescence, as a chemical sensor in thin films [9, 17].

It also has very interesting electromechanical properties, which allows it to be used, on a large scale, as a transparent conductor in acoustic devices and in microwave delay lines or as a piezoelectric material [18].

For photo catalytic applications, ZnO has a conduction band that is mainly composed by the Zn: 4s and 4p orbitals. This can affect the rate of transfer of photo-generated electrons from the valence band to the conduction band under irradiation. For this reason, the electron mobility in single crystal ZnO is much higher [28].

In the field of photovoltaic, most solar cells are currently made from silicon. In this application, zinc oxide can be used as a transparent electrode on the top "front contact" layer to allow electric current to flow through the component while allowing light to pass through [16].

III.8. Properties and applications of SnO_2 films

There are two types of tin oxide:

- **Tin monoxide or stannous oxide (SnO)** unstable in air, brown-black in color, insoluble in water, soluble in strong acids and bases. The SnO decomposes on heating. It is used as a reducing agent and as a chemical intermediate [29].
- **Tin dioxide or stannic oxide (SnO_2)** which is found in the natural state as the mineral cassiterite. Cassiterite is an oxide of variable color, ranging from yellowish to black, it has been known and exploited since ancient times. Her name (from the Greek kassiteros, pewter) given to it by the French mineralogist Beudant in 1832. However, cassiterite has been known for over 5000 years. It is characterized by an adamantine brilliance. It can be transparent or translucent. Of imperfect cleavage, it is hard and heavy. Tin oxide is relatively refractory and has an extremely high melting point (about 1600°C). It is resistant to attacks by mineral acids except concentrated sulfuric acid [30].

The latter will be the subject of our study and we will use the name "oxide tin" to designate it

III.8.1. Properties

Tin oxide is a wide bandgap n-type semiconductor. Tab III.3 summarizes some physical properties of this material:

Table III.3: Some physico-chemical properties of SnO_2 [30]

Property	Value
Molar Mass ($g.mol^{-1}$)	150.70
Specific density ($g.cm^{-3}$)	6.915
Melting point °C	1630
Boiling point °C	2330
Hardness (MOHS [2] Scale)	7.8

III.8.2. SnO_2 gap

The gap of tin oxide in thin layers varies between 3.6 and 4.2 eV. These variations are related to the techniques used for its elaboration. The oxide gap of tin is of the direct type. The extremes of the valence band and the band of conduction are on the same axis of vectors k (Fig III.4) (k is the wave vector in the Brillouin area). The transitions of electrons from the valence band to the conduction band are vertical [31].

III.8.3. Electronic structure of the band gap of SnO_2

The electronic band structures of oxygen and tin are:

O: [He] $2s^2 2p^4$ Sn: [Kr] $4d^{10} 5s^2 5p^2$

Sn^{4+} ions have 10 electrons in their outer d shell which is $4d^{10}$ and the inner layers are all filled. In these ions, the lowest energy level and completely empty is a level s and must presumably contribute to the bottom of the conduction band [32].

Due to the electric field of the crystal, the s-levels of non-equivalent cations separate in Γ^{1+} and Γ^{4+} but by considerations of symmetry and by measurements optics, it has already been assumed that in SnO_2 , the state Γ^{1+} is below the state Γ^{4+} (Fig III.4). In 1974, J. L. Jacquemin made a calculation using the KKR^3 method to specify the position of the minimum of the conduction band in the first zone of Brillouin and confirmed the work of Arai that he had already assumed in 1964 that this minimum was at k = 0. For the energy level at the top of the valence band several authors claim that the top of the valence band is due to level p of the ion O^{2-} since the layer $2p^6$ is full[32].

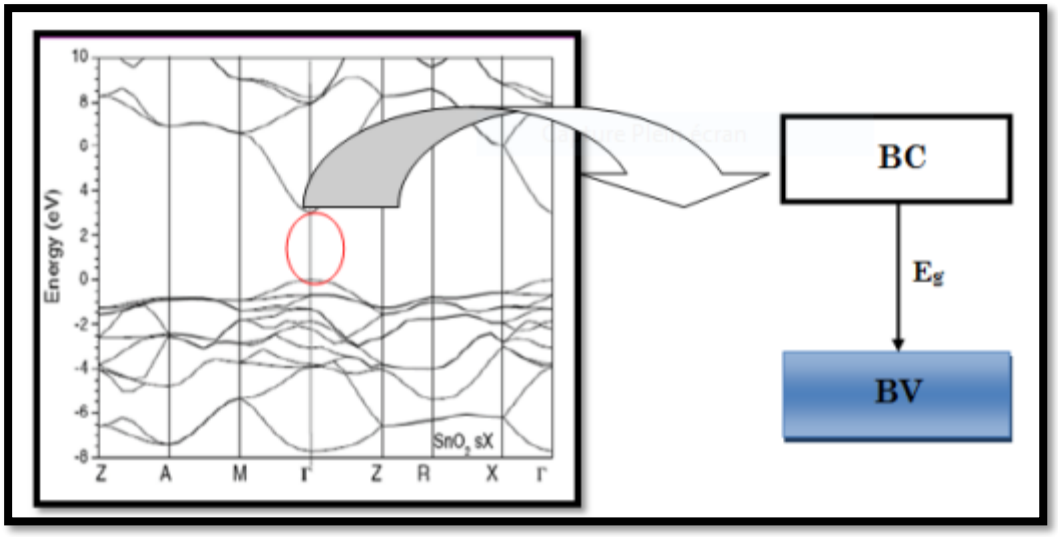

Figure III.4: Introduction to the Band Gap of Tin Oxide [32]

III.8.4. Crystallographic Structure

Tin oxide has a single stable phase at ambient pressure called cassiterite and adopts a quadratic lattice of the rutile type. Its space group is P4/mnm. The unit cell has parameters a = b = 0.475 nm and c = 0.318 nm and contains six atoms. Each Sn^{4+} tin ion is at the center of an octahedron almost regular formed by six oxygen ions, O^{2-}, while each O^{2-} is surrounded by three Sn^{4+} located at the vertices of an isosceles triangle**[33]** (Fig III.5).

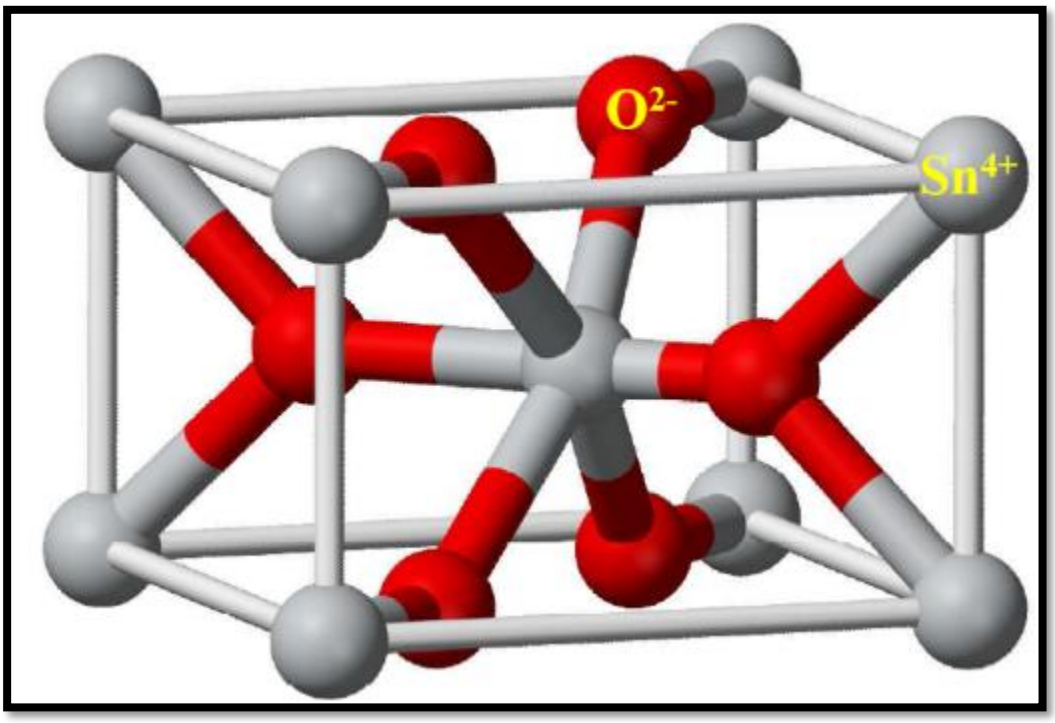

Figure III.5: Unit cell of SnO_2 (rutile structure)

The ionic radii of the Sn^{4+} cation and the O^{2-} anion are respectively 0.071 and 0.14 nm. Oxygen is in position 4f (space group P42/mnm) given by (1 − u; 1 − u; 0), (1/2 + u; 1/2 − u; 1/2) and (1/2 − u; 1/2 + u; 1/2) with u = 0.31. Tin occupies position 2a, (1/2; 1/2; 1/2) and (0; 0; 0).

III.8.5. Electrical structure

In its stoichiometric form, SnO_2 is an insulator, but in its oxygen-deficient form, tin oxide behaves like an n-type semiconductor with a gap of 3.6 eV (for the Spray Eg method = 3.9 eV). Gaps of oxygen formed by the transfer of an oxygen atom, from a normal site to the gaseous state, make it possible to obtain an n-type semiconductor. Indeed, the oxygen deficiency thus created has 2 electrons -it is then said to be neutral- that it can yield under the effect of the temperature. There is then single or double ionization of the latter. Electrons released can bind to Sn4+ tin atoms. They then become Sn^{2+} and behave as electron donors (Fig III.6) [34].

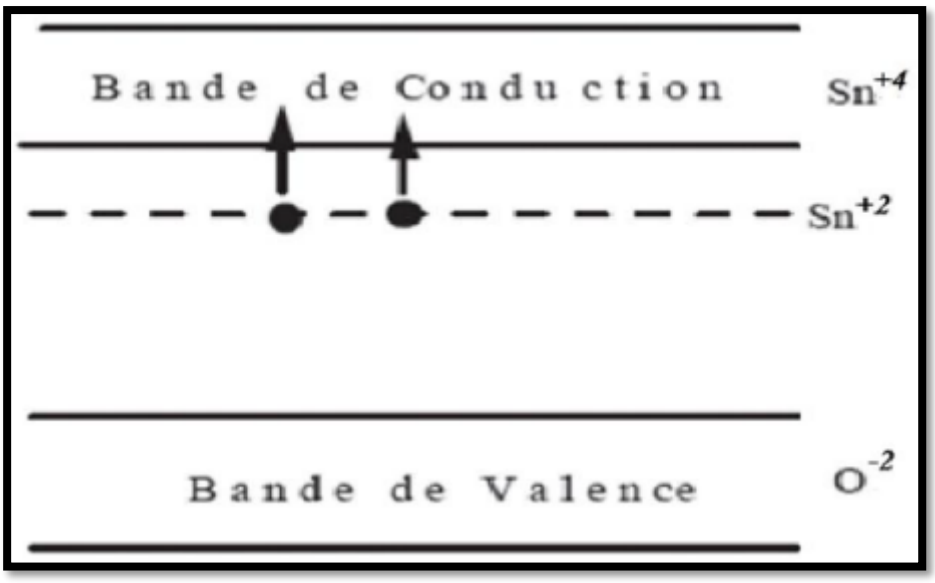

Figure III.6: Energy diagram of SnO_2

In the temperature range 200-1350°C, have been demonstrated in SnO_2, the existence of an oxygen deficit in relation to its stoichiometric composition. There vacancy density (defined by x in $SnO_{2^{-x}}$, strongly dependent on temperature and the partial pressure of oxygen which varies, in general, between 10^{-3} and 10^{-2}% atm. The concentration of electrons in pure SnO_2 is directly proportional to that of shortcomings. Moreover it can be shown that, if we

consider the oxygen vacancies doubly ionized as the majority defect, the electrical conductance is proportional to the partial pressure of oxygen and follows a law in

$(PO_2)^{-1/6}$[29]

III.8.6. Optical properties

The optical properties of SnO_2 depend on the interaction of electromagnetic waves with the electrons of the semiconductor. An electromagnetic wave interacting with this material will be completely absorbed by it if the associated energy $E = h\nu = hc/\lambda$ is able to transfer electrons from the valence band to the band conduction, that has to say. To be at least equal to the width of the forbidden band (gap) [30].

Thus, if one wants the material to be transparent in all the extent of the visible, the gap must be at least as wide as the largest of the energies associated with the frequencies of the visible spectrum (400 nm to 800 nm). A good transparency in the entire visible spectrum will therefore be ensured by a value of forbidden band at least equal to 3.1 eV. Therefore, in the form of a thin layer, the SnO_2 is a good transparent material in the visible optical range.

III.9. Photovoltaic applications

The principle of the solar cell lies in the conversion of photon energy into electric energy. If a photon arrives on the semiconductor material with energy less than the value of the optical gap, it will not be absorbed; the middle will then be transparent. If the energy of the photon is greater than or equal to the energy of gap (Eg), the photon will transmit its energy to an electron in the valence band with transfer to the conduction band.

Once the electrons are formed, it is necessary to separate the electrons and the holes formed in order to be able to drive the electrons towards the collecting electrodes. This separation is obtained by an electric field (permanent and indestructible) which is the more often generated by the junction of two semiconductors of different nature (heterojunction), by the potential barrier between a metal and a semiconductor or well by the interface between two semiconductors whose density of charge carriers is different [33].

In the case of metal oxides, solar cells consist of a layer conductive transparent oxide deposited on type-n or -p silicon. Silicon allows the conversion of photons into electrons and the metal oxide layers play the role of conductor of electrons towards the electrodes in order

to allow the collection and the transmission of the electrical signal created by the silicon (Fig III.7).

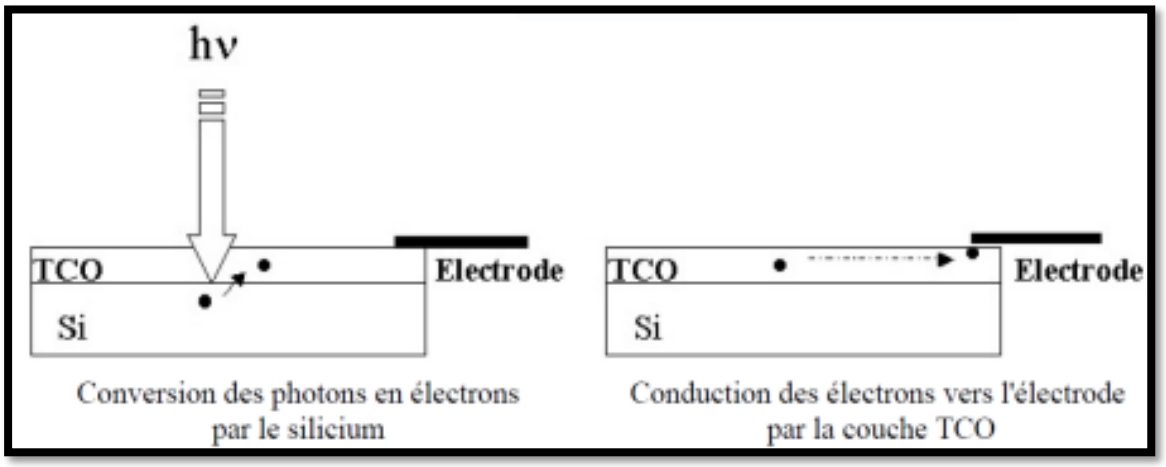

Figure III.7: Schematic diagram of an Si-TCO electrode

To be able to be used in this type of application, the layers must have very high optical transmission combined with the highest electrical conductivity possible: we will then speak of a TCO (Transparent Conductive Oxide) layer [34].

III.10. Conclusion

The role of the anti-reflection layer is very important; it is used to minimize the losses by reflection. The energy efficiency obtained for the homojunction cell (without window layer) we have briefly presented the properties of the dioxide of tin (SnO_2) and Properties of ZnO (optical, electrical….etc.) with the aim of its application in the field of photovoltaic cells.

Moreover, in the next chapter we will use the PC1D simulation software, which allows the calculation of the electrical and photovoltaic parameters of the solar cell.

CHARTER IV:

SIMULATION BY PC1D AND OPTIMIZATION

Chapter IV: Simulation By PC1D And Optimization

IV.1. Introduction

The efficiency of a photovoltaic solar cell is dependent on optimizing all the layers that make up the cell. This study focuses on finding the best parameters for the two cells being studied in regions with the highest yields. In the world of simulation and characterization of optoelectronic devices, including photovoltaic cells, there are many simulation environments and tools available such as Synopsys, Silvaco, Scaps, AMPS-1D, and PC1D. We chose to use the PC1D simulator, as it is simple, quick, and effective for straightforward structures. By using the current-voltage $\boldsymbol{I(V)}$ characteristics provided by PC1D, we can determine the values of the key factors that affect the cells such as the current $\boldsymbol{I_{cc}}$, voltage $\boldsymbol{V_{co}}$, efficiency η , and fill factor **FF**.

IV.2. Simulation Program PC1D

PC1D is a numerical simulation software, is widely utilized for simulating solar cells. Developed at the University of South Wales in Sydney, Australia, it enables simulation of photovoltaic structures based on semiconductors with one-dimensional axial symmetry.

The software contains library files with parameters for commonly used crystalline semiconductors in photovoltaic technology such as GaAs, a-Si, AlGaAs, Si, InP, and Ge. It also features files for solar spectrums, primarily AM0 and AM1.5 spectrums.

The main interface of PC1D is displayed as follows:

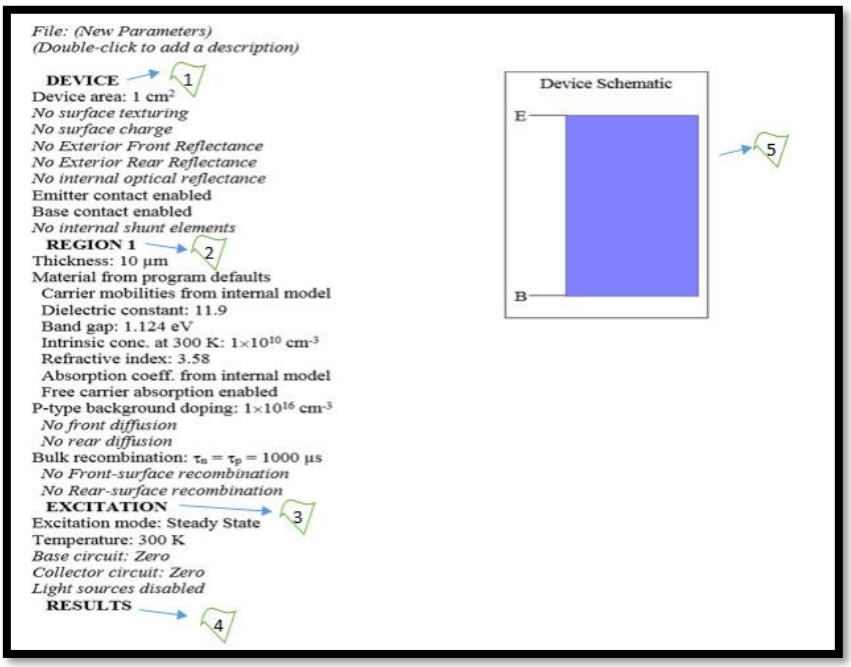

Figure IV.1: PC1D software window used in digital simulation [1]

➢ **Essentially, there are 5 key parts to this system:**

1. The "device" section contains general information about the device being simulated.

2. The "region" section includes critical information about the device region such as material type, thickness, doping type, etc. The system allows up to 5 regions to be added or removed, but must have at least one region.

3. The "excitement" section includes the parameters for exciting the device and determining its behavior, such as radiation and operating temperature for solar cells.

4. The "results" section displays the results of the simulation, including values for Icc, Voc, and the maximum power.

5. The "device schematic" section displays the visual representation of the device, which can be updated as soon as changes are made to the region parameters.

➢ **Pc1d has two ready files with standard parameters for simulating solar cells:**

1. The "one-sun.exc" file gives the following results:

- ✓ Short circuit current value.
- ✓ Open circuit voltage value.
- ✓ Maximum power value.

2. The "scan-qe.exc" file gives :

- ✓ The short circuit current value.
- ✓ The maximum power value.

The figure below shows the basic cell:

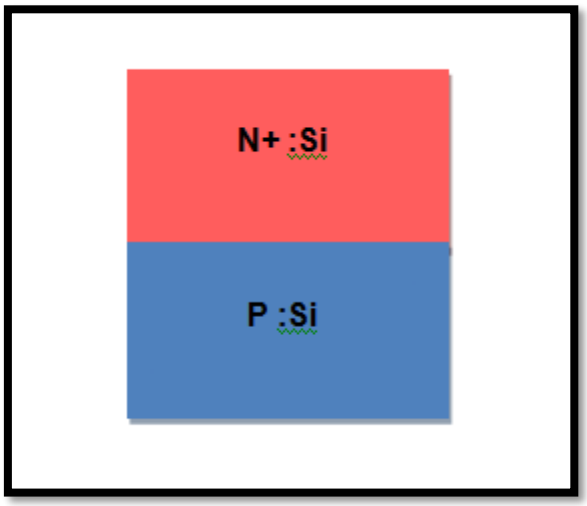

Figure IV.2: The basic cell

The figure shows the *I-V* curve of the basic characteristics:

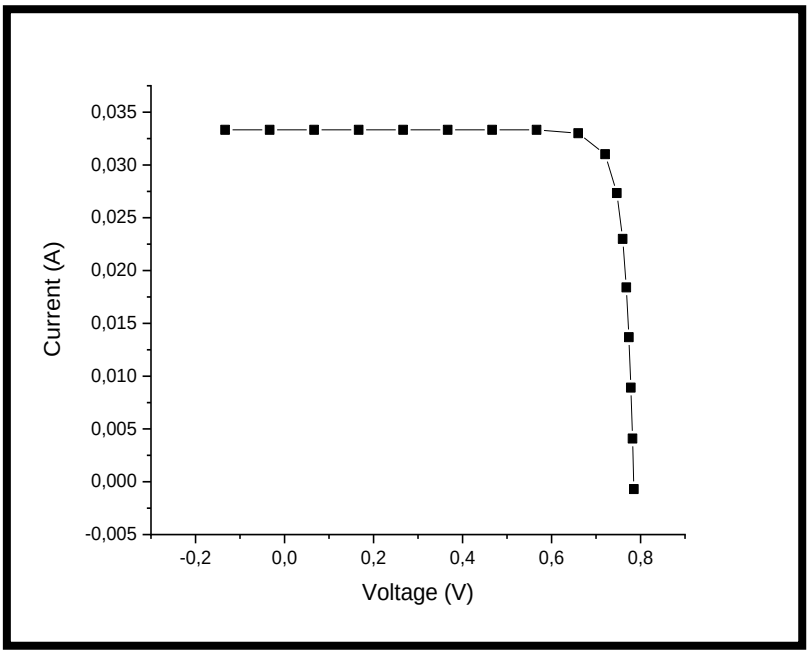

Figure IV.3: characteristic of the basic cell.

IV.3. Simulation results

Part one :

IV.3.1.Influence of the area surface on the characteristic I-V/Power

We took these parameters:

- **N-type background doping** : 10^{17} cm^{-3}
- **P-type background doping** :10^{15} cm^{-3}
- **Bulk recombination :** 3000µs

In addition, we changed the area latters as follow:

(a) Surface of 100cm².

(b) Surface of 120cm².

(c) Surface of 150cm².

(d) Surface of 200cm².

These next results were obtained from the simulated cell above:

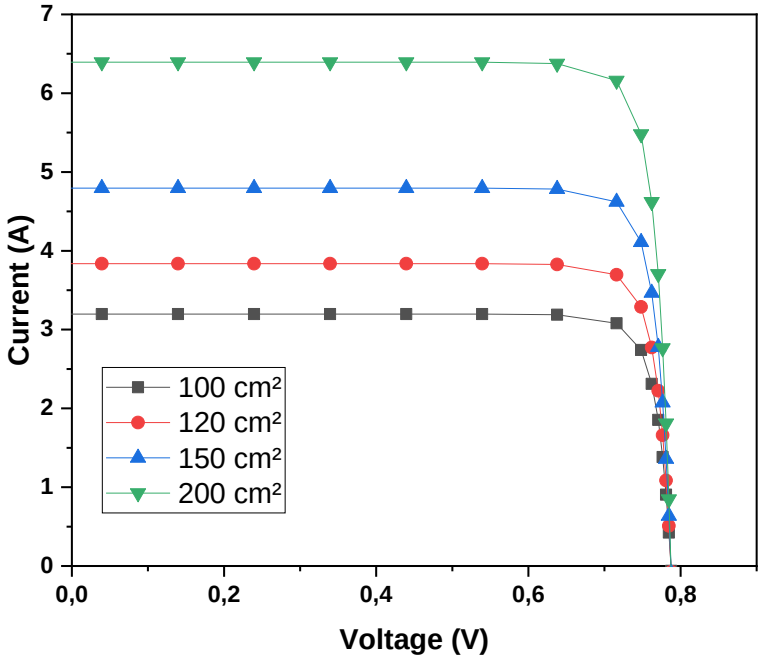

Figure IV.4: Influence of the area on the I-V characteristic

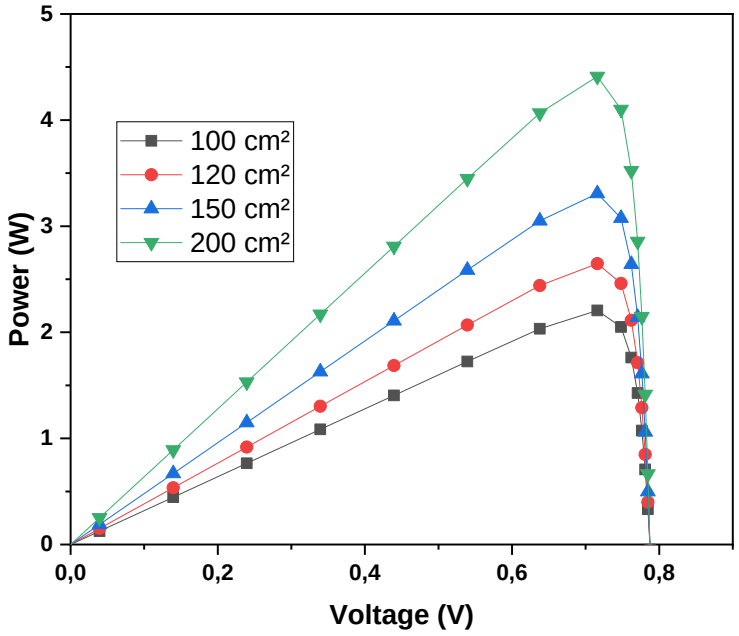

Figure IV.5: Influence of the area on the Power characteristic.

The P (V) curve demonstrates that the power output increases to a peak, and then decreases. The peak of the power curve represents the highest amount of power that the cell can produce.

➢ **Form Factor FF and Efficiency :**

The efficiency refers to the percentage of the incident solar energy that the module is able to convert into usable electrical energy, and it's also The ratio of the power generated by the cell, **P = V x I** , and the power of the incident solar radiation P_0.

The value of P_0 is 0.1W per cm² of cell surface area.

The form factor FF indicates how the shape of the I (V) curve affects the performance of the cell. A closer match to a rectangular shape results in a higher FF, which is closer to 1.

$$FF = \frac{P\max}{P1} = \frac{Vm \times \mathrm{Im}}{Vco \times Icc} \qquad \textbf{(IV.1)}$$

This leads to:

$$\eta = \frac{P\max}{P_0} \qquad \textbf{(IV.2)}$$

With:

Icc: Short-circuit current.

Vco: Short-circuit voltage.

Pmax: Max base power out.

FF: Form Factor.

η : Efficiency.

Table IV.1: Comparison of different area values

Device area (cm^2)	**100**	**120**	**150**	**200**
Icc (A)	-3.197	-3.837	-4.796	-6.395
Vco (V)	0.7874	0.7874	0.7874	0.7874
Pmax (W)	2.206	2.647	3.308	4.411
FF	0.8763	0.8761	0.8759	0.8759
η (%)	22.06	22.06	22.06	22.06

We started by investigating whether the size of the solar cell surface has any impact on the power it produces. When you vary the surface area of a solar cell, you are effectively changing the amount of sunlight that the cell can capture. Increasing the surface area of the solar cell allows it to capture more sunlight, which can lead to an increase in power output Table IV.1 and Fig IV.5. The larger the surface is, the higher the output power will be [1].

Our analysis of the I-V characteristics revealed that this increase in power is primarily due to a rise in the current value (influenced by the photo-current and in turn influenced by the amount of light received), as the surface expands, this is because the voltage does not change significantly with the change in surface size.

An increase in cell surface area can result in more electrons channels and transporters in the surface, leading to a reduction in the electrical resistance of the cell membrane and an increase in the electrical current (Table IV.2) Additionally, the increased surface area can also

result in a greater effective area for electrons transfer, which can further increase the flow of them.

The efficiency of a solar cell is determined by the ratio of the amount of electrical power output to the amount of sunlight that the solar cell receives. It depends on several factors, such as the bandgap energy of the semiconductor material, the efficiency of the electron-hole separation and collection, and the reflectivity of the cell surface.

When we increase the surface area of a solar cell, we are essentially increasing the amount of sunlight that the cell can absorb. This increase in sunlight leads to an increase in the number of electron-hole pairs that can be generated and, hence, an increase in the amount of electrical power output.

However, the efficiency of the solar cell remains the same because the additional power output is proportional to the additional sunlight that is being absorbed. Since the solar cell is converting the additional sunlight into electrical power at the same efficiency as before, the overall efficiency of the solar cell remains constant.

IV.3.2. Influence of the thickness of the n-region on the I-V characteristic/Power and efficiency

We took the next parameters:

- **N-type background doping** : $10^{17}cm^{-3}$
- **P-type background doping** :$10^{15}cm^{-3}$
- **Bulk recombination** : 3000 µs
- **Surface area** :200cm^2

And we changed the thickness as follow:

(a) Thickness of 7µm.

(b) Thicnkess of 14µm.

(c) Thickness of 21µm.

(d) Thickness of 30µm.

The following results were obtained from the previously simulated cell:

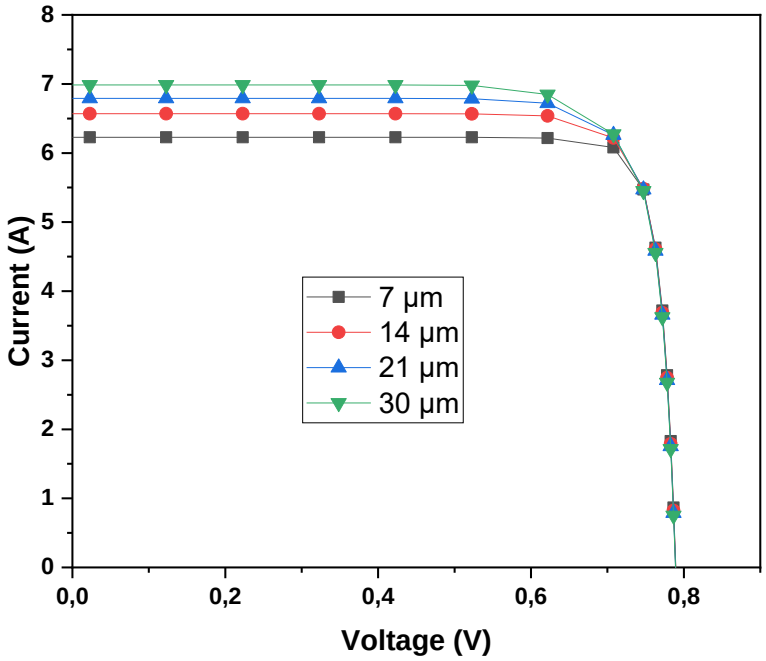

Figure IV.6: Influence of the thickness on the I-V characteristic .

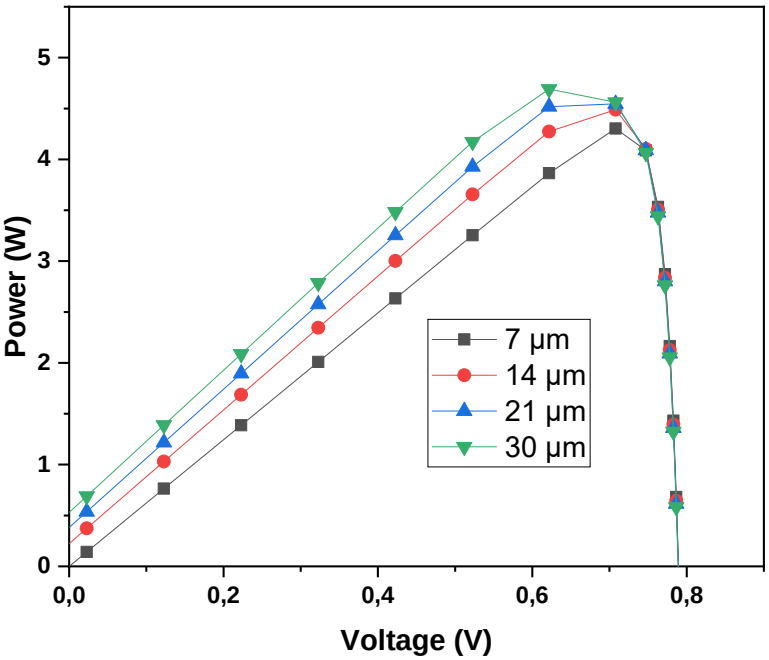

Figure IV.7: Influence of the thickness on the Power characteristic.

Table IV.3: Comparison of different thickness values

Thickness of the n-region	7	14	21	30
Icc (A)	-6.228	-6.569	-6.791	-6.986
Vco (V)	0.7894	0.7849	0.7812	0.7773
Pmax (W)	4.313	4.495	4.593	4.720
FF	0.8772	0.8717	0.8657	0.8692
η (%)	21.57	22.48	22.97	23.6

We played on the thickness of the n-region. Each time we increased the thickness of this region the power Fig (IV.7) and the current increased Fig (IV.6), which leads us to a higher efficiency Table (IV.2), and this suggest that the I-V characteristic is indicating a lower resistance to current flow.

This behavior can be explained by the reduction in the width of the depletion region, which is a result of the increased thickness of the n-type region. When the depletion region is narrower, the barrier potential is lower, making it easier for current to flow across the junction.

IV.3.3.Influence of the texturing on the characteristic I-V/Power and the efficiency

We took the next parameters:

- **N-type background doping :** $10^{17} cm^{-3}$
- **P-type background doping :** 10^{15} cm^{-3}
- **Bulk recombination :** 3000 µs
- **Surface area :** 200 cm^2.
- **Thickness :** 30 µm.

The results shown were obtained from the previously mentioned simulated cell above:

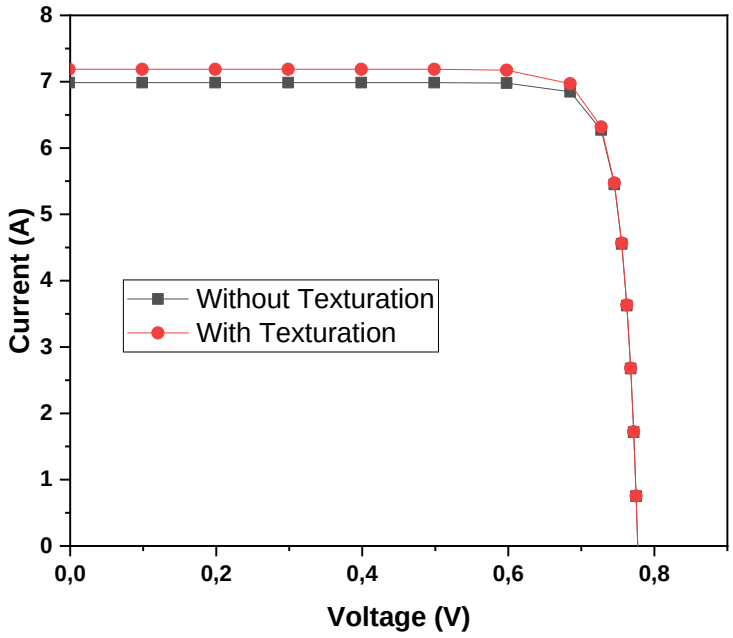

Figure IV.8: Influence of the characteristic I-V With and without texturing

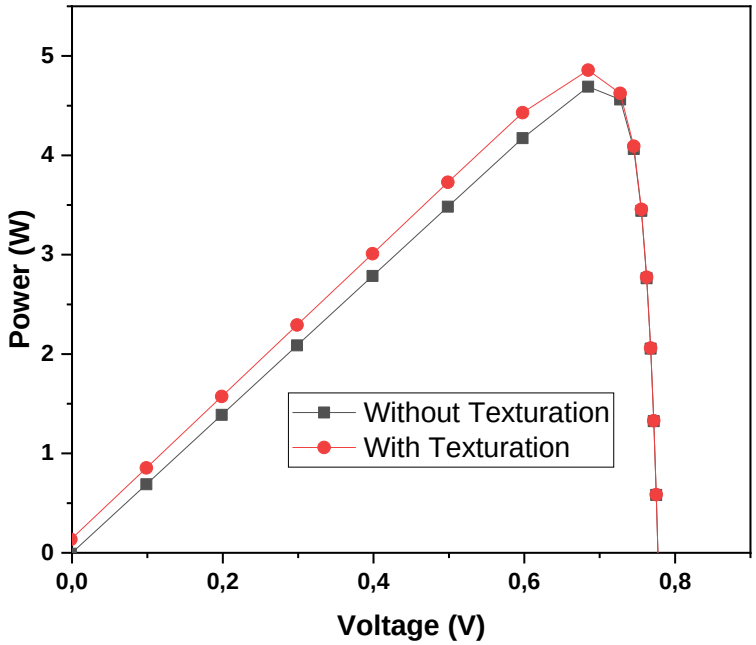

Figure IV.9: Influence of the characteristic Power with and without texturing

Table IV.4: Cell comparison with texturing and without texturing

Front surface	Without texturing	With texturing
Icc (A)	-6.986	-7.188
Vco (V)	0.7773	0.7776
Pmax (W)	4.720	4.865
FF	0.8692	0.8703
η (%)	23.6	24.33

The texturation of the device increased the current Fig) IV.8), the power Fig) IV.9) and the efficiency Table (IV.3), this suggests that the texturing process has improved the device's performance.

The increased current can be explained by the increased effective surface area of the junction, which allows for more carriers (electrons and holes) to contribute to the flow current and it can also explained by the reduction of the reflected radiation which caused current rising which leads to a better efficiency.

IV.3.4.The influence of the angle of texuring on the characteristic I-V/Power and Efficiency

The parameters taken are the same parameters above :

- **N-type background doping :** 10^{17} cm^{-3}
- **P-type background doping :** 10^{15} cm^{-3}
- **Bulk recombination :** 3000 µs
- **Surface area :** 200cm^2.
- **Thickness :** 30µm.

We made changes to the texturing angle as described below:

(a) Angle of 30°.
(b) Angle of 60°.
(c) Angle of 80°.
(d) Angle of 95°.

The parameters above gave us the next results:

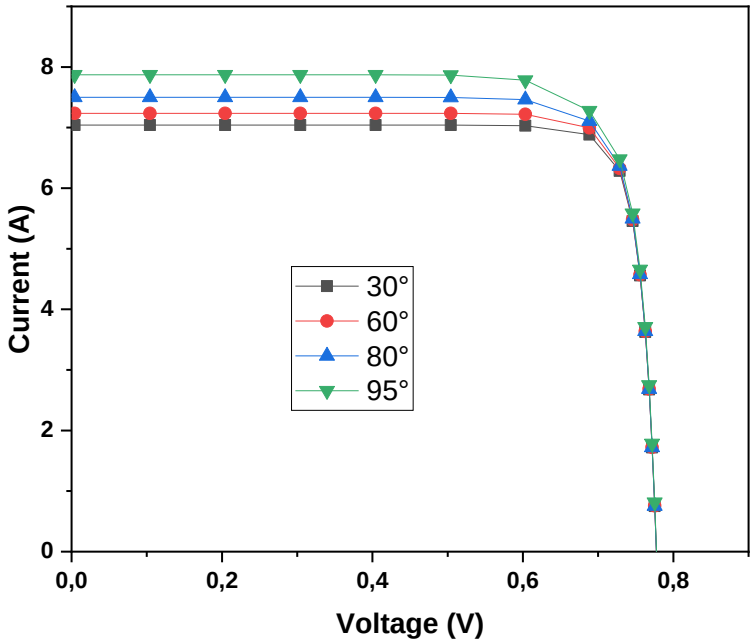

Figure IV.10: Influence of the texturing angle on the I-V characteristic .

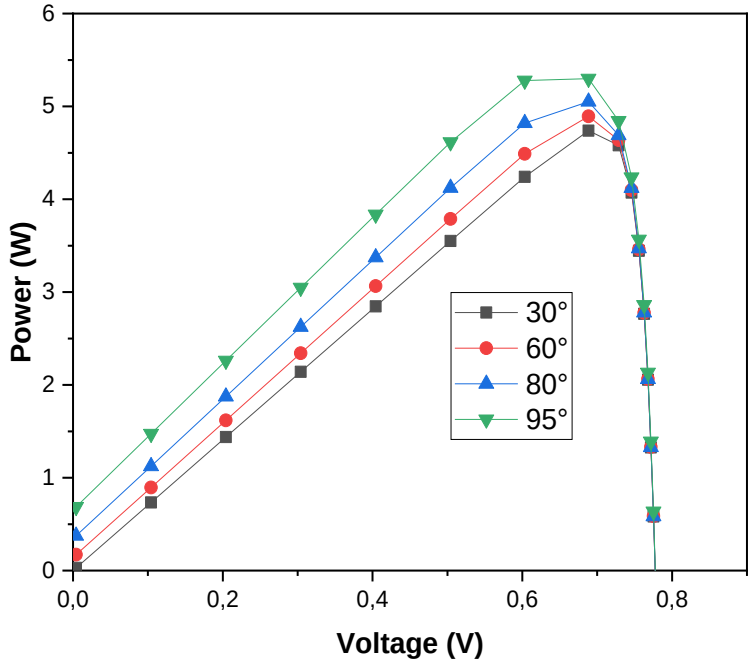

Figure IV.11: Influence of the texturing angle on the Power characteristic.

Table IV.5: Comparison of the different angle of texturing

Angle of texturing	30°	60°	80°	95°
Icc (A)	-7.041	-7.236	-7.499	-7.872
Vco (V)	0.7774	0.7777	0.7773	0.7835
Pmax (W)	4.761	4.897	5.054	5.348
FF	0.8697	0.8702	0.8670	0.8670
η (%)	23.81	24.49	25.27	26.74

We tried with different angles and we found these results:

Whenever the angle of texturing grows the current Fig) IV.10), power Fig) IV.11) and the efficiency increases Table (IV.4) because the solar cells become more exposed to the solar rayonement. This is because the texturing creates a larger surface area for light to be reflected and absorbed.

The angle of texturation that is most effective for a solar cell will depend on the type of cell and the amount of sunlight that it will be exposed to. For example, a cell that will be exposed to a lot of sunlight may need a higher angle of texturation than a cell that will be exposed to less sunlight. Overall, the optimal angle of texturation for a solar cell will depend on the type of cell, the amount of sunlight that it will be exposed to, and the cost of the cell. It is important to consider all of these factors when making a decision about the angle of texturation for a solar cell.

IV.3.5.Influence of the depth of texturation on the characteristic I-V/Power and Efficiency

For the simulation, we used the subsequent parameters:

- **N-type background doping :** 10^{17} cm^{-3}
- **P-type background doping :** 10^{15} cm^{-3}
- **Bulk recombination :** 3000 µs
- **Surface area :** 200cm^2.
- **Thickness :** 30µm.
- **The angle of texturation :** 95°.

And we modified the depth of texturation as follows:

(a) Depth of 1µm.

(b) Depth of 2µm.

(c) Depth of 3µm.

(d) Depth of 4µm.

The subsequent findings were acquired from the simulated cell mentioned earlier on:

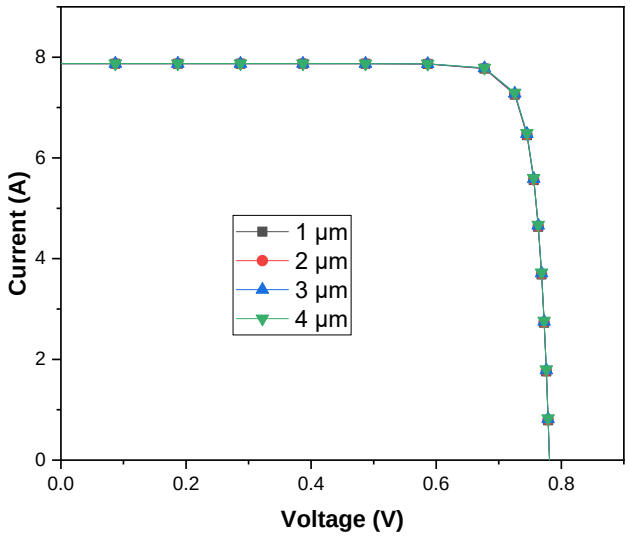

Figure IV.12: Influence of the texturation angle on the I-V characteristic .

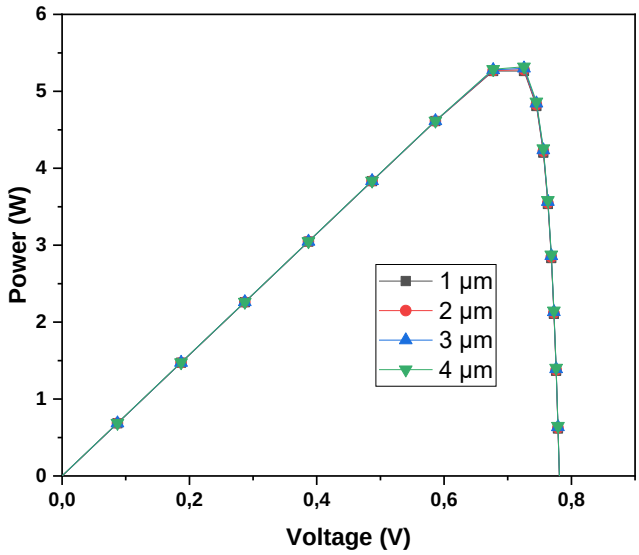

Figure IV.13: Influence of the texturation angle on the Power characteristic .

Table IV.6: Comparison of the different depth texturations

Depth of texturation	1µm	2µm	3µm	4µm
Icc (A)	-7.870	-7.871	-7.872	-7.873
Vco (V)	0.7810	0.7822	0.7835	0.7849
Pmax (W)	5.321	5.334	5.348	5.365
FF	0.8657	0.8663	0.8670	0.8681
η (%)	26.61	26.67	26.74	26.83

The depth of texturing is the distance from the surface of the solar cell to the bottom of the grooves. The deeper the texturing, the more light is reflected and absorbed by the cell.
The previous table represents the depth changes we notice a slight improvement, where the current Fig) IV.12), the power Fig) IV.13) and the efficiency Table (IV.5) increases when the depth value increases.

That refers to the thickness of the absorbing layer in the solar cell, which can have a significant impact on the efficiency of the cell. In general, a thicker absorbing layer in a solar cell can increase its light absorption and conversion efficiency.

Part two :

- **Cell SnO_2/Si(N^+) /Si(P) :**

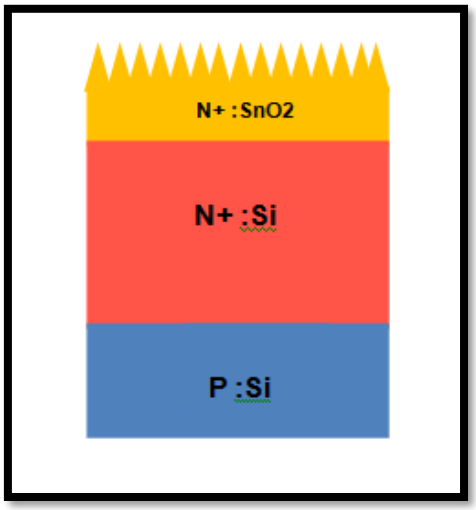

Figure IV.14: Cell SnO_2

IV.4.The Influence of the thickness of SnO_2 region on the characteristic I (V)/P (V) and Efficiency

- ✓ **The parameters introduced for the simulation :**

Table IV.7: The parameters for the simulation SnO_2

Device area	$16cm^2$
Front surface texture angle	110°
Front surface texture depth	4µm
1st device region	Layer SnO_2
Electron mobility	$25cm^2/Vs$
Hole mobility	$2500cm^2/Vs$
Dielectric constant	9
Gap Energy	3.8eV
Instrinsic concentration at 300K	$10^{-14}\ cm^{-3}$
Refractive index	1.9
F-type background doping	$1\times10^{17}\ cm^{-3}$
Bulk recombination	$\tau n = \tau p = 1000\ \mu s$
2nd device region	Junction $Si(N^+)$
Thickness	30µm
Electron mobility	from internal model of silicon
Dielectric constant	11.9
Gap energy	1.124Ev
Instrinsic concentration at 300K	$10^{10}\ cm^{-3}$
Refractive index	3.58
Absoprtion coefficient	si300.abs
N-type background doping	$1\times10^{17}\ cm^{-3}$
Bulk recombination	$\tau n = \tau p = 3000\ \mu s$
3rd device region	Junction Si(P)
Thickness	10µm
P-type background doping	$1\times10^{15}\ cm^{-3}$

Bulk recombination	$\tau n = \tau p = 3000\ \mu s$
Excitation	from one-sun.exc

- We simulated with the parameters above and we changed the thickness as follow :

(a) 0.10µm.

(b) 0.17µm.

(c) 0.25µm.

(d) 0.30µm.

- The next graphs and the table were obtained from the simulated cell above :

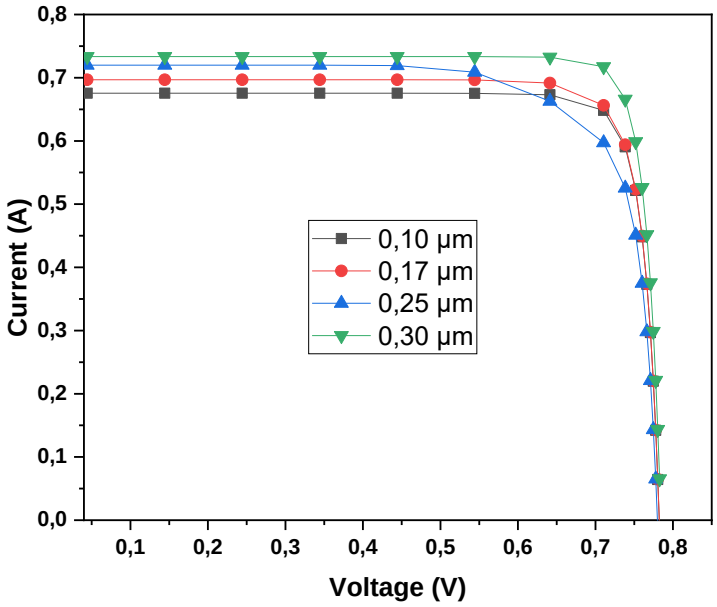

Figure IV.15: Influence of the thickness of SnO_2 region on the I-V characteristic

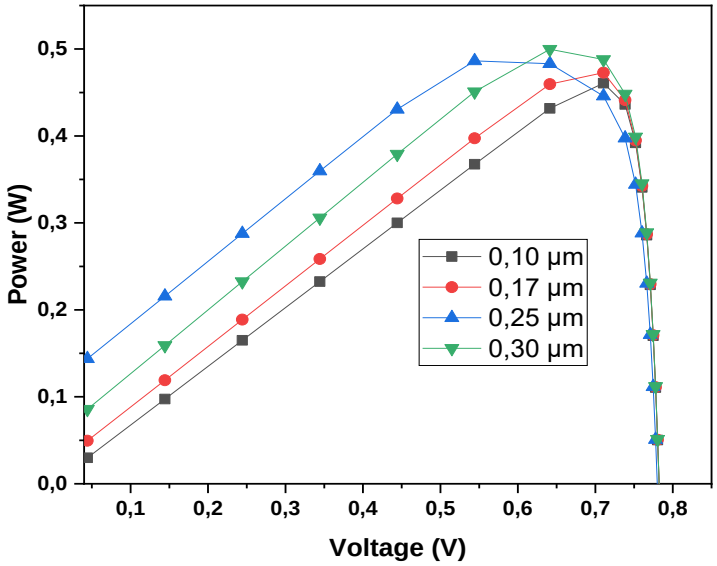

Figure IV.16: Influence of the thickness of SnO_2 region on the Power characteristic .

Table IV.8: Comparison of the different thickness of ARL in SnO_2 region

Thickness of ARL (µm)	0.10	0.17	0.25	0.30
Icc (A)	-0.675	-0.696	-0.720	-0.733
Vco (V)	0.7823	0.7828	0.7833	0.7836
Pmax (W)	0.4608	0.4738	0.4921	0.5026
FF	0.8726	0.8696	0.8725	0.8750
η (%)	28.80	29.61	30.76	31.41

The table above summarizes the efficiency results obtained for the different thicknesses of the anti-reflective layer (ARL) with SnO_2, ranging from 0.10µm to 0.30µm. The corresponding efficiency values were found to be 28.80%, 29.61%, 30.76%, and 31.41% respectively.

As shown in the table, the efficiency of the solar cell increased with increasing thickness of the anti-reflective layer. In addition, the current and the power increased, this trend can be more clearly visualized in the Figures (IV.15) (IV.16) above, which shows the variation of current and power with the thickness of the ARL.

These efficiency results are comparable to those reported in previous studies [2]. The optimal thickness of the ARL reported in our study (0.30µm) was slightly higher than that reported in study I mentioned above (0.13µm) which leads us to a higher efficiency. This may be due the variation of other parameters in our study such as texturation, Doping and Depth of texturation.

In general, a thicker SnO_2 layer can provide better anti-reflective properties, allowing more light to be transmitted into the solar cell and potentially improving the cell's current and efficiency as the table shows. However, if the layer is too thick, it can start to absorb more light itself, reducing the amount of light that reaches the active layer of the cell and potentially decreasing efficiency.

Additionally, if the SnO_2 layer is too thick, it can start to interfere with the flow of charge carriers in the solar cell, leading to reduced performance. This is because charge carriers may have to travel further through the SnO_2 layer to reach the electrode, leading to higher levels of resistance and a reduction in the overall current that the cell can produce.

On the other hand, a thinner SnO_2 layer may not provide as much anti-reflective benefit, but may allow for better charge carrier flow and overall cell performance. However, if the layer is too thin, it may not provide sufficient anti-reflective properties, leading to a reduction for light that is transmitted into the cell.

Overall, the optimal thickness for the SnO_2 layer will depend on the specific characteristics of the solar cell and the desired performance goals. It is important to carefully measure and analyze the performance of the cell with varying thicknesses of SnO_2 layers to determine the optimal thickness for the specific application.

- **Cell ZnO/Si(N^+) /Si(P) :**

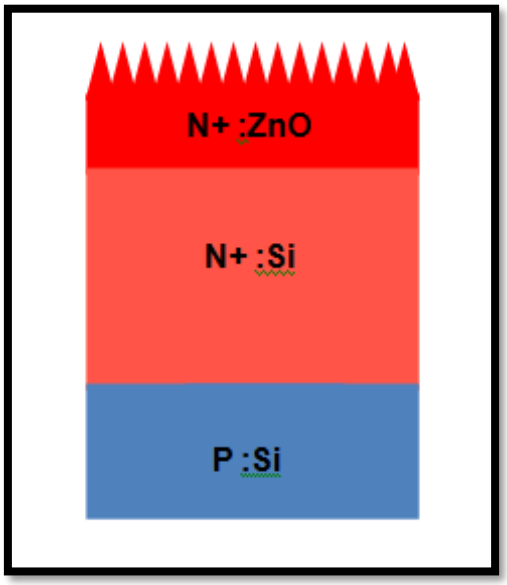

Figure IV.17: Cell ZnO

IV.5.The Influence of the thickness of ZnO region on the characteristic I(V)/P(V) and Efficiency

- ✓ **The parameters that are implemented for the simulation :**

Table IV.9: The parameters for the simulation ZnO

Device area	16cm²
Front surface texture angle	110°
Front surface texture depth	4µm
1st device region	Layer ZnO
Electron mobility	50cm²/Vs
Hole mobility	50cm²/Vs
Dielectric constant	8.66
Gap Energy	3.27eV
Instrinsic concentration at 300K	10^{-14} cm^{-3}
Refractive index	2
F-type background doping	1×10^{17} cm^{-3}
Bulk recombination	$\tau n = \tau p = 1000$ µs
2nd device region	Junction Si(N^{+})
Thickness	30µm
Electron mobility	from internal model of silicon
Dielectric constant	11.9
Gap energy	1.124Ev
Instrinsic concentration at 300K	10^{10} cm^{-3}
Refractive index	3.58
Absoprtion coefficient	si300.abs
N-type background doping	1×10^{17} cm^{-3}
Bulk recombination	$\tau n = \tau p = 3000$ µs
3rd device region	Junction Si(P)
Thickness	10µm
P-type background doping	1×10^{15} cm^{-3}
Bulk recombination	$\tau n = \tau p = 3000$ µs
Excitation	from one-sun.exc

- Using the aforementioned parameters for the simulation, we varied the thickness as follows:

(a) 1µm.
(b) 2µm.
(c) 3µm.
(d) 4µm.

- The succeeding outcomes were derived from the simulated cell above, as mentioned before :

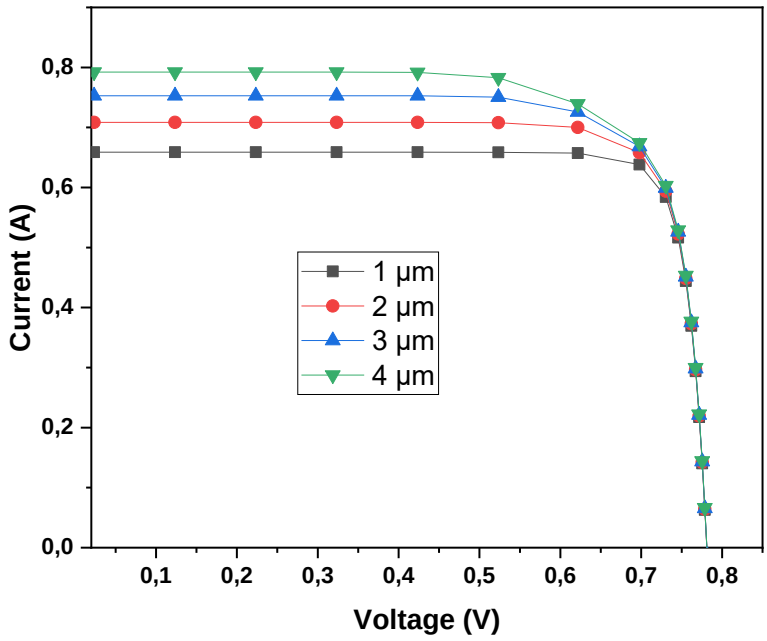

Figure IV.18: Influence of the thickness of ZnO region on the I-V characteristic.

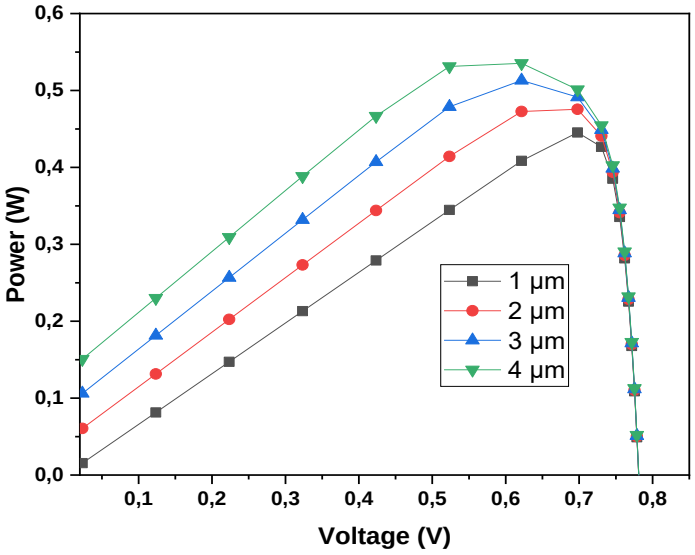

Figure IV.19: Influence of the thickness of ZnO region on the Power characteristic .

Table IV.10: Comparison of the different thickness of ARL in ZnO region

Thickness of ARL (µm)	1	2	3	4
Icc (A)	-0.6587	-0.7084	-0.7527	-0.7922
Vco (V)	0.7811	0.7823	0.7836	0.7848
Pmax (W)	0.4461	0.4789	0.5135	0.5382
FF	0.8670	0.8641	0.8706	0.8656
η (%)	27.88	29.93	32.09	33.64

The results obtained from our study on the effect of varying the thickness of a ZnO anti-reflective layer (ARL) on the efficiency of a solar cell are summarized in the Table IV.9 and illustrated in the Figures (IV.18) (IV.19) As shown, increasing the thickness of the ZnO ARL from 1µm to 4µm led to a steady increase in efficiency from 27.93% to 33.66% and increase current and power remarkably. These results demonstrate the potential of the ZnO ARL as an effective means of increasing the efficiency of solar cells. Optimizing the thickness of the ZnO layer is a trade-off between maximizing light absorption and minimizing electrical losses.

The increase in efficiency observed in our study can be attributed to the ability of the ZnO ARL to reduce the amount of light that is reflected at the surface of the solar cell. As the thickness of the ZnO ARL increases, the layer, reducing the amount of light that is reflected back into the air, absorbs more light. This increases the amount of light that is transmitted into the solar cell, leading to a greater amount of power generated.

Our results are consistent with previous studies that have demonstrated the effectiveness of ZnO ARLs in improving solar cell **[3].** However, the optimal thickness of the ZnO ARL reported in our study (4μm) is much promising than that reported in the study i mentioned. Comparing the efficiency results to theirs, they found an efficiency of 24.8% which is inferior to ours this is because we investigated the influence of multiple parameters and we took the perfect one from each parameter in order to seek a higher efficiency.

Comparing the higher efficiency, we got to others. In the article, the authors studied a ZnO/Si HJ solar cell and they found a 24.8% **[3]** efficiency, which is inferior to ours that is because we investigated the influence of multiple parameters and we took the perfect one from each parameter in order to seek a higher efficiency.

However, this may be due to differences in the materials used or the fabrication process, and suggests that further optimization is necessary to fully exploit the potential of ZnO ARLs in improving solar cell efficiency.

GENERAL CONCLUSION

GENERAL CONCLUSION

In this present work, our study is based on the simulation using PC1D software of three solar cells, which are cell homojunction Si (N^+)/Si (P) and two cells heterojunction SnO_2 /Si (N^+)/Si (P), ZnO/Si (N^+)/Si (P), where SnO_2 and ZnO used as an anti-reflective layer.

In the first part of this study, an optimization of the parameters of the Si (N^+)/Si(P) homojunction cell, determining the optimal values of these parameters, namely : area surface, thickness of the n-region, apply texturation on the front surface to reduce reflection losses and also investigating the texturation's angle and depth. The results if this first part show a significant improvement in efficiency compared to the initial values, increasing from 22% to approximately 26%.

In the second part, we added SnO_2 and ZnO as an anti-reflective layer in order to highlight the importance of an ARL (Anti-reflective Layers) on the silicon solar cell, we studied the effect of the thickness of the ARL on the textured solar cell, and we used an experimental data of reflectivity, absorption coefficient and refractive index.

The simulation results of the cells: Si (N^+) /Si(P), SnO_2 /Si (N^+) /Si(P) and ZnO/Si (N^+)/Si (P) show that the utilization of SnO_2 and ZnO on the surface of the homojunction solar cell remarkably improves the conversion efficiency. It increases from 26% to 31% for SnO_2 and from 26% to 33% for ZnO.

BIBLIOGRAPHY

Chapter I

[1] Le photovoltaïque–Module 3 – Fonctionnement et Technologies Novembre2010 page 3,4,5,6/10.

[2] Andre Susanto, ChitraPriambodo, CastlerockConsulting_ Rooftop Solar PV System Designers and Installers APEC Secretariat March2015

[3] Andrej Čotar, dipl.ing._ Andrej Filčić, dipl.oec REA Kvarner Ltd _ PHOTOVOLTAIC SYSTEMS Rijeka, January 2012

[4] Miro Zeman _Delft University of Technology_INTRODUCTION TO PHOTOVOLTAIC SOLAR ENERGY

[5] H. Mathieu, "Physique des semi-conducteurs et des composants électroniques", 2ème Edition, Masson, 1990.

[6]S. M. Sze, Physics of semiconductor Devices, second edition, Copyright. C.1981 by John, Wiley and Son, Inc.

[7] Roshanak Radbeh « Réalisation et caractérisation des cellules solaires organiques à couches composites polymères incluant des nanotubes de carbones ». Thèse de doctorat, Université de Limoges, 2008.

[8] A. Luque, Practical Handbook of Photovoltaics (Second Edition) -2012.

[9] FAHRENBRUCH, Alan et BUBE, Richard. Fundamentals of solar cells: photovoltaic solar energy conversion. Elsevier, 2012.

[10] KOSYACHENKO, Leonid A. (ed.). Solar Cells: New Aspects and Solutions. BoD–Books on Demand, 2011.

[11] REINDERS, Angèle, VERLINDEN, Pierre, VAN SARK, Wilfried, et al. Photovoltaic solar energy: from fundamentals to applications. John Wiley & Sons, 2017.

[12] GOETZBERGER, Adolf et HOFFMANN, Volker Uwe. Photovoltaic solar energy generation. Springer Science & Business Media, 2005.

[13] NELSON, Jenny A. The physics of solar cells. World Scientific Publishing Company, 2003.

[14] WINTER, C.-J., SIZMANN, Rudolf L., et VANT-HULL, Lorin L. (ed.). Solar power plants: fundamentals, technology, systems, economics. Springer Science & Business Media, 2012.

[15] FONASH, Stephen. Solar cell device physics. Elsevier, 2012.

[16] FRAAS, Lewis M. et PARTAIN, Larry D. Solar cells and their applications. Hoboken, NJ: Wiley, 2010.

[17] HARROU, Fouzi, KADRI, Farid, et SUN, Ying. Forecasting of photovoltaic solar power production using LSTM approach. Advanced statistical modeling, forecasting, and fault detection in renewable energy systems, 2020, vol. 3.

[18] SUHAIMI, Suriati, SHAHIMIN, Mukhzeer Mohamad, ALAHMED, Z. A., et al. Materials for enhanced dye-sensitized solar cell performance: Electrochemical application. Int. J. Electrochem. Sci, 2015, vol. 10, no 4, p. 2859-2871.

[19] SAGA, Tatsuo. Advances in crystalline silicon solar cell technology for industrial mass production. npg asia materials, 2010, vol. 2, no 3, p. 96-102.

[20] GRATZEL, M. Les nouvelles cellules solaires nanocristallines. Actualité chimique, 2007, vol. 308, p. 57.

[21] MEMOIRE de ARBAOUI Kawter et MAZOUNI Mohamed Amin "Effet de la couche antireflet sur la réponse d'une cellule solaire" Université Djillali LIABES-Sidi Bel Abbes Faculté de Génie électrique Département d'électronique

[22] D. A. Clugston and P. A. Basore, PC1D version 5:32-bit solar cell modelling on personal computers", 26th IEEE.

[23] H. HELLALE, " Optimisation des grandeurs photovoltaïques des cellules solaires à base du composé GaAs1-xNx", mémoire de master, université Djillali Liabes, sidi bel abbes,2016

[24] A. Aho, A. Tukiainen, V. Korpijärvi, V. Polojärvi, AIP Conférence Proceedings, Toledo, Spain (2012).

[25] X. M. Teng, H. T Fan, S. S. Pan, C. Ye, and G. H. Li, Journal of Vacuum Science & Technologie 24 (2006).

Chapter II

[1] E. A. AlNuaimy and J. M. Marshall, « Excimer laser crystallization and doping of source and drain regions in high quality amorphous silicon thin film transistors », Ap pl. Phys. Lett. 69 (1996) 38573859.

[2] C. Anderson and U. Kortshagen, « Seeded solid phase crystallization of amor phous silicon films with embedded nanocrystals », Mater. Res. Soc. Symp. Proc. 1066 (2008) 185190.

[3] G. Andrä, H.D. Geiler, G. Götz, K. H. Heinig, H. Woittennek, « Explosive LiquidPhase C rystallization of Thin Silicon Films during Pulse Heating », physica status solidi (a) 74 (1982) 511515.

[4] G. Andrä, J. Bergmann, F. Falk, « Laser crystallized multicrystalline silicon thin films on glass », Thin Solid Films 487 (2005) 7780.

[5] G. Andrä and F. Falk, « Multicrystalline silicon films with large grains on glass: preparati on and applications » Phys. Stat. Sol. (c) 5 (2008) 32213228.

[6] : G. Andrä, J. Bergmann, A. Gawlik, J. Plentz, I. Höger, T. Schmidt, F. Falk, « Thin Film Solar Cells Based on Diode Laser Crystallized Polycrystalline Silicon », 26th E uropean Photovoltaic Solar Energy Conference and Exhibition, (Hamburg, Germany), 2011, 28032806.

[7] T. R. Anthony and H. E. Cline, « Surface rippling induced by surface tension gradients during laser surface melting and alloying », J. Appl. Phys. 48 (197 7) 3888-3894.

[8] G. Auvert, O. Bensahel, A. Perio, V. T. Nguyen, and G. A. Rozgonyi, « Explosive crystal lization of aSi films in both the solid and liquid phases », Appl. Phys. Lett. 39 (1981) 724 726.

[9] M. Avrami, « Kinetics of Phase Change. I: General Theory », Journal of Chemical Physics 7 (1939) 11031112. [10] M. Avrami, « Kinetics of Phase Change. II: Transformation Time Relations for Random Distribution of Nuclei », Journal of Chemical Physics 8 (1940) 212224.

[11] M. Avrami, « Kinetics of Phase Change. II I: Granulation, Phase Change, a nd Microstructure Kinetics of Phase Change » 9 (1941) 177184.

[12] A. Aydinli, Y Gündüç and C Topical,« Simulation of explosive crystallisation in pulsed l

aser irradiation aSi », J. Phys. D: Appl. Phys. 22 (1989) 693698.
[13] G. Baertschi, R. P. Salathé, and H. P. Weber, « Dynamics of Laser Crystal lization in Amorphous Ge Films », Appl. Phys. 25 (1981) 9193.

[14] P. Baeri, C. Spinella, and R. Reitano, « Fast Melting of Amorphous Silicon Carbide Indu ced by Nanosecond Laser Pulse », International Journal of Thermophysics 20 (1999) 1211 1221.

[15] U. Bangert, P. J. Goodhew, C. Jeynes and I. H. Wilson, « Lowenergy (25 keV) argon da mage in silicon » J. Phys. D: Appl. Phys. 19 (1986) 589603.
[16] D. Bensahel, G. Auvert, and M. Dupuy, « Explosive crystallization in single crystal - silicon amorphized by implantation », J. Appl. Phys. 54 (1983) 395397.
[17] E. Berthoumieux, B. Berthier, C. Moreau, J.P. Gallien, A.C. Roux, « Paramet erization of nuclear reactions cross section using Rmatrix theory », Nuclear Instruments and Methods in Physics Research B 136138 (1998) 5559

[18] M. F. Best, R. A. Condrate, « A Raman study of TiO2SiO2 glasses prepared by sol- gel processes », J. of Mat. Sci. Lett. 4 (1985) 994998.
[19] W. Beyer, « Hydrogen effusion: a probe for surface desorption and diffusion », Physica B: Condensed Matter 170 (1991) 105114.
[20] W. Beyer, « Infrared absorption and hydrogen effusion of hydrogenated amorphous sili conoxide films », Journal of NonCrystalline Solids 266269 (2000) 845849.

[21] D. K. Biegelsen, N. M. Johnson, D. J. Bartelink and M. D. Moyer, « Laser and Electron Beam Solid Interactions and Materials Processing », edited by J. F. Gibbons, L D. Hess, and T. W Sigmon, NorthHolland, NewYork, 1981, 487.
[22] D. K. Biegelsen, N. M. Johnson, D. J. Bartlelink, M. D. Moyer, « Therm al gradient control for enhanced laser induced crystallization of predefined semiconductor are as », United States Patent, 4 330 363, 1982.05.18
[23] J. L. Bobin, H. Nifenecker, C. Stéphan, « L'énergie dans le monde : bilan et perspectives », EDP Sciences, 2001.
[24] S. Bourdais « Etude du Dépôt et des Propriétés Physiques du Silicium Polycristallin obte nu par le procédé RTCVD sur Substrats de Mullite. Application aux Cellules Photovoltaïques en Couches Minces » Thèse de l'Université Louis Pasteur, Strasbourg, 1999.
[25] B. Bourouga, G. Le Meur, B. Garnier, J. F. Michaud, T. Mohammed_Brahim, « Heat tra

nsfer during a cw laser crystallisation process of a silicon thin film on a glass substrate », Exc erpt from the Proceedings of the COMSOL Multiphysics User's Conference, Paris, 2005.

Chapter III:

[1] http://forums.futura-sciences.com/physique/129469-optique-difference-demarche.html

[2] Castro -hurtado et all, applied surface science, 276 (2013)229-235.

[3] Touria benbakhti, ″caractérisation des semi-conducteurs composés par les techniques d'imagerie de photoluminescence″. Thèse de doctorat, l'état Est science en microélectronique, (1999).

[4] https://media4.obspm.fr/public/AMC/pages_lois-snell-descartes/lsd-rfr-mise-enevidence.html

[5] MEMOIRE de ARBAOUI Kawter et MAZOUNI Mohamed Amin "Effet de la couche antireflet sur la réponse d'une cellule solaire" Université Djillali LiabeS-Sidi Bel Abbes Faculté de Génie électrique Département d'électronique

[6] J. Thomas, Georg Hass, vol.2, in: physics of thin films, G.Hass, Academic press, New York (1963).

[7] FERHATI Fariza ″élaboration de l'oxyde de vanadium v2O5 par APCVD application PV″, Mémoire de magister, Université Mouloud MAMMERI Tizi-Ouzou, (2011).

[8] Hind Tabet-Derraz, Thèse de Doctorat d'état (2007), Laboratoire d'Élaboration et Caractérisation des Matériaux (LECM) de SBA, Algérie.

[9] J. L. Deschanvres, 'Elaboration par le procédé pyrosol de couches minces texturées de ZnO pour la réalisation de microcapteurs', Thèse de doctorat, Laboratoire des matériaux et du génie physique, CNRS-Ecole Nationale Supérieure de Physique de Grenoble, France

[10] Nam Ho Kim, Hyoun Woo Kim, 'Room temperature growth of Zinc oxide films on Si substrates by the RF magnetron sputtering', Materials Letters. 58 (2004) 938-943.

[11] H. L. Hartnagel, A. L. Dawar, A. K. Jain, C. Jagadish, 'Semiconducting Transparent Thin Films'. Bristol and Philadelphia: Institute of Physics Publishing (1995).

[12] Bengisu Ergin, Elif Ketenci, Ferhunde Atay, international journal of hydrogen energy 34 (2009) 5249 –5254.
[13] Ü. Özgür, Ya. I. Alivov, C. Liu, A. Teke, M.A. Reshchikov, S. Doğan, V. Avrutin, S. J. Cho and H. Morkoç, Journal of Applied Physics 98 (2005) 041301.
[14] Jérôme Garnier, 'Elaboration de couches minces d'oxydes transparents et conducteurs par spray CVD assisté par radiation infrarouge pour applications photovoltaïques', Thèse de doctorat (2009), Laboratoire d'Arts et Métiers ParisTech d'Angers.
[15] E.M. Bachari, G. Baud, S. Ben Amor, M. Jacquet, Thin Solid Films. 348 (1999) 165.
[16] T.K. Subramanyam, B. Srinivasulu Naidu, S. Uthanna. Cryst. Res. Technol. 35 (2000) 1193

[17] Lekiket Hichem, Elaboration et caractérisation des hétérojonctions à base de couches minces de ZnO et ZnS, Mémoire de magister (2008), Université de Constantine.
[18] Balla Diop Ngom, Etude Expérimentale de la microstructure et des propriétés optiques des nanorods d'oxyde de zinc dopé au tungstène préparés par ablation laser pulsé, Thèse de doctorat (2009), Dakar.
[19] Jiefang Zhu, Dinko Chakarov and Michael Zäch, "Nanostructured Materials for Photolytic Hydrogen Production", L. Zang (ed.), Energy Efficiency and Renewable Energy Through Nanotechnology, Green Energy and Technology, DOI: 10.1007/978-0-85729-638-2_13, Springer-Verlag London Limited 2011.

[20] H. Tabet-Derraz, N. Benramdane, D. Nacer, A. Bouzidi, M. Medles, Solar Energy Materials et solar cells 73 (2002) 249-259.
[21] A. F. Kohn, G. Ceder, D. Morgon, C. G. Van de Walle, Phys. Rev.B, 61 (2000) 15019.
[22]S. M. Sze, Physics of Semiconductor Devices, 2nd ed. (Wiley Eastern Limited, 2000).

[23] B.J. Jin, S.H. Bae, S.Y. Lee, S. Im. Mat. Sci & Eng. B71 (2000) 301.
[24] K. I. Hagemark, L. C. Chacka, J. Solid State. Chem, 15 (2001) 261.
[25]Noua Bouhssira, Elaboration et caractérisation des couches minces D'oxydes de Zinc par évaporation, Mémoire de magister (2005), Université Mentouri-Constantine.
[26] G. bogner, J. phys. Chem. Solids 19 (1961) 235.
[27] N. Sakagami, M. Wada, Trans. IECE (japan) E60 (2000) 78.
[28] N. Ito, Y. Sato, P. K. Song, A. Kaijio, K. Inoue, Y. Shigesato, Thin Solid Films 99 (2006) 496.

[29] C. M. Ghimbeu, Préparation et Caractérisation de couches minces d'oxydes métalliques semi-conducteurs pour la détection de gaz Polluants atmosphériques, Thèse doctorat. Université Paul Verlaine de Metz, (2007).

[30] T. Dauzhenka, Couches minces d'oxyde d'étain : la localisation faible et les effets de l'interaction, Thèse doctorat. Université de Toulouse, (2011).

[31] M. Khachane, Étude des matériaux ferroélectriques céramiques et couches minces à base de nimbâtes alcalino-terreux et multicouches ferroélectriques-catalytiques pour capteur de gaz, Thèse doctorat. Université du Sud Toulon- Var, (2007).

[32] T. Brouri, Élaboration et étude des propriétés électriques des couches minces et de nano fils de ZnO, Thèse Doctorat, Université Paris-Est, (2011).

[33] K. Lagha-Menouer, Étude et réalisation d'une cellule solaire multicouches du type Si − SiO2 − SnO2 − ZnO par APCVD, Thèse Doctorat, université Mouloud Mammeri Tizi-Ouzou, 2011.

[34] D. Lambe et al., Thin solid films, 518(2009)1222-1224

Chapter IV:

[1] BELARBI, Moussaab, BENYOUCEF, Abdellah, et BENYOUCEF, Boumediene. Simulation of the solar cells with PC1D, application to cells based on silicon. *Advanced Energy: An International Journal (AEIJ)*, 2014

[2] TALA-IGHIL, R. et BOUMAOUR, M. Numerical simulation of silicon based solar cells with a degenerated SnO2: F window layer. *The European Physical Journal-Applied Physics*, 2007

[3] NAIM, Houcine, SHAH, Deb Kumar, BOUADI, Abed, *et al.* An In-Depth Optimization of Thickness of Base and Emitter of ZnO/Si Heterojunction-Based Crystalline Silicon Solar Cell: A Simulation Method. *Journal of Electronic Materials*, 2022.